MASTER OF SCIENCE

An evaluation of computer assisted skull re-assembly using hand held and automated laser scanners

Mackenzie, Stenton

Award date:
2007

Awarding institution:
University of Dundee

MASTER OF SCIENCE

An evaluation of computer assisted skull re-assembly using hand held and automated laser scanners

Stenton Mackenzie

2007

University of Dundee

An evaluation of computer assisted skull re-assembly using hand held and automated laser scanners.

Stenton Mackenzie

The Unit of Anatomy
and Forensic Anthropology

Dissertation submitted to the University of Dundee
for the degree of MSc. in Human Identification
2007

Supervisor: Dr. C. Wilkinson

CONTENTS

Illustrations

Discussion

Nomenclature

3D (3-D)	three dimensions (of perspective)
3D-DM	three dimensional digitised model
CAD	computer aided design
CAS	computer-assisted surgery
.cly	FreeForm file
CT; CAT	computed tomography; computer assisted tomography
.fsn	FASTSCAN files
GB	gigabyte (unit of computer data information storage capacity)
GHz	gigahertz (unit of frequency – one billion cycles per second)
IBM PC	International Business Machines - personal computer
.jpg	Joint Photographic Expert Group (image file type)
MB	megabyte (unit of computer data information storage capacity)
MHz	megahertz (unit of frequency - one million cycles per second)
MVA	motor vehicle accident
psi	pounds per square inch
RAM	random access memory
RP	rapid prototyping
RV	real virtuality
.STL	stereolithography files
VR	virtual reality

Abstract

Computer assisted skull re-assembly is an alternative to classical manual methods of physical restoration and reconstruction. The technique is reliant on high quality images produced by radiological CT or optical surface laser scans. The accuracy of CAD re-assembly and the contribution the technologies of image production make to the process are largely unevaluated. This research uses four 3D models produced by a hand held laser scanner (Scorpion FASTSCAN by Polhemus) and one model produced by an automated, stationary laser scanner (Minolta by Hyperfocal) to re-assemble 5 skulls using a computer modelling program (Freeform Modelling). Hand held scanning, model production and quality are assessed; skull restoration accuracy is described and quantified by a reverse engineering software program (Geomagic Qualify) which measures overlap between the contour shells of original and restored skulls.

The level of acceptable accuracy for skulls which might support facial reconstruction following re-assembly was determined to be $\leq$ +/- 2.0 mm of error. Crania and mandibles were assessed individually. Accuracy results for five crania were unacceptable (40%), acceptable (40%), and reasonable (20%). Results for five mandibles demonstrated accuracy which was acceptable (40%), reasonable (20%), and good (40%).

Optimising CAD potential for skull restoration depends on further research which examines: 1) the affect upon model quality resulting from the partnership between interdependent computer software, and 2) a comprehensive comparative analysis of surface capture technologies in relation to the models used in restoration.

Declaration

No portion of the work referred to in this thesis has been submitted in support of an application for another degree or qualification of this or any other university, or institute of learning.

Copyright

Acknowledgements

I want to thank Dr. Caroline Wilkinson for her supervision and guidance in the completion of this dissertation. Any errors or omissions are entirely my own.

I am indebted to Caroline Needham for her endless patience and humour, Amy Tillotson and Dr. Chris Rynn for their assistance, and to Professor Sue Black for inspiration from on high.

Janice Aitken helped with the preparation of images and Dr. Stephen Richmond in their processing. I am appreciative of their contributions.

I extend my gratitude to those whose skulls are reminders of their former presence amongst us.

INTRODUCTION

The reconstitution of skulls from a fragmented or degraded state is required before facial restoration of deceased individuals can be accomplished (Neave, 1986). In recent years, concern about the untested use and nature of computer aided programs for the reconstruction of soft facial tissues has arisen (Wilkinson, 2005). A facial resemblance can provide an ancillary, but important contribution to legally accepted forensic methods of positive human identification, such as DNA and dental analysis (De Greef and Willems, 2005).

There is little documentation as to the reliability and efficiency of skull re-assembly using computers. When the fragmented skull must be restored or remodelled, the degree to which the skull is returned to its original state is of the utmost importance because a restored facial appearance will primarily rely directly upon the morphology of the skull. This research seeks to both qualify the process of computer-assisted skull re-assembly and to quantify accuracy by comparing the surface contour profiles of five skulls before, and after fragmentation and restoration.

Whether in forensic circumstances where the identification of the recently dead is called individuation, an archaeological context where health, diet and biological affinity form the basis of population history, or in evolutionary relationships revealed by palaeontological studies, fragmented skulls must be as fully and accurately restored as possible to extract the maximum evidence from remains (White, 2000).

White (2000) defines restoration (or re-assembly) as “putting pieces of broken bones back together”, differentiating it from reconstruction – the fabrication of missing bone. This document uses this division to indicate such a clarification in skull re-assembly.

In 2005, Davy and her colleagues commented that although the processes of capturing skull images for the purpose of facial reconstruction now exist, similar technologies for the re-assembly of the skull have yet to document promises of speed and accuracy. Subke (2005) identifies it as “hitherto missing component in a completely digitized reconstruction”. In this regard two systems, a hand-held laser scanner, a mounted laser scanner and computer modelling software program are used to examine the efficacy of 3D virtual skull re-assembly.

The choice of technology and technique were guided by the availability first, of a new hand-held laser scanner (purchased primarily for its portability), and existing computer hardware and software systems, which are regularly used for facial reconstruction but not as often for skull restoration or reconstruction. Accuracy of results were tested using Geomagic Qualify (Geomagic, 2007), a reverse engineering software program, similar to software which has previously been used in comparisons between facial reconstructions and corresponding CT scans from living subjects (Wilkinson, *et al*., 2006).

A brief orientation to the skull and a review of literature relating to facial reconstruction, the manual restoration technique, virtual reality and a computer restoration method follow immediately. A training regime is described. Methods, results, discussion and conclusion with accompanying references, and bibliography proceed in order.

The skull

In all references to the skull the following is assumed: directional and positional terms relating to the body (and skull) are in the context of the standard anatomical perspective and accompanying planes. The skull is positioned according to the Frankfurt Horizontal plane (FH), a horizontal line between craniometric points of the left and right porion (external auditory meatus) and the left orbitale (lowest point on the infraorbital margin). The skull refers to the entire framework inclusive of the mandible; the cranium describes the skull without the mandible, and the calvarium is the cranium without the face. The bones of the facial skeleton are referred to as the splanchnocranium (White, 2000).

Made up of 28 bones in total (excluding accessory wormian bones which are found along suture lines) - 8 unpaired, 6 paired, and 2 sets of 3 small auditory ossicles - the skull is a complex structure. The skull houses and protects the brain, and the primary organs of sight, smell, hearing, taste, smell and mastication (Bass, 1995). It supports the functions of breathing, swallowing, and speech, and is the structure upon which the soft tissues of the face are positioned - serving human communication through expressive movement.

The skull is comprised of both cortical and trabecular tissue, each of which contribute their own structurally characteristic properties to bone behaviour. Collagen, a protein, imparts elasticity, while calcium and phosphorous in the form of hydroxyapatite crystals contribute to bone stiffness (Galloway, 1999). “Weight for weight it is stronger than wood, concrete or steel” (Kau, *et al*., 2005). Skull size and robusticity vary within population groups and according to biological sex and ancestry group; the more gracile skulls of females, the elderly, and children are more vulnerable to trauma. Elements of

its morphology may best be described as an assembly of ridges, projections, openings and depressions (Seeley, *et al*., 2006).

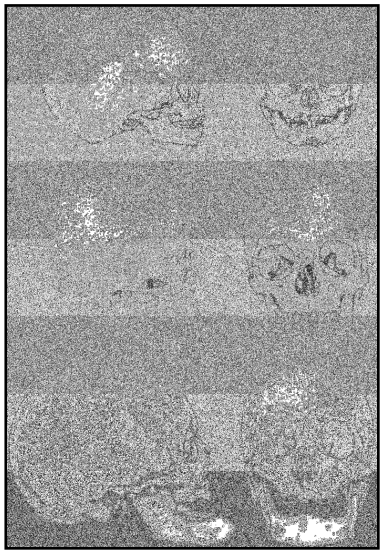

Fig 1: Child, adult and senescent skull.

From: Matshes, E. *et al*. (2005) Human Osteology & Skeletal Radiology: An Atlas and Guide.

The skull is not only the most recognised (Quigley, 2001) element of the human skeleton, but in physical anthropology, the most studied as well (Iscan and Helmer, 1993). In social terms, the skull signifies death and mortality. As such, it is central to human ritual, religion, and art - it is resident in the very fabric of symbolic intercourse (Wilson, 2001). Currently skulls in human skeletal collections serve many areas of scientific study in anatomy, biology and physical anthropology (Quigley, 2001). Osteologists are able to generate both qualitative and quantative information about the morphology and morphometry of the skull through observation and measurement (White, 2000).

Facial reconstruction

Facial reconstruction or approximation is employed as an adjunct to other forensic methods of identifying an individual (Vanezis, *et al*., 1989). The purpose is to create a sufficient likeness to promote recognition amongst people who knew a subject. Differentiating this process from those which lead to positive identification, such as DNA or dental records, is important - facial reconstruction cannot replicate a face exactly - what is desired is a resemblance strong enough to initiate recollection of a unique craniofacial morphology within communities familiar with that person (Wilkinson, 2005; Rynn and Wilkinson, 2006). Interestingly, it is argued that a caricature of a person (as penned by the political cartoonist), is more easily recognised than an ultra-realistic rendering of appearance (Davy, et al., 2005).

A facial resemblance may be achieved through a variety of methods, according to the availability of practitioners, the context attached to, and surrounding the subject in question, preferences of police, and the willingness of the media to distribute and promote the recognition process in the public view (Wilkinson, *et al*., 2006). The following techniques are most common: 1) an artist sketches a likeness of the face in 2D using a photograph of the skull as a template and guide; 2) a face is sculpted in 3D on a cast of the original skull in clay; 3) a computer program 'sculpts' a 3D face on an image of a skull generated by a CT, MRI or laser surface scanner (Wilkinson, 2004).

As a result of a relationship between soft facial tissues and the bones to which they attach (Fedosyutkin and Nainys, 1993), facial reconstitution based on anthropometric, anatomical, and anthropological analysis is possible when (and only if) an intact or a restored/reconstructed skull is available (Neave, 1986; Wilkinson and Neave, 2001). A high order of probable individuation (less than 1 in 1 billion will demonstrate matching

coordinate profiles) in skulls is possible when craniometric measurements are made with an error margin of 0.5 mm; within this restriction, “the craniometric individuality of a skull is as distinctive as a fingerprint” (Schimmler, *et al*., 1993). One of the principal aims therefore, of skull re-assembly is to provide the scaffold upon which a facial resemblance may be based.

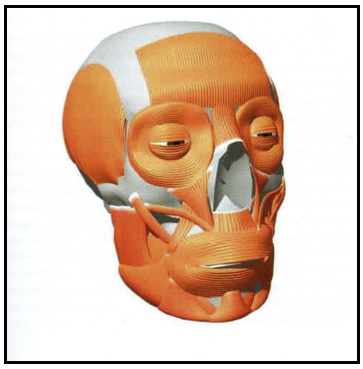

Fig 2: Muscle placement - computer 3D.

From: Clement, J.G. and Marks, M.K. eds. (2005) Computer-Graphic Facial Reconstruction

As utilised by Neave (Prag and Neave, 1997) and others, computer facial reconstruction adheres to the Manchester method, (aligned conceptually and practically with reconstruction rather than approximation because it relies on an extrapolation of muscle tissue from prescriptive anatomic detail in the skull). The Manchester method is a combination of the US (approximation), and the Russian style (reconstruction), using tissue depth guides as a secondary instrument, allowing the indications of the craniomorphology to over-ride the depth pegs when there is disagreement (De Greef and Willems, 2005).

One of the potential benefits to computerized systems for facial reconstruction is the prior use of such a system for the restoration of the skull (Subke, 2005). Incorporation of new techniques can be rapid, particularly if they are seen as attractive. This can pull

technology into practice before validity and accuracy are adequately demonstrated (Wilkinson, 2005). It is these claims of speed, efficiency, and accuracy which prompt the research which is the subject of this paper. The accuracy of facial reconstruction, though still controversial, has withstood the rigor of blind studies and practitioners of facial reconstruction demonstrate various success rates, as high as 70% and 50% above chance (Wilkinson and Whittaker, 2002; Wilkinson, *et al*., 2006). As a precursor to, and an integral element of either manual or computer facial reconstruction techniques, computer-aided skull re-assembly and reconstruction must be subject to the same tests and standards for accuracy and reliability (Wilkinson, 2005).

Manual restoration and reconstruction

Presumably, from the time of the earliest investigations of discovered fragmented skeletal remains, such inquiry has demanded restoration and or reconstruction. These processes however, can irreparably damage a dissembled skull: the Le Moustier 1 Neanderthal fossil skull initially unearthed in 1908 underwent five manual rebuilds (the last one was done in 1925), each successive attempt resulting in accrued loss of bone and erosion of that which remained (Ponce de Leon, and Zillokofer, 1999). Although the techniques of the physical method have changed little in the meantime, restoration materials have improved - but physical renovation always involves risk to the material and its originality (White, 2000).

Generally, in the case of human remains, says White (2005), “restoration is often quick and easy for the competent osteologist”. There are numerous (particularly in the human skull) morphological features which assist in identifying whole or partial pieces and the side of the skull to which they belong. These include changes in bone thickness, muscle

attachments, tooth roots, tooth sockets, sutures, foramina, sinuses, surface textures and blood vessel impressions. Variants in the number of wormian bones, teeth as well as type, articular facets, and anomalies in any of the morphologies listed above are non-metric elements since they cannot be measured (Quigley, 2001). An example of their usefulness in restoration is demonstrated by the posterio-superior direction of impressions made by the meningeal blood vessels on the endocranial surface of parietal bones – by observing these directional clues, a portion of, or a whole parietal bone may thus be sided.

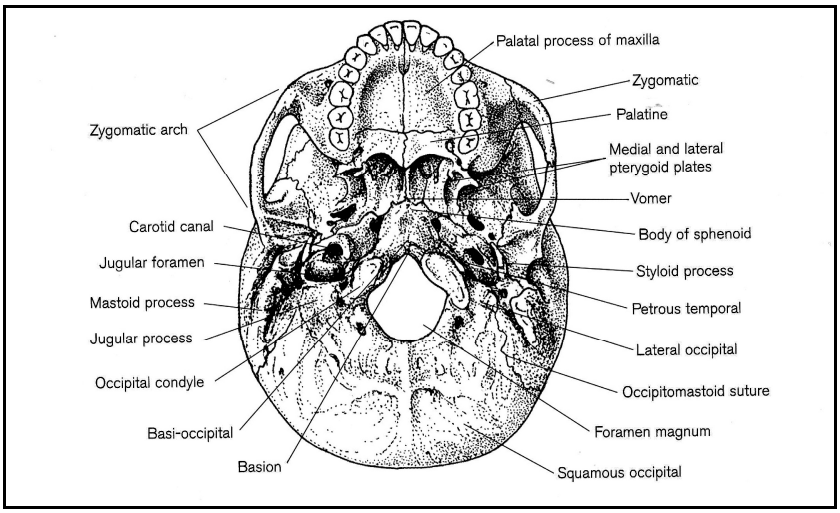

Fig 3: Inferior skull surface.

Complex exterior morphology

From: Scheuer, L. & Black, S. (2000) Juvenile Developmental Osteology.

In relation to fragility, White (2000) emphasises that bones are in a technical sense as precious to science as books are to a library; specific protocols must be observed to ensure specimens in collections and labs are not damaged, lost, or mixed one with another. From an ethical and philosophical perspective, bones represent former living people, and are therefore entitled to our respect. Irreplaceable bones possess originality which is obscured in the process of digitalising their image for use in virtual

environments on computers:

> "with either two- or three-dimensional digital images scanned from original osteological specimens, ...problems are compounded dramatically as the investigator moves another step away from the original. Color, texture, internal anatomy, matrix cover, preservative cover, preparation damage, erosions and distortions of all kinds may be faithfully recorded by such imaging... but for the osteologist seated at a computer monitor on the other side of the planet, these features are often not digitally distinguishable from actual bony anatomy."
>
> [White, 2000]

The need to curate original specimens remains, in spite of the growth and flexibility of digital capture and storage systems (White, 2000). Replicas, such as casts and models made from silicon, rubber and plastic, while immensely useful as teaching and research tools, inherit from the modelling process a substantial loss of internal morphology and general distortions which lead to misinterpretation "based on inaccurate observations and measurements" (White, 2000).

Accepted manual skull restoration guidelines and order of practice have evolved and continue in usage (Bass. 1995; Prag and Neave, 1997; Wilkinson, 2004; Knott, 2002). "Construction starts from the inside, progressing to the outside" in order to avoid the time consuming opening of that which has already been restored to add an internal piece (Subke, 2005). Construction of the facial complex, the basi-cranium and the vault as semi-independent units initially reduces the tendency for error propagation (Zollikofer and Ponce de Leon, 2005). Continual checking and re-checking is required to prevent such an error in alignment perpetuating itself in ever greater increments as other fragments bones are added (Prag and Neave, 1997; Wilkinson, 2004); to this end it is best to use a non-permanent adhesive material whose removal does not harm the bone surfaces - so that pieces may be disengaged from each other and repositioned. Dental sticky wax or vinyl acetate maintains continuity between pieces as assembly proceeds;

further stability can be provided with wooden dowels which support weight and create some rigidity (Wilkinson, 2001).

Of crucial importance to the consideration of any subsequent facial reconstruction is the designation of distortions (arising from plastic deformation as a result of fracture mechanics or post-depositional forces), to an overlap area at the back of the cranial vault - "where errors in shape should not affect the accuracy of the reconstruction" (Wilkinson, 2004). In this way, facial bones are the focus of accuracy to optimise any potential for correct identification.

Cranium breadth may be judged by using the placement of the mandibular condyles in the temporal fossae as a guide (White, 2000). Space for the soft tissue cushioning between condyle and fossa must be taken into account (Prag and Neave, 1997). If pieces require gluing, use only an adhesive which may be dissolved without destroying the bone to which it adheres (water soluble), and which will not chemically inhibit the later use of moulding materials (White, 2000). A sandbox for holding pieces as wax or adhesives cure and allowing gravity to assist naturally in the process may make fragments easier to join (Bass, 1995). Structural tension release as a result of skull fracture means some pieces can not be restored to the same degree of conjunction as their pre-fracture state (Wilkinson, 2004).

When bone is so fragmented that anatomical (morphological) landmarks are difficult to determine and make contiguous, each fragment will be matched by trial and error in an edge-by-edge manner, against every other fragment edge in turn, until pieces are joined by process of elimination (Prag and Neave, 1997; White, 2000). An overhead flexible magnifier and directed light are helpful - a microscope can be enlisted to determine

whether two edges match (White, 2000). Wilkinson (2004) notes that few skulls are symmetrical, while acknowledging that the mirror image created by modelling in wax an area missing from one side of the face or cranium creates an artificial symmetry, but adds, the symmetry does not seem to effect the overall accuracy of the reconstruction. Other documenters of facial reconstruction techniques concur with this conclusion (Prag and Neave, 1997, p.22). Colledge (1996) found the mandible was most susceptible to creating distortion on a resulting facial reconstruction having a significant effect upon accuracy. When the area missing is bilateral instead of unilateral, the surrounding areas of bone must act as a constructive guide (Wilkinson, 2004).

Virtual reality

What is the importance of virtual reality (VR) to computer-assisted restoration/reconstruction of skeletal remains? Or, as Zollikofer and Ponce de Leon (2005) ask, “what is the relationship between a real body and its reconstructed, virtual counterpart?”

Historically, the scientific examination of the human body has largely involved a 'taking apart' of structures, a literal dissecting of materials that constitute the body. Investigation focussed on a dismantling of form and function to the smaller, and smallest, of pieces, particles and elements (Dyer and Thorndike, 2000). Computer technology makes possible an investigation of the interior scale, or the internal landscape of the body (Verhoff, *et al*., 2007; Virtopsy, 2007). Virtual reality as it is manifested by computer graphics is something new, a re-assembling of the original in representative form (Zollikofer and Ponce de Leon, 2005; Galantucci, *et al*., 2006). Representation and transmission of information via computers may be recent, but

ethnobotanist and philosopher Terence Mckenna says virtual reality has been a constitutional facet of our species since the moment language occurred - that virtual reality *is* language, - that they are indivisible in function (History Ends in Green, 1993).

The definition of virtual reality is "still in flux"(Sherman and Craig, 2003), because it is still so new. Researchers, designers, cyberspace travellers, video-gamers, and technicians interpret it variably. Sherman and Craig (2003), define it as a medium, and link it directly to the cave paintings of our ancestors, qualifying VR as the latest media in a series of progressive conceptual and technical steps in communication. *Virtual* denotes an essentiality (an experience); *reality,* for the purpose of this discussion, is defined as being a place or a thing that exists because it can be experienced (by us) (Sherman and Craig, 2003). The basis of VR is perceptual equivalents; physical reality depends on technical devices, skills to implement them, and (ultimately) our perceptual systems, which manage the responses facilitating communication:

> "technically, it can be defined as a computer-based environment in which the user interacts with geometric representations of real-world or model objects, utilizing tools and performing manipulations that emulate physical tools and actions while being immersed in this virtual world."
>
> [Zollikofer and Ponce de Leon, 2005]

Physical interaction between an operator and virtual skull fragments are mediated via the computer screen display of those fragment images and a manipulation arm: a pen-like wand mounted on a jointed swing arm sits next to a keyboard; a facsimile of this tool on screen corresponds with directional movements of the operator's hand holding the pen (figure 4). A virtual skull fragment floats in three dimensions (length, width and volume) on screen; sensations of attraction/resistance transmitted through the pen assist the operator in attaching to an 'anchor' origin point placed within the fragment.

Using six degrees of movement, up, down, forward, back, and tri-axonal rotation (Sherman and Craig, 2003), a fragment can be visually guided into position with another fragment. With sufficient hand-eye coordination and clarity of image detail, an entire skull may be rebuilt in such a manner. Clarity of morphological detail depend on the density of algorithmic voxels of which the image is composed (Galantucci, *et al*., 2006).

Fig 4: Human arm operating haptic arm.

Photograph: Amy Tillotson

Matching hand movements and visual observations in order to direct the wand appropriately on screen is a demanding perceptual task. Even with the sensation of touch relayed via the on-screen tool, the contours of a piece - the convexities, ridges, and planes, and their relationship to other pieces - frequently evade one's grasp, confusing both mind and hand. Human neural networks however, are adept at 'filling in the blanks' (Zollikofer, 2002). When the perception of reality is endangered by a lag in response time, or the immaterial behaviour of matter on screen (when a tool pops 'through' a target piece, appearing on the other side), the human brain negotiates and translates the gaps in time and suspension of the usual laws of physics. Discontinuities are perceived as *relative static* – and do not interfere significantly with task execution

(Zollikofer and Ponce de Leon, 2005). The importance of lag time reduction between operator input and movement completion was demonstrated by a medical application for the first time in 2001 – telesurgery. Using robotics and a laparoscopic approach, gall bladder removal was performed across a transatlantic distance by surgeons operating tiny cameras and microsurgery instruments. A computer console and optic fibre cables allow the rapid transfer of data in "near real time" (Sherman and Craig, (2003), or at less that one-fifth of a second.

In 1991, paleoanthropology used virtual reality and real virtuality in skull restoration and reconstruction for the first time. The discovery of the Tyrolean Iceman invited fresh interpretations of human evolution, in addition to ushering in a new era in investigative computer-assisted technology. It also contributed to the medical professions' first use of the technology in 1992 in the planning of plastic and maxillo-facial surgery (Recheis, *et al*., 1999). Using computed tomography (CT) scans, 3D computer image analysis, and a stereolithographic skull model, Recheis *et al*. (1999) determined endocranial morphology, confirmed endocranial volume, and clarified the type and extent of facial fractures and dental erosion of the Neolithic Age Iceman's mummified remains. The stereolithographic copy of the Iceman's head made from CT data was accurate to $\pm$ 0.5 mm in all directions in comparison to the original. They confirmed their findings using other skulls - and computer guided geometric morphometrics have subsequently come into routine employment in physical anthropology (Zollikofer, *et al*., 1998).

Computer aided restoration and reconstruction

At the time of writing descriptions of skull restoration using computer assistance are in a paleoanthropological context (Zollikofer, *et al*., 1995; Ponce de Leon and Zollikofer, 1999; Zollikofer, 2002; Subke, 2005). Computer aided skull restoration as a prelude to facial reconstruction in a forensic context is not documented - the assumption presumably being that an intact skull is present, or that a fragmented skull is restored and reconstructed by the manual method. In some literature it appears as though the term 'skull reconstruction' is referring to re-assembling the facial soft tissues, not the bony skull, but the writer has not bothered to make a differentiation between the two (Davy, *et al*., p.183).

The goal of fossil restoration/reconstruction in paleoanthropology is to understand the three-dimensional morphology of an individual at the time of death, and to relate the structure and ontogeny of one or more individuals to overall patterns of species development. (Ponce de Leon and Zollikofer, 1999). Brain size, vocal capacity, and bipedality are central to primate and hominid evolution. Skull morphology which contains information about endocranial volume, the upper/mid pharyngeal area, and the relative position of the foramen magnum are therefore of interest to paleoanthropologists (Wind, 1984; Zollikofer, *et al*., 1998; Vialet, *et al*., 2005).

Computer assisted re-assembly of skull fragments however, is dependent upon an initial method of imaging fragments which impart enough 3D detail to make reconstitution feasible. Prior to computed tomography, conventional radiography's principal drawbacks were superimposition (one bony part obscuring another), and an inability to demonstrate the interior skull anatomy. Wind (1984), in her work on mineralised *Homo erectus* skulls, recognised that the (then) newest generation of CT scans produced

smaller pixels (picture elements), allowing a kind of detailed image analysis that previous CT technology could not deliver.

In 1984 Conroy and Vannier, lauded the non-invasive computer programs which manipulated 2D CT slices into 3D images allowing “precise data on area, volume, symmetry, and linear and angular dimensions”...and linear measurements in the sub-millimetre range, “more accurate, objective, and reproducible than the same measurements taken by hand on the original specimen”. It was now possible to view intracranial structures by 'removing' the obscuring matrix encasing fossils. Making sections of the image transparent overcame the superimposition problem without ever dissecting the real fossil (Conroy and Vannier, 1984; Taylor, 2004).

In 1992, Klemt and Infantosi, reported on the increasing resolution achieved with CT scans (2 mm), and the resulting computational 3D modelling used in education - particularly medicine, clinical diagnostics, orthopaedics, and biology. They predicted that the difficulties imposed by lengthy computation time in image production would decrease as the technology was adapted and developed. In 1992, 3D models were created by what now seem in comparison, small and underpowered computers – IBM PC units running at 12 MHz, with 1 MB of memory.

By the late 1990's the combination of computer hardware capacity and software specificity reached a point where it was “possible to disassemble earlier reconstructions, isolate the original material, realign distortions, and reintegrate the parts in a novel reconstruction” (Ponce de Leon and Zollikofer, 1999). Fossil re-assembly with computer assistance had acquired not only a truly visionary ability, but by incorporating tests of reproducibility, also ensured that results represented testable hypotheses (Ponce

de Leon and Zollikofer, 1999). Accuracy can be tested in certain graphics programs by measuring the distance between fragments with an onscreen tool (Subke, 2005), or, an intact skull may be scanned and it's surface area compared with that of the same skull restored after fracture by a program which measures their degree of similarity (Ponce de Leon and Zollikofer, 1999).

These advances are exemplified by reports in 2005 of two fossil skulls, a *Homo erectus* in China (Vialet, *et al*., 2005), and a *Sahelanthropus tchadensis* (Zollikofer, *et al*., 2005) in Africa, both of which suffered combinations and degrees of fracture, embeddment, and distortions due to post-depositional forces. To return the *Homo* skull to pre-depositional proportions it was treated with a global active deformation technique (Vialet, et al., 2005). The *Sahelanthropus* restoration involved matrix removal using "integrated data segmentation tools" (Zollikofer, et al., 2005), (which means the CT scan perceives and transmits enough information about non-fossil substances to set definable thresholds for variation in image presentation). Virtual disarticulation of the distorted bones into discrete fragments meant they could be counter-fitted to create continuity of anatomical features of bone and fracture lines.

Computational restoration/reconstruction requires a computer with sufficient memory and speed to run the large, complex graphics programs used to import and manipulate scan file formats and facilitate 3D assembly. Once images are converted to the file format the graphics program uses, each piece is fitted using visual clues. Each fragment on screen is recognised by a set of x, y, and z coordinates derived from a 3D measurement by scanning instruments (Zollikofer and Ponce de Leon, 2005); they are individually fitted to a 'global' set of anatomical coordinates (figure 5).

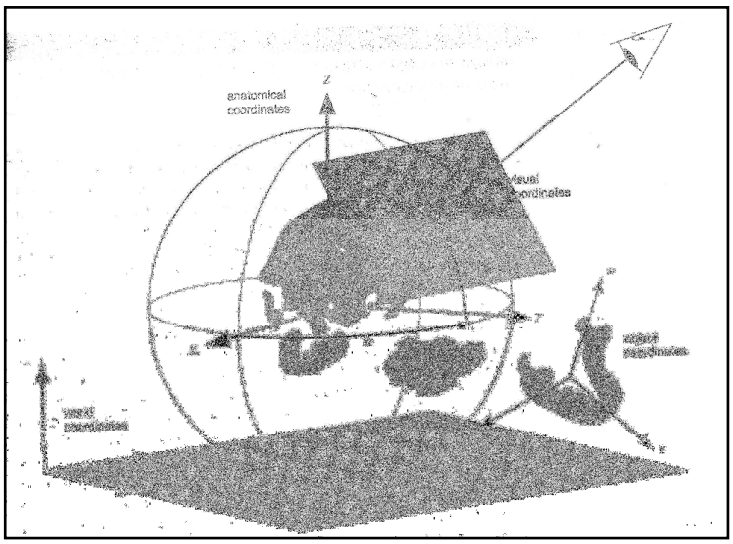

Fig 5: The x, y, and z coordinates and virtual reality; weightless, matter-less, and 6 degrees of freedom.

From: Zollikofer, C.P.E. and Ponce de Leon, M.S. (2005). Virtual Reconstruction: A Primer in Computer-Assisted Paleontology and Biomedicine.

Commands are accessed both through the keyboard and via manual control of the haptic feedback arm; 6 degrees of freedom means pieces onscreen may be freely manipulated in any direction relative to each other, and they may be made see-through at various gradients for examination of a critical edge-to-edge fit (Subke, 2005). Internal structures may be done first, last, or at any stage desired, as there are no rigid rules of assembly order in virtual reality as there are manually. As each fragment is fitted the file may be saved, or multiple files saved as progress is made, so the operator can return to a previous level of restoration if necessary. If at any time it is decided a piece is incorrectly placed, the piece may be repositioned, mirrored, or deformed to align with the particularity of the reconstruction (Subke, 2005).

Because the digital skull can be perforated by on-screen instruments, internal and external measurements are done any time during construction; multiple planes of perspective through the skull may be chosen for metric assessment at any stage in the

process. The distance between fragment pieces at fracture lines may, because of the coordinate points prescribed by the computer aided design (CAD) program which delineate every edge, be measured *en masse* for the entire skull, rendering a colour graduated scale of accuracy (Subke, 2005). Rules of parsimony apply: continuity follows standard anatomical landmarks, as it does in manual restoration; and the fabrication of mirrored image parts is based on the theory that "the left and right sides of the same individual are more similar to each other than left and right sides of any two different individuals" (Zollikofer and Ponce de Leon, 2005).

Time is an important factor: measurement and manipulation, with some degree of acclimatization and practice, are rapid and repeatable. Producing copies of 3D objects is quick because there is no repetition of processing steps or deterioration of material; once a file is saved, it may be returned to as quickly and as often as the operator wishes. Wilkinson (2005), claims a fragmented skull is more efficiently and quickly pieced together using computerised methods because support mechanisms are not required as they are in manual restoration, and that in the case of remodelling missing fragments, or mirroring bilateral fragments, computers offer a potentially significant reduction in the time it normally takes to complete those procedures by hand.

The ultimate speed of computing is dependent on the speed and size of the processors themselves. The human operator is limited by the constraints of their own hand-eye coordination, and their ability to spend long periods of time in awkward positions with scanning apparatus (if a mobile, hand held unit is used). Long periods of time at the computer terminal manoeuvring the haptic feedback arm, mouse, and keyboard are in and of themselves, physically wearing to the operator.

The initial purchase price of computerised systems and the ongoing expense of their maintenance is a disadvantage. Hardware and software upgrading is repetitious and unavoidable. Depending on the degree of the operator's tolerance for, and accord with computer systems in general, re-assembly in virtual reality may prove inefficient unless the person is thoroughly trained on the system in question. Acclimatization to the altered sense of space when using haptic feedback requires time; there is a sense of moving against a normal ordering of space and movement, a mismatch between human senses and the manner of 'doing' as dictated by program parameters. Sequences of tool use and selection of categories of tools require memorisation and constant usage to retain fluency.

Efficient use of computer-assisted methods also relies on anatomical training; a thorough grasp of the morphology of the skull is necessary (Zollikofer, *et al*., 1998). If the ability to portray adequate detail of an object is below the detection threshold of the scanning device, a degraded or incomplete image is imported into the re-assembly program. Human beings can individuate minute details of shape and texture if adequately trained and experienced, if not, there is risk of compounding any technical insufficiency of scanner and computer programs with the untrained abilities of the human director, resulting in lengthy and inaccurate renderings.

In summary, the advantages of the computerised method are considerable: freedom from gravity, adhesives, and concern for the fragility of fragments; unrestrained movement provides non-destructive measurements which are impossible in the physical counterpart; and controlled deformation using compression models limit unwanted distortion of the whole skull (Zollikofer and Ponce de Leon, 2005). Accuracy of skull restorations with computer assistance however, remain untested and reports on the

speed and general efficacy of computer systems used in this way are, as yet, not sufficiently cross-qualified. This research aims to:

(1) to scan the fragments of four skulls using a hand held laser scanner and restore them to the highest degree of accuracy possible using FreeForm Modelling computer software (a fifth set of fragments previously scanned by an automated laser scanning system will also be restored in FreeForm);

(2) quantify restoration accuracy by comparing scans of the original and restored skulls using Geomagic Qualify software;

(3) qualify restoration accuracy of the same skulls using superimposition in Photoshop; and quantify accuracy using a measuring tool in Photoshop to generate proportional measurements of differences in width, length and height;

(4) qualify the processes of computer assisted image capture and skull re-assembly in terms of time, productivity, and ease of use.

METHOD

Scanning

The FASTSCAN (Polhemus, 2007) Scorpion laser surface scanner (Polhemus, Colshester, Vermont, USA) is a handheld device utilising two cameras positioned equidistant on either side of a laser beam generator mounted on a lightweight aluminium frame wand (Park, *et al*., 2006). It requires Windows 2000 (service pack 4 or above), or Windows XP (service pack 2 or above), a USB port, a minimum of 512 MB RAM, and a 2 Ghz Intel Pentium IV or better are necessary for image processing.

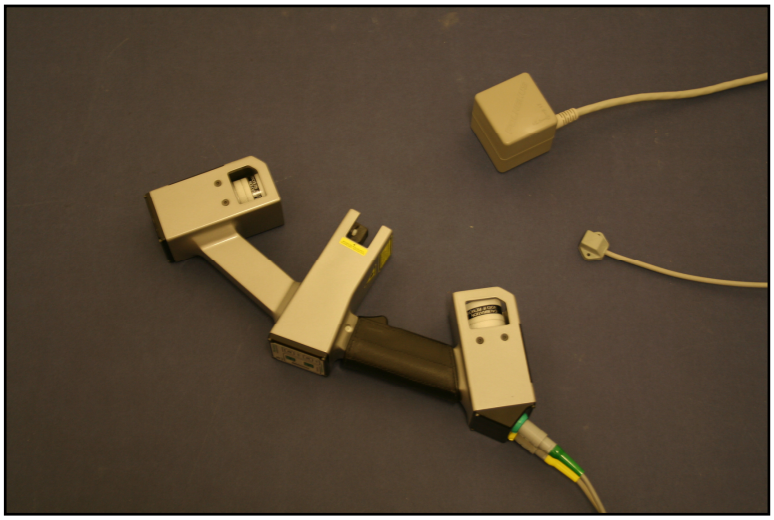

Fig 6: FASTSCAN hand held laser scanner, large and small receivers.

The processing unit records triangulations generated by a non-contact range finder, in combination with the laser projection and subsequent detection of the beam, as the means of determining the position and orientation of the finder relative to the object scanned (Polhemus, 2007). Software coordinates multiple scans (passes of the wand over the object at varying angles) using a video processor and tracker electronics, to create and transmit the 3D object image on a computer screen. Correct use of the laser

required a semi-darkened room and a surface of sufficient stability and size to support the object.

The intact cranium and mandible of four skulls were scanned separately prior to fragmentation. The pieces of each skull were then scanned after fragmentation. The way in which fragments of skulls were scanned varied: (1) some were scanned one side only, (2) or two sides (interior and exterior) against a black synthetic felt background, then combined later in image processing; (3) some were scanned through a freestanding plexiglass shelf (40 x 60 x 30 x 5 centimetres), and others (4) through clear regular glass (2.09 mm thick). Fragments smaller than approximately 20 by 20 mm or originating from an interior bone of the skull (such as the ethmoid) were not scanned. Bone fragments (especially those from the sinuses, orbits, ethmoid, and interior aspects of the sphenoid bone) which were particularly small or powdered were not included for scanning or computer restoration, (or the physical restoration of the specimens at project end).

Scanner parameters (Polhemus, 2007) were as follows: smoothing was set at 1.00, decimation at 0.50. This was the baseline - smoothing was adjusted in some instances (those changes are specified where they occur). Profile smoothing was set at low (in a range of high, medium and low), sensitivity at number 3 (in a range of 1 to 6, where 1 is equal to least sensitive and 6 is equal to most sensitive), objects were limited to 1, maximum scanning distance (from object) was 750 mm, and angle was 30 degrees. When the through-glass refraction correction was used, the refraction number was set at 1.52 mm for glass measured at 2.09 mm thickness. No refraction was set for plexiglass. The (larger) receiver (Tx), (approximately 55 mm in width, length and height), was placed as close as possible to the bone while allowing for full movement of the wand

around the bone. The wand was passed over the object the minimum number of times required to generate a complete image (Park, *et al.*, 2006). A table supported the scanner processor, the wand when not in actual use between scan movements, the felt (and the plexiglass stand) upon which the objects were placed. A laptop was positioned within easy visual and physical distance of the table, to make the screen accessible while the operator scanned.

Skull A

Skull A had previously been manually re-assembled by Professor Richard Helmer, a forensic scientist from Germany. The intact cranium was scanned on and through plexiglass; the intact mandible was scanned in two sets, once on the superior surface, and again (by turning the piece over), on the inferior surface. The two separate scans of mandible A, imported to FreeForm, were combined into one image. Fragments of skull A were scanned on black felt; either on their exterior surface only, or, when necessary, the interior and exterior surfaces were scanned and then combined. Pieces of sphenoid bone or the petrous portion of the temporal bone fell within this category.

Skull B

Skull B was not fragmented in this research. The reconstructed intact skull and fragments were scanned with a stationary automated Minolta laser (Hyperfocal, 2006). The specific procedures of those scans are unknown. Discrepancies were present in the files: although the mandible had been fractured (two pieces), no images of those fragments were evident, and duplicates of both the left and right temporal bones existed. The mandible had not been permanently glued, so the two pieces were scanned on and through regular glass and subsequently processed in FreeForm Modelling. Two large pieces which lay on either side of a smaller fragment were scanned, each with the same

fragment attached along the same fracture line. As a result the duplicated surface area (the small fragment) had to be deliberately overlapped as a result.

skull (in order done)	transected	hand held scan through glass	hand held scan through plexiglass	hand held scan 1 side	automated Scan
A			x (cranium and mandible)	x (pieces)	
C	x			x	
B	x	x (mandible fragments)			x (whole skull and fragments)
D	x		x		
E	x	x			

Table 1: Summary of skulls (transected status) and and scanning methods.

Skull C

The cranium of skull C was transected (horizontally above the orbits and occipital protuberance) for demonstration purposes prior to use in this project. The vault and the rest of the cranium were each placed separately (transected edge down) on black felt. They were scanned on the exterior surface – the vault from a superior perspective and the remaining cranium from an inferior perspective, which included 360 degrees to capture lateral, posterior, and anterior surfaces. Mandible C was scanned on two surfaces – interior and exterior – and combined in FreeForm Modelling into one piece.

Skull D

The cranium of skull D was also transected. The 'cap' and the remainder of the cranium were placed as a contiguous unit and scanned through plexiglass. The mandible was scanned in the same manner, as, after fracture, were the fragments.

Skull E

The cranium of skull E had been transected. 'Cap' and cranium were placed as one, and scanned through regular clear glass (2.09 mm thick) placed across the upturned legs of the plexiglass shelf. Glass refraction correction was set at 1.52 mm. The glass refraction settings were selected as follows: (1) the transceiver (Tx) was on the same side of the glass as the object, and (2), set on the glass next to the object.

Files

Two sets of files resulted from scanning: completed scans were saved as FASTSCAN file (.fsn) to a folder on the laptop. Information captured by the laser requires processing to make the image usable (Zollikofer and Ponce de Leon, 2005). Each file was named according to the area or part of the bone of the skull the operator felt it originated. These initial .fsn files were stored for the remainder of the length of the project.

One option for optimising sweeps compiled in a scan was chosen depending on whether it improved the image detail and reduced noise: if “register sweeps” (Polhemus, 2007) improved detail and reduced distortion it was retained, if it did not, sweeps were de-registered. Assessing improvement as a result of registering the sweeps was possible either by a visual comparison between the unregistered and registered image, or by viewing an analysis of the degree of alignment (shown in millimetres) for the image

before and after registration. The second set of files consisted of those produced by "Basic" formatting (Polhemus, 2007). Basic format was performed on each scan and the image retained as an .STL file, which may or may not have included registration of sweeps as the first stage of processing.

3D models of skulls before fracture, all fragments, and re-assembled skulls were prepared for export in FreeForm modelling. Fragment resolution was reduced to ten percent, and skull resolution to ten, twenty, or thirty percent. Professor Stephen Richmond processed the resulting images using Geomagic Qualify. He was asked to use which ever resolution possessed the highest quality (thirty percent for instance, instead of ten or twenty percent) when possible.

Skull fragmentation

Five skulls were provided from the skeletal collection in the Department of Anatomy and Forensic Anthropology at the University of Dundee. Four skulls possessed metal hardware installed for the purposes of attachment and articulation of the mandible with the cranium, or the transected vault to the cranium. This was removed with needle-nose pliers. The mandible and the cranium of four of the five skulls were placed in plastic bags individually to contain fragments and fractured by hitting them with a rolling pin. The separated cranium and mandible were set on a solid, inflexible surface and struck an average of 2-4 times.

The mandible and cranium of each skull were individually labelled A, B, C, D, and E. For example, skull A consisted of cranium A and mandible A. Fragments of each skull were kept separately in plastic zip-lock type bags labelled appropriately. Separateness

was maintained during processing and restoration.

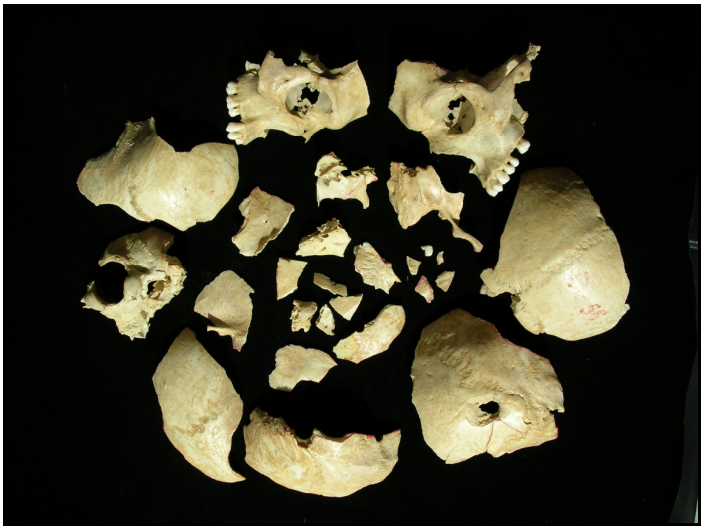

Fig 7: Skull A physical fragments.

Photograph: Amy Tillotson.

Fragments of each skull used as a physical reference during computer processes were handled with care and placed on carpet mats. Foam lined aluminium baking trays with sides to contain fragments were used for transport between work stations. The four skulls which it was necessary to restore before returning to the teaching collection from which they came, were restored with dental wax.

Computer re-assembly

.STL (stereolithography) files were imported into FreeForm Modelling (SensAble Technologies, Inc., Woburn, MA., USA), a computer software system paired with a haptic force feedback device, the PHANTOM Desktop arm (SensAble technologies, Inc.). FreeForm Modelling version 9.0 is a 32-bit edition software requiring a recommended Genie Pro 2 Vig396 computer with Windows XP Professional SP2, dual processors (Xeon 5150 2.66 Ghz), 4 GB of RAM, a Quadro FX3500 256 MB graphics card and a 1280 by 960 (or higher) display resolution (SensAble Technologies, 2007). At the time of writing a parallel port was necessary to connect the haptic arm.

The integrated system was actually run on a Viglen (Genie 945) desktop computer, using Windows XP 2002 SP2, a single Pentium processor (3 GHz), 2 GB of RAM, a Quadro FX 500/FX600/AGPSSE2 (version 1.5.3) graphics card, and a screen display resolution of 1280 by 1024 pixels.

The FreeForm Modelling software which is used for virtual 'clay' modelling, often in industrial design, is capable of performing restoration, reconstruction and construction of objects in virtual 3D (Zollikofer, *et al*., 1998; Subke, 2005). Haptic feedback is a touch-based interactive tool which enables such manipulation (Sherman and Craig, 2003; Subke and Wittke, 2005); it is often described as 'intuitive' (Taylor, 2004). The .STL files, in the process of importing, were treated in one of two ways: if “fill holes” preserved morphological detail sufficiently to render that detail useful in identification during re-assembly, then it was chosen as the mediator for transformation into FreeForm usable format; if “fill holes” command eliminated too many details (by filling in concavities for instance), “thicken” command was used instead (Polhemus, 2007). A request for thickening at minimum values resulted in a value offered automatically;

which was accepted and the file, after conversion, designated as FreeForm (.cly) in agreement with the file name chosen during scanning to ensure continuity throughout the process. Converted mandible and cranium fragment files were assigned to separate folders.

Each skull re-assembly in the FreeForm program was accompanied by a skull template, scaled to approximate the size of the skull under construction. The template was made more, less, or completely invisible on an adjustable gradient to verify developing skull conformity with template shape. An object list was created with the importing of the first fragment from the .STL files, and a small window which provides a choice of alternate views other than the main screen perspective was opened. The mandible was restored first in all skulls. Pieces were re-labelled one at a time as they were imported onto a working screen from FreeForm files. When all pieces had been imported, fitted, and checked for discrepancies, their resolution was reduced to export (as per description above) and submitted as .obj files to Geomagic Qualify (Geomagic Inc., North Carolina, USA), for quantitative comparison (Kau, *et al*., 2005; Wilkinson, *et al*., 2006).

Timing

The re-assembly time in FreeForm Modelling was recorded for each skull. The time for skull A included, in addition to the actual examination and manipulation of fragments, the combining of two scans to produce a single piece (the mandible for instance), and cleaning fragments of obvious 'noise'. It did not include the importing and conversion of .STL files into .cly format. Skulls C, D, and E differed, in that their approximate recorded assembly time *did* include the .STL file importation and conversion. It was not necessary to import the .STL files for skull B, as they were already present in the computer system. Each of those .STL files, however, required conversion to .cly FreeForm.

Training regime

Prior to this project the author had restored two skulls manually but had no experience with computer assisted restoration. Instruction on and practice with the laser scanner and FreeForm Modelling software was required. Skulls and fragments were scanned repeatedly to develop a steady 'sweeping' movement. Experimenting with laser settings yielded images for comparison; appropriate parameters were noted. Repeated use of commands and functions in FreeForm continued until reasonable confidence in the ability to manoeuvre objects in 3D was achieved; three sets of practice fragments were available for restoration rehearsal, and a day was spent using FreeForm in a facial reconstruction workshop. Guidance was available from experienced practitioners in FreeForm. These practice sessions, in addition to previous education in skeletal anatomy, formed the foundation of training. The use of tools for skull (and facial) reconstruction in FreeForm Modelling was not attempted in this research; mirror and deformation techniques are an addition to skills learned for restoration.

Measurements and statistical analysis

Shell contour deviation assessment

Analysis of accuracy was provided by Geomagic Qualfiy software. The program is reported to be “accurate to < 0.1 micrometers in length and 1/36,000 of a degree in angle" relative to a reference value (Geomagic, 2007). It compared images of the original and restored skulls, illustrating the degree of overlap between shells (exterior surfaces), by providing colour coded maps of maximum and minimum ranges of deviation in millimetres for each mandible and cranium (Kau, *et al*., 2005). The process compares shells by assessing each fractured restored surface as it corresponds to the original and determining a ‘best fit’ (alignment) for the combined fracture surfaces with that of the original object over all (Richmond, 2007). The maximum and minimum tolerances for shell to shell deviation analysis of the skulls were set by the Geomagic Qualify operator at: (+) 10.000 and 0.500 mm and (-) 10.000 and 0.500 mm. The software generates and compiles average and standard deviation figures for each set analysed.

The framework for analysing agreement between shell contour profiles of original and restored skulls was dependent on a threshold of error ensuring sufficient accuracy of a restoration if it were to support a facial reconstruction. That limit was hypothesised to be +/- 2 millimetres (Wilkinson, 2007). The limits of acceptable error in a computer 3D-DM skull re-assembly upon which a facial reconstruction can be based have not yet been established. This limit is therefore based upon the experiential knowledge and training of a recognised facial reconstruction practitioner (Wilkinson, 2007), and is used in the Department of Anatomy and Forensic Anthropology at the University of Dundee. It is conjectured that it is impossible to restore a skull using the manual method without incurring error which (at the very least) is $\leq$ +/- 1 mm (Wilkinson, 2007).

If the percentage of the contours which were less than or equal to (≤), +/- 2 mm error were 80% or better, accuracy was considered good. If the points in agreement were equal to or greater than 70% they were considered reasonable. Percentages 60% or over were acceptable; less than 60% was unacceptable (Wilkinson, 2007). Percentages of contours registering as ≤ +/- 2.0 mm error required contextual analysis for each skull individually in order to assess their usefulness in regard to potential facial reconstruction applications.

In describing and analysing the deviations classified by the incremental scale accompanying the Geomagic Qualify colour mapped images, some aggregation was employed in collating data. For instance: the category ≤ + 2.1 and ≤- 2.1 mm is coded by colour in the legend for each mapped image in Geomagic (figure 8). The ≤ +/- 2.1 mm range represented in the deviation tables gives the number of points (with percentages) on the object contained in that category – technically these points fall between +/ - 0.5 mm and ≤ +/- 2.1 mm.

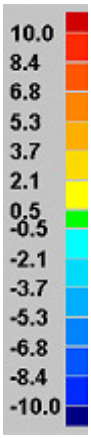

Green = greatest accuracy, or 'no significant differences'. Lightest yellow starts at + 0.5 mm error (meaning contour profile is more prominent in comparison to the original object's contours), and continues rising in + increments toward the maximum tolerance which is + 10 mm. The reverse is true on the less prominent (-) scale, where lightest blue = - 0.5 mm error, and continues toward darker blue and the maximum (negative) tolerance, which is – 10 mm error.

Fig 8: Colour scale for shell deviation maps.

In formatting summaries of results however, the author has constructed the ≤ +/- 2.1 mm category to represent all points included in the range ≤ +/- 0.5 mm *and* ≤ +/- 2.1 mm. In this way two categories are condensed into one for the purpose of simplifying an understanding of point weight in each category as they relate to levels of accuracy acceptable for facial reconstruction. The summary tables of shell deviation results (pp. 47 and 48), demonstrate the use of two further aggregate classes: ≤ +/- 5.3 mm includes values which are ≤ +/- 3.7 mm. The values which are > +/- 5.3 mm and range up to and include +/- 10 mm also encompass the increments which are ≤ +/- 6.8 mm, and ≤ +/- 8.4 mm. Values referred to in the text as being within a category by *percentage*, shall be understood to mean the combined increment values, not a value specific to one increment only.

It is noted that the baseline 'no significant difference' (light green on the colour code bar), although the most significant category in the analysis, does not have corresponding points listed in the deviation tables. Since increments on the tables only begin with ≤ +/- 0.5 mm, it appears that the green, or 'no significant difference' figures are included in ≤ +/- 0.5 mm classification in this shell comparison process.

Superimposition and proportional measurements

A secondary analysis of accuracy was performed by superimposing and comparing images in Photoshop CS2 software (version 9.0.2; Adobe Systems Incorporated). Superimpositions were performed without reference to the deviation maps or superimpositions provided by Geomagic Qualify. Skull images were saved in FreeForm as .bmp (bitmap) files, and converted in Photoshop to .jpg file format. Superimposition was achieved by using different colours to represent 'before fracture' (cream) and 'after re-assembly' (grey). 'Perspective' was engaged. Cranium images were superimposed using, (1) the superior edge of the orbits and (2), the inferior surface of the mastoid

processes. The distribution and predominance of one colour (cream or grey) in images varied in relation to the approximation of balance achieved by using the borders of these two landmarks as a guide. Mandibles were treated similarly, aligning the anterior, inferior edge of the mandible body and the oblique line of the mandible laterally.

Proportional measurements (in centimetres) of widths, lengths, and height were made in Photoshop using a line tool and a ruler tool, and the results calculated in percentages. Each figure was derived by measuring each distance twice and taking an average. Saved screen images of original and restored craniums and mandibles were positioned either side by side or one above the other and straight lines were drawn which abutted superior, inferior, lateral or medial surfaces of the original (reference) image. The restored image (test) was manoeuvred so that one of its edges (corresponding with the original) abutted the same line.

RESULTS

Geomagic Qualify shell deviations summary

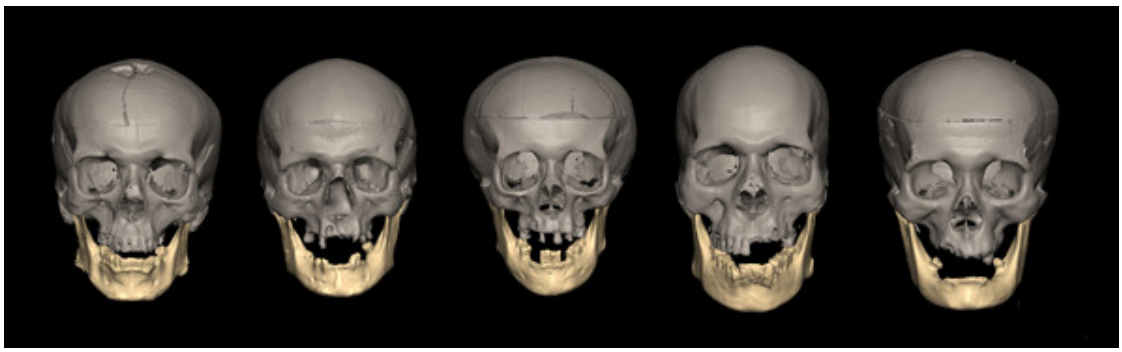

Fig 9: Skulls A-E; scan images before fracture.

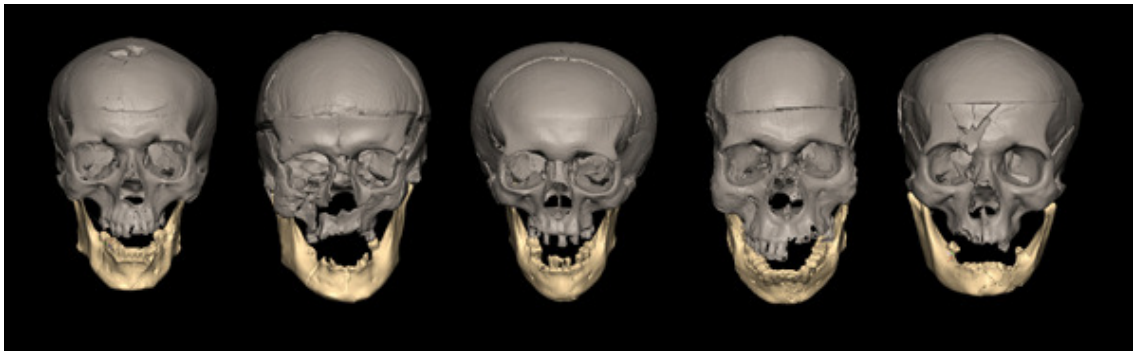

Fig 10: Skulls A-E; scan images after restoration

All restorations – both crania and mandibles - were recognisably distinct from each other and at a glance, easily paired with their corresponding original by overall shape and size. Cranial facial areas were composite maps of different error levels, but presented, in the largest part, an error which was ≤ +/- 0.5 mm to ≤ +/- 2.1 mm. Based primarily on the percentages of the restorations which were ≤ +/- 2.1 mm of error in agreement with the original, two craniums (A and D) were unacceptable at 54 and 56%. Craniums B and E were acceptable at 64%, and C reasonable at 70% (graph 1).

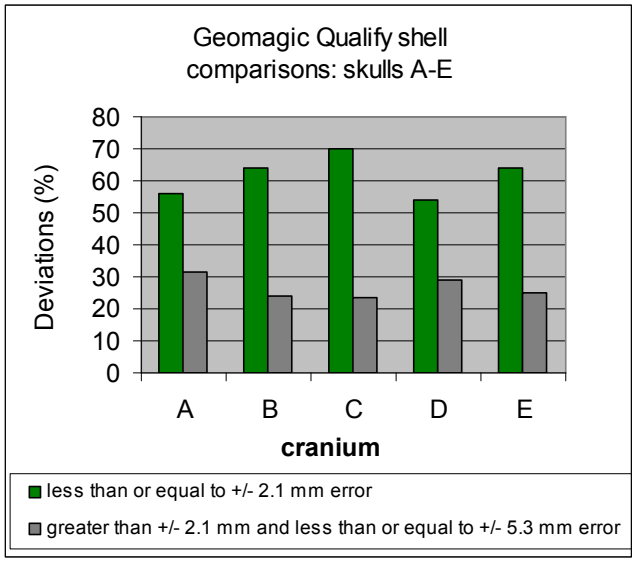

Graph 1: Cranium shell deviation totals.

Mandibles (graph 2) exhibited higher accuracy ratings (based on the same standard used for the crania): B and D had good ratings at 88 and 82%, E was reasonable at 77%, while mandibles A and C each scored 66% (acceptable). The standard deviation for crania ranged from 2.8 mm to 4mm; for mandibles the range was from 1.6 mm to 2.4 mm. All mandibles except D had 1 condyle (either head or process as well) which showed no overlap between the original and restored images. Without exception all mandible condyles demonstrated incorrect angling ('under built') toward the midline. Three restored craniums exhibited no overlap in some areas: cranium A at the palate, vertical posterior left maxilla, and the left pterygoid process; cranium B at the inferior sphenoid, maxillae, right palatine, and left temporal bone, and D at the right occipital, right temporal (mastoid), both zygomatic, and the anterior tips of the nasal bones.

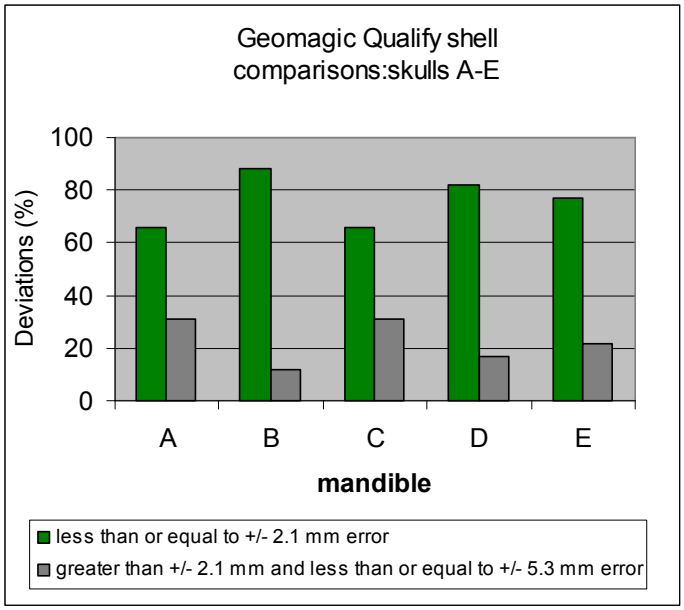

Graph 2: Mandible shell deviation totals

A summary table including all +/- mm error increments for skulls A-E is in Appendix 2. Contour Shell deviation tables for individual crania and mandibles are in Appendix 3 through Appendix 7. No values appear in the "out of maximum +/- tolerance" category in any of the tables, even though some re-assembled craniums and mandibles exhibit areas of no overlap with their original images. This is explained by the inability of the Geomagic Qualify program to recognise surfaces which are separated in distance from each other which is far beyond the values set for maximum tolerances (+/- 10 mm). Where restored mandible condyles are aggressively under built toward the midline, the lateral surface of the restored condyle may partially overlap the medial surface of the original condyle, and the lateral surface of the restored condyle may be so far from the lateral surface of the original condyle as to make the overlap detection function incapable of registering an extreme range in condyle dimensions. The portions of original and restored images positioned relative to each other in this way are 'unmappable'. In the text this is described as "no overlap" instead of as "out of maximum +/- tolerance" in order to avoid confusion with the labelling and categories of the deviation tables.

Superimposition and comparison summary

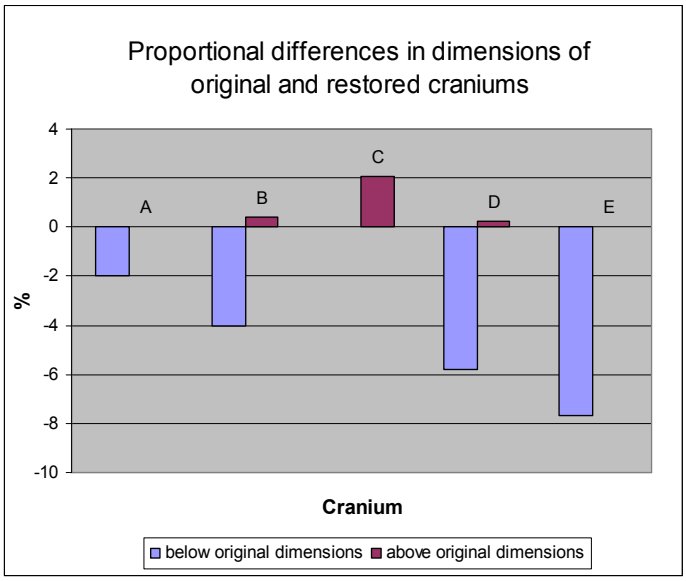

Graph 3: Summary of cranium measurements.

General agreement exists between the superimposition/proportional measurement comparisons and shell deviation results for the five skulls: restored crania A and C and mandible D and B were the best in order in terms of measurement differences; restored cranium C and mandible B and D (reverse order to the measurement results) were first or second in the deviation scores.

All of the crania appear 'under built', (including cranium C despite the misleading percentage in graph 3) – which means the greater portion of proportional measurements in Photoshop showed the restored images to be less prominent than the original, and in superimposition, restored craniums appeared smaller than original images. Best fit occurred through the facial regions at the supraorbital and infraorbital margins, at the zygomatic bones, as well as the frontal processes and anterior bodies of the maxillae. Proportional height measurements of restored crania were closest to the original dimensions, and length the farthest.

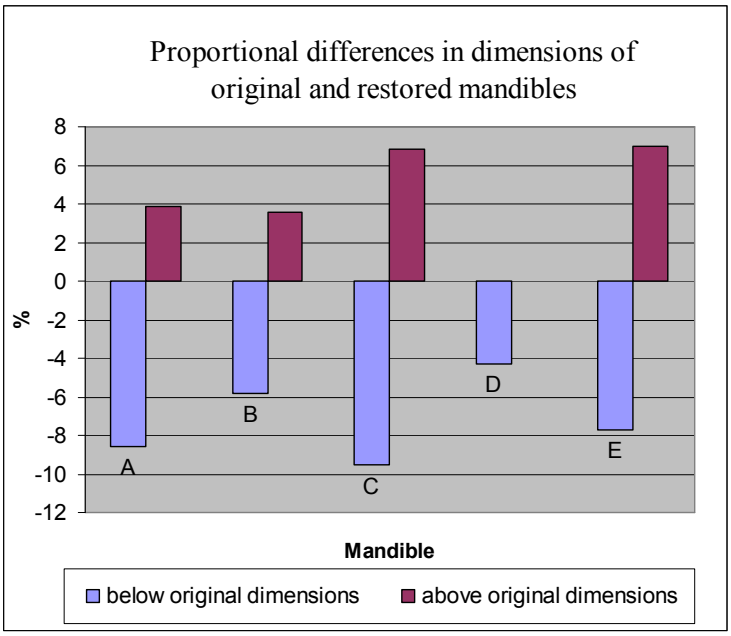

Graph 4: Summary of mandible measurements.

All restored mandibles exhibited less prominence than the originals, although in terms of proportional measurements, a more equal balance between less and more prominent differences than that in the craniums was evident. Width, then length and height were farthest from the original image dimensions. Combined proportional differences were larger in the mandible set than in the crania. All mandible condyles appeared to angle incorrectly toward the midline, both in proportional comparison measurement and in superimposition. The anterior mandible body appeared to be the best fit in superimposition.

Restoration time

The approximate time taken to re-assemble a skull using computer assistance ranged from 60 hours for the first skull (A), to 6 hours for the last skull (E). The number of fragments resulting from fracture ranged from 17 (skull C) to 35 (skull E). The skulls with the fastest restoration time, at 6.5 and 6 hours (skulls D and E), also had a higher number of fragments - 34 and 35 pieces respectively.

skulls (in order of Completion)	**pieces**	**time** (approximate hours)
A	30	50
C	17	20
B	28	25
D	34	6.5
E	35	6

Table 2: Fragments and completion time; skulls A – E

Shell deviation maps/table/graphs: skull A

Cranium A

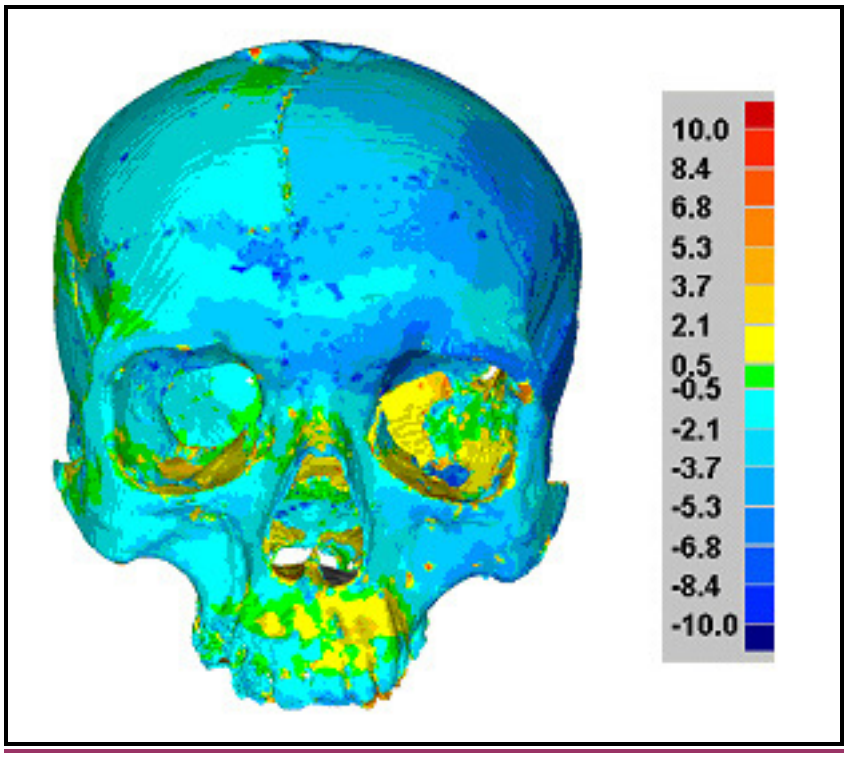

Fig 11: Cranium A anterior.

Green = no significant difference (mm);
lightest yellow = less than or equal to + 0.5 mm error;
lightest blue = less than or equal to – 0.5 mm error

560,927 data points were evaluated on cranium A. Areas demonstrating no significant difference (mm) were present in disparate patches on the anterior maxillae, the superior edges of the nasal opening, the right temporal area, the right parietal and upper right occipital bones and inferiorly along the sphenotemporal and temporooccipital articulations. The cranium is predominantly 'under built'. The right side (excepting a prominence of ≤ + 0.5 mm on the right parietal bone), demonstrates error mostly in the ≤ - 0.5 mm to ≤ - 2.1 mm range. The left vault is more severely affected, exhibiting error ranging from ≤ - 5.3 to ≤ -8.4 mm (increasingly less prominent).

The total amount of the restored cranium shell less than or equal to (≤), +/- 2.1 mm error

was 56%. Of that total, 29% was less prominent (≤ -2.1 mm) in relation to the original cranium, and 27.5% was more prominent (≤ +2.1 mm). 31.5% of the remaining contours expressed an error ≤ +/- 5.3 mm and 12% was greater than +/- 5.3 mm error. The palate and posterior vertical left portion of the left maxilla, and the left pterygoid process showed no overlap. The standard deviation was 4 mm and the variance was 16 mm.

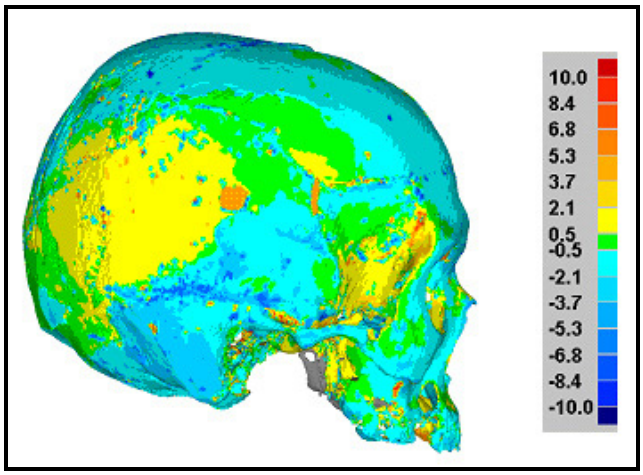

Fig 12: Cranium A lateral right.

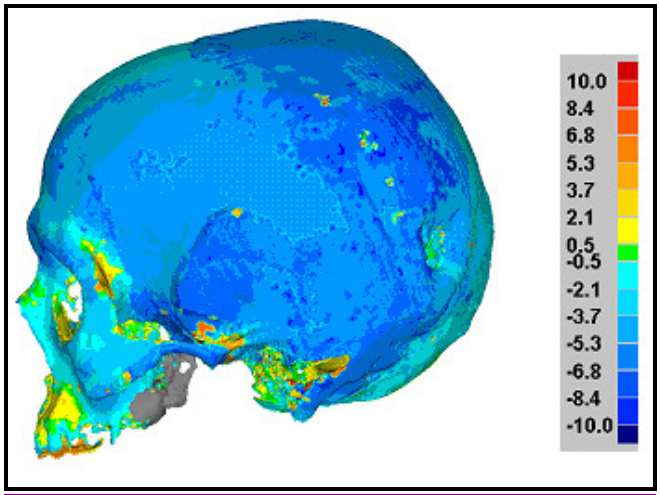

Fig 13: Cranium A lateral left.

Mandible A

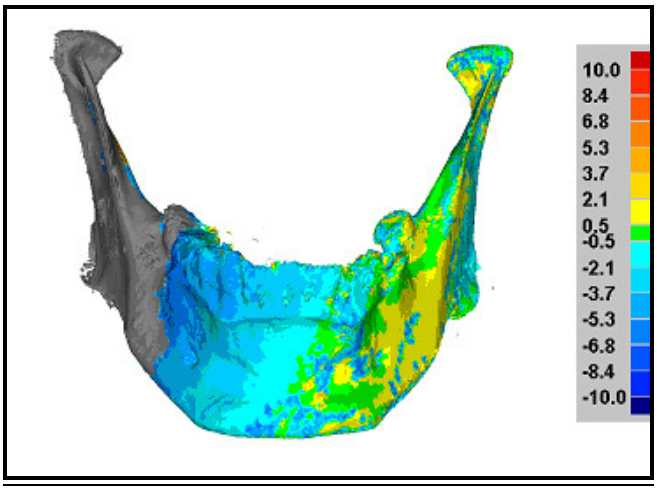

Fig 14: Mandible A anterior.

Green = no significant difference (mm);
lightest yellow = less than or equal to + 0.5 mm error;
lightest blue = less than or equal to – 0.5 mm error

146,726 data points were evaluated on mandible A. The right condyle and a portion of the right ramus (laterally and medially), show no overlap between the original and the restoration. The inferior oblique line, portions of the anterior and left ramus and the head of the left condyle show no significant differences, while the remainder of the left side, anterior and interior, and the lateral and medial surface of the left condyle demonstrate error ≤ +/- 2.1 mm.

The total amount of the restored mandible shell profile which was less than or equal to (≤) +/- 2.1 mm error was 66%. Of that total, 39% was less prominent (≤ - 2.3 mm), and 27% was more prominent (≤ + 2.3 mm) in relation to the original mandible. 31% of the remaining contours demonstrated an error ≤ +/- 5.3 mm while 3% was less prominent (≤ - 8.4 mm error). The standard deviation was 2.4 and the variance 5.8 mm

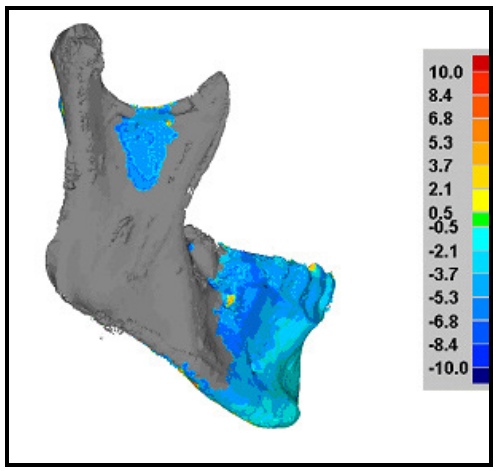

Fig 15: Mandible A lateral right.

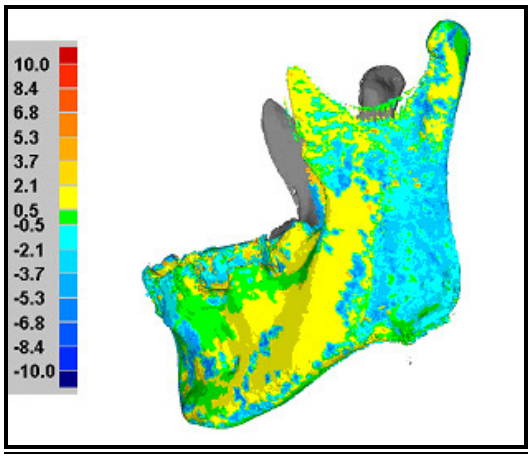

Fig 16 : Mandible A lateral left.

Superimposition and comparison: Skull A

Cranium A.

In superimposition the vertical height and width of the original and the restored face are the same. The vertex, the superior border of the right orbit, and the inferior edge of the right upper incisor align horizontally. Proportional measurements confirm this (0% difference in width and height). Cranial length of restoration is insufficient (1.95% less than original). In total, 1.95% of the restored cranium A measured greater than or less than the original dimensions.

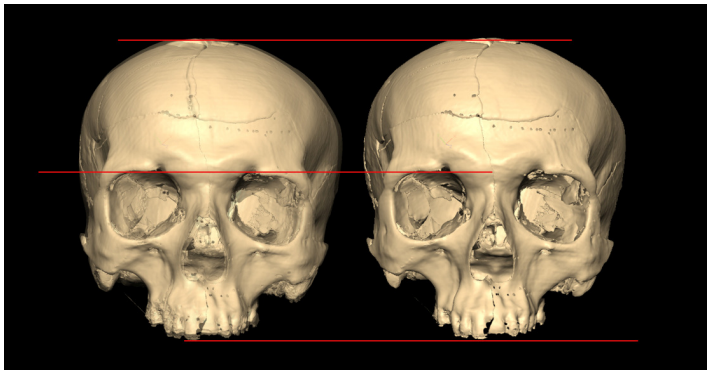

Fig 17: Cranium A -comparison anterior.

Right hand position = after restoration

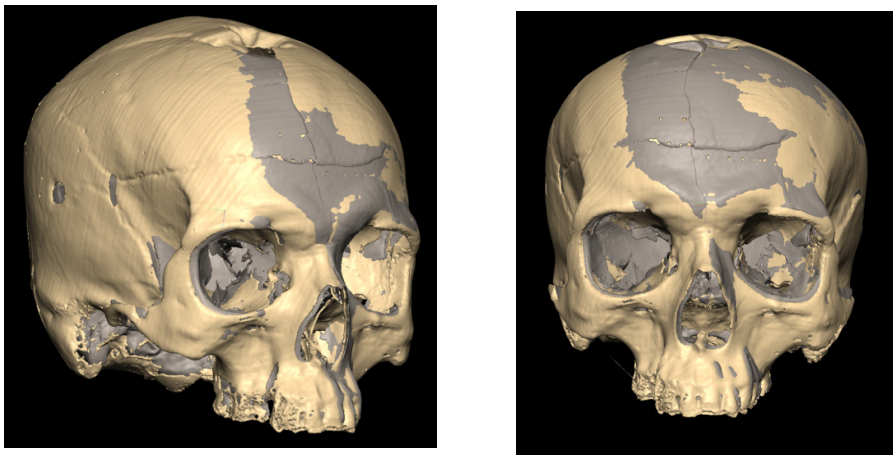

Fig 18: Cranium A - superimposition anterior and oblique.

Cream = before restoration, grey = after restoration

Mandible A.

Restored mandible A is narrower in breadth than the original (4.69% less), and 3.83% greater in length. The height of the restored rami was 3.87% less than the original. In total, 12.39% measured greater than or less than the original mandible. In superimposition, the restored condyles appear incorrectly angled toward the midline.

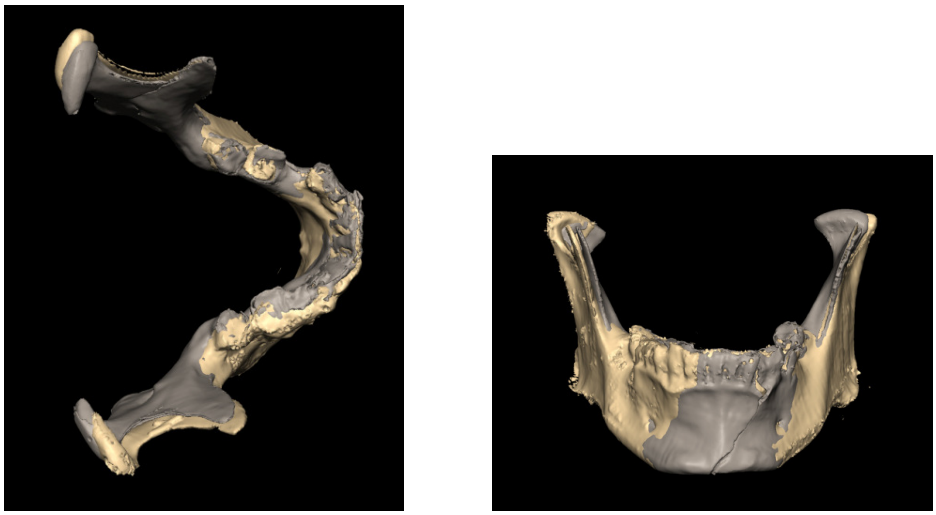

Fig 19: Mandible A - superimposition superior and anterior.

Cream = before restoration, grey = after restoration.

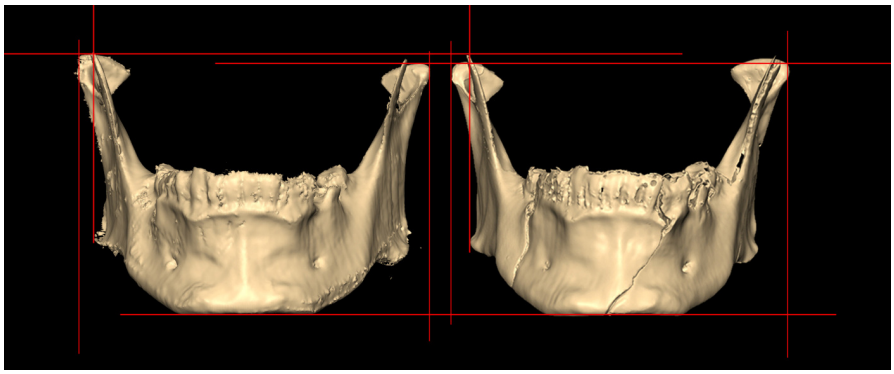

Fig 20: Mandible A - comparison anterior.

Right hand position = after restoration.

Shell deviation maps/tables/graphs: skull B

Cranium B.

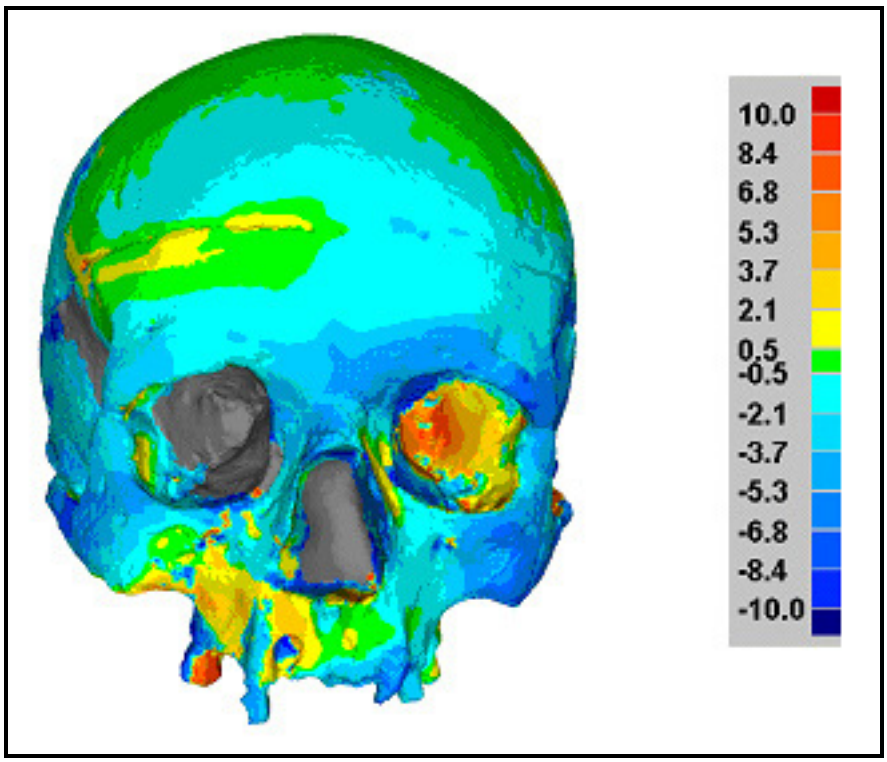

Fig 21: Cranium B anterior.

Green = no significant difference (mm);
lightest yellow = less than or equal to + 0.5 mm error;
lightest blue = less than or equal to – 0.5 mm error

148,270 data points were evaluated on cranium B. The greatest accuracy (no significant differences) was reflected predominantly in the frontal and parietal bones of the vault and in the most anterior maxillae. The inferior zygomatic bone (body and arch), the zygomatic process of the frontal bone, the postero-inferior temporal bone, and the postero-inferior occipital bone - all on the left side - were least accurate: up to ≤ - 8.4 mm deviation (less prominent).

The total amount of the restored cranium shell ≤ +/- 2.1 mm error was 63%. Of that total, 53% was less prominent (≤ - 2.1 mm) and 10.3% was more prominent (≤ + 2.1 mm) in relation to the original cranium. 25% of the contours remaining expressed an

error ≤ +/- 5.3 mm and 12% was > +/- 5.3 mm error. The inferior surface of the sphenoid, part of the posterior maxillae bodies, the right palatine bone, some of the most inferior left temporal bone (and mastoid) demonstrate that there was no discernable overlap between these portions of the original and restored cranium. The standard deviation was 2.8mm and the variation, 7.8 mm.

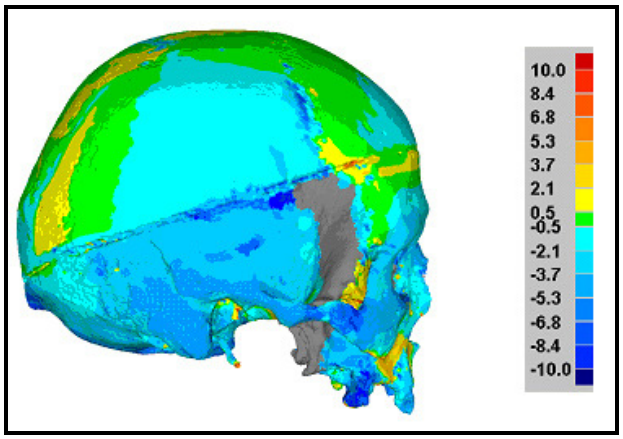

Fig 22: Cranium B lateral right.

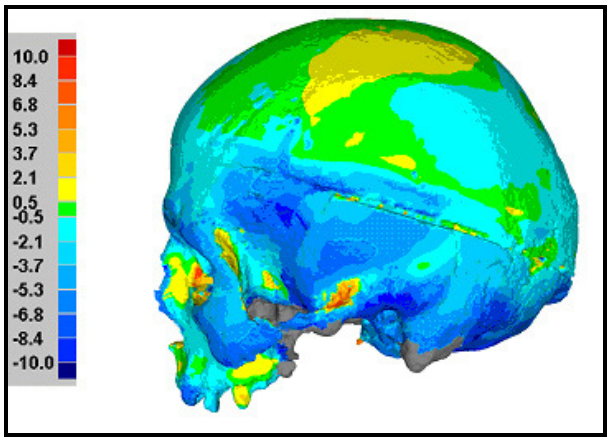

Figure 23: Cranium B lateral left.

Mandible B

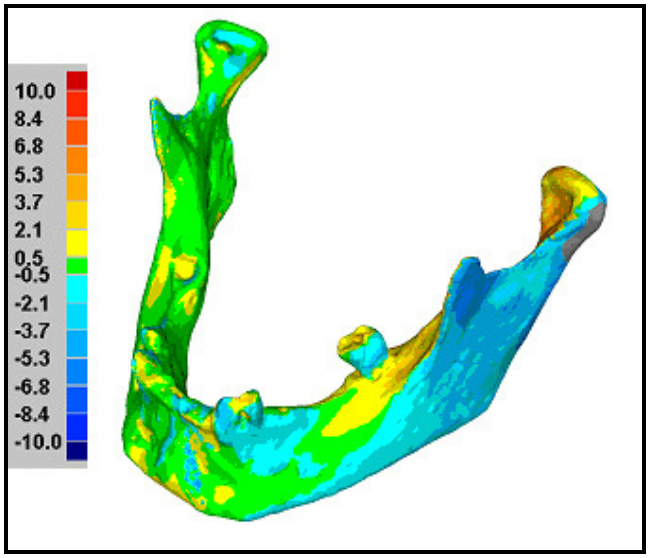

Fig 24: Mandible B anterior oblique left.

Green = no significant difference (mm);
lightest yellow = less than or equal to + 0.5 mm berror;
lightest blue = less than or equal to – 0.5 mm error

41,905 data points were evaluated on mandible B. The anterior and anteroinferior edge, the right lateral portion of the mandible body , the right ramus and right condylar process (excepting the lateral surface at the tip of the coronoid process), and the interior surface of the mandible body display no significant differences. The left condyle is less in agreement: it is more prominent on the medial surface of the upper portion of the left ramus (≤ +3.7 mm error), while the left coronoid process and the lateral ramus is less prominent (≤ - 3.7 mm error) – the restored mandible appears insufficienct in width.

The total amount of the restored mandible shell ≤ +/- 2.1 mm error was 88%. Of that total, 66% was less prominent (≤ - 2.1 mm) and 22% was more prominent (≤ + 2.1 mm) in relation to the original mandible. 12% of the remaining contours profile was ≤ +/- 5.3 mm error. Less than 1% error was ≥ - 6.8 mm deviation. The lateral surface of the left condylar process indicates that no contours of the original and restored mandible

overlapped at this location. The standard deviation was 1.6 mm and the variation was 2.6 mm.

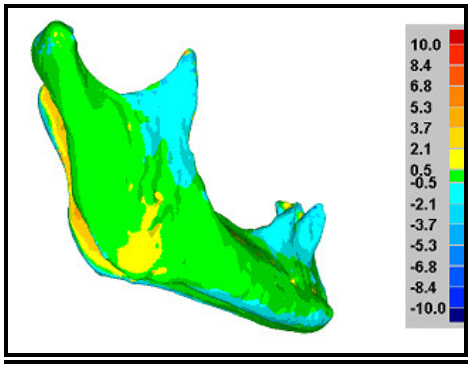

Fig 25: Mandible B lateral right.

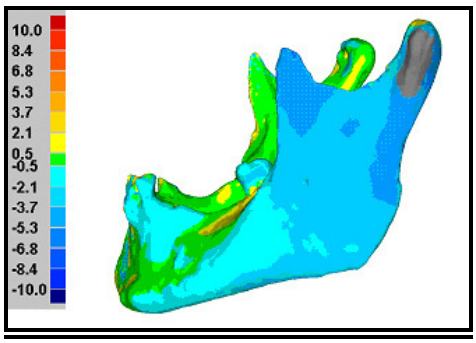

Fig 26: Mandible B lateral left.

Superimposition and comparison: Skull B

Cranium B

The closest agreement in vertical proportions was in the height of the face (restoration is 0.38% greater than the original); cranial width was less than the original (2.39%), when measured at the widest point laterally on the parietal bones, and length was less by 1.62%. The total amount of the re-assembled cranium which measured greater than or less than the original was 4.39%. In superimposition, the right maxilla, right zygomatic and the frontal bone (bilaterally) were in closest approximation with the original.

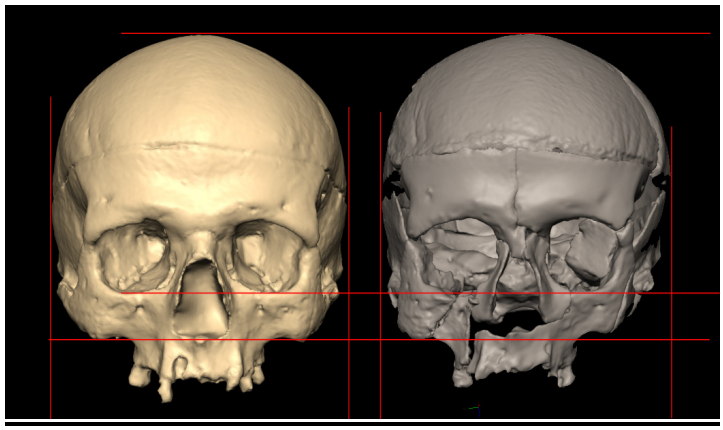

Fig 27: Cranium B - comparison anterior.

Right hand position = after restoration

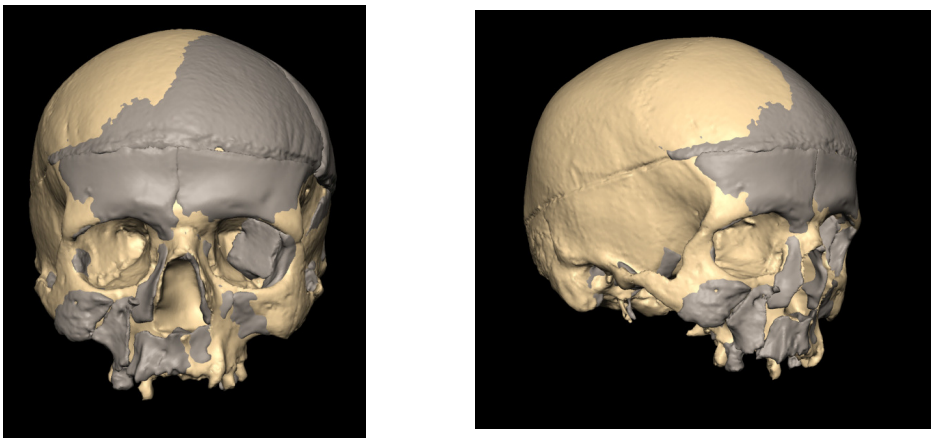

Fig 28: Cranium B - superimposition anterior and oblique right.

Cream = before restoration; grey = after restoration

Mandible B

9.43% of re-assembled mandible B measured greater than or less than the dimensions of the original mandible. Restored condyle width was less than the original (3. 46%), as was height (2.37%). Length of the body was greater after restoration (3.60%). The condyle angles appear incorrect in superimposition. The height of the anterior body at the midline was in close approximation to the original.

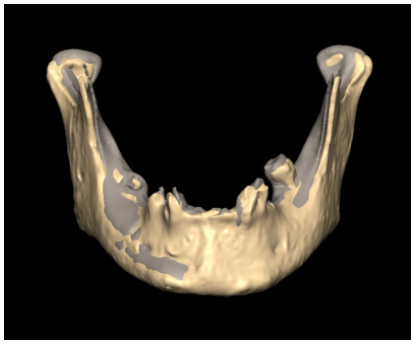

Fig 29: Mandible B - superimposition anterior.

Cream = before restoration; grey = after restoration

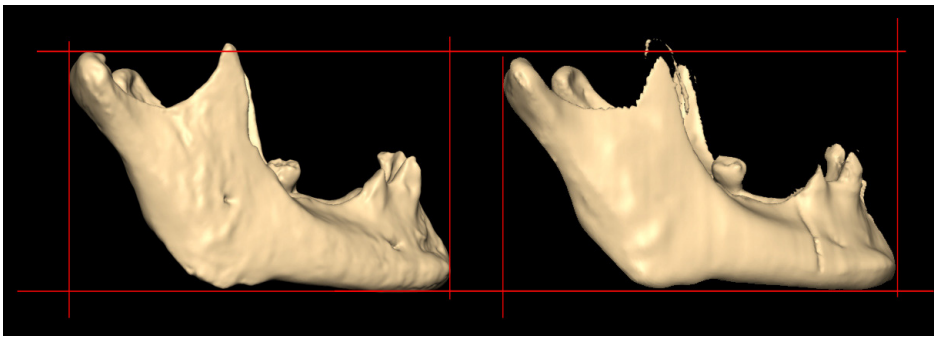

Fig 30: Mandible B - comparison lateral.

Right hand position = after restoration

Shell deviation maps/tables/graphs: skull C

Cranium C

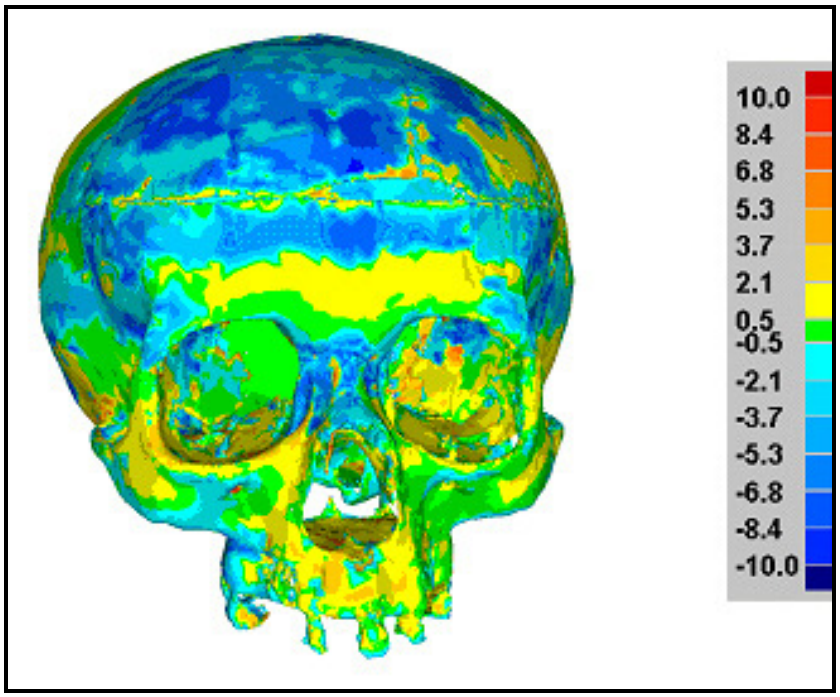

Fig 31: Cranium C anterior.

Green = no significant difference (mm);
lightest yellow = less than or equal to + 0.5 mm error;
lightest blue = less than or equal to – 0.5 mm error

537, 383 data points were evaluated on cranium C. The superior and medial edges of both eye orbits, the frontal process of both zygomatics, most of the left maxilla, the left zygomatic, the posterior occipital bone, and both parietal bones demonstrate mostly discontinuos patches of no significant difference (as error) between the restored and original cranium. Anterior sections of the maxillae, the upper right maxilla, right zygomatic, right mastoid, central lateral area of both temporal bones, a horseshoe shaped section of the upper vault, and a horizontal band through the lower forehead are more, rather than less prominent; Areas less prominent (between $\leq$ - 6.8 and $\leq$ -8.4 mm error) include the anterior and superior frontal bone, the sagittal and lambdoidal suture lines, the nasal bones, and scattered areas on the left and right lateral walls of the greater wings of the sphenoid.

The total amount of the restored cranium shell ≤ +/- 2.1 mm error was 71%. Of that total, 42% was less prominent (≤ - 2.1 mm), and 29% was more prominent (≤ + 2.1 mm) in relation to the original cranium. 23% of the profile remaining was ≤ +/- 5.3 mm error, and 6% was > +/- 5.3 mm error. No part of the cranium exhibited error > +/- 10 mm. The standard deviation was 2.8 mm, and the variance therefore was 7.84 mm.

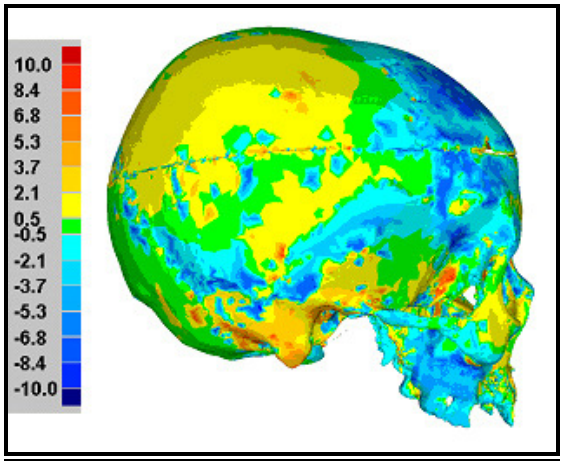

Fig 32: Cranium C lateral right.

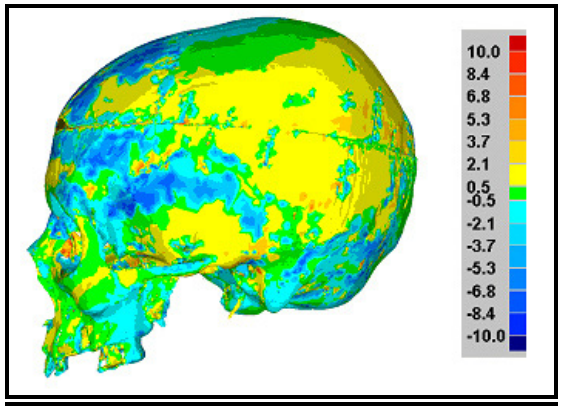

Fig 33: Cranium C lateral left.

Mandible C

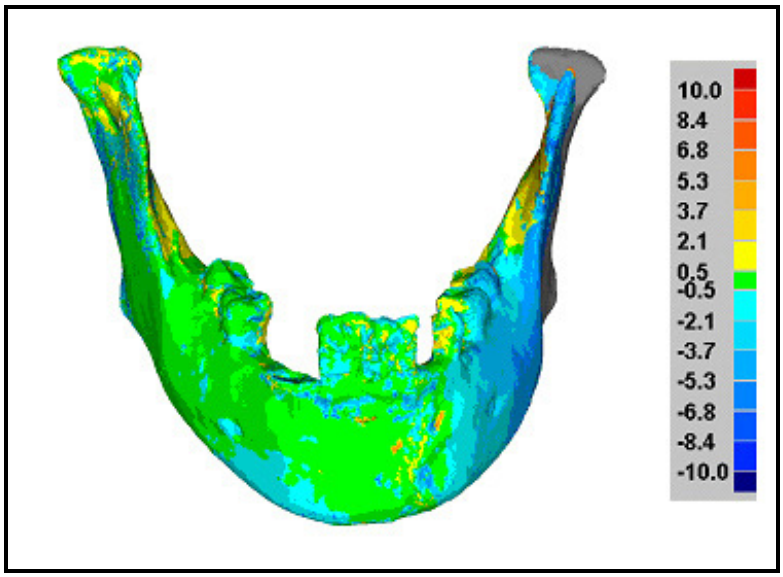

Fig 34: Mandible C anterior.

Green = no significant difference (mm);
lightest yellow = less than or equal to + 0.5 mm error;
lightest blue = less than or equal to – 0.5 mm error

85,267 data points were evaluated on mandible C. The anterior and latera/medial right body, as well as the medial ramus and head of the right condyle showed no signifcant differences between the original and restored mandible. Patches of decreasing prominence (≤ - 2.1 mm to ≤ - 3.7 mm error) appeared in the posterior (interior) midline of the body, the lateral upper portion of the left ramus and part of the medial surface of the left condlyle.

The total amount of the restored mandible shell ≤ +/- 2.1 mm error was 66%. Of that total, 42 % was less prominent (≤ -2.2 mm) and 23% was more prominent (≤ + 2.1 mm in relation to the original mandible. 31% of the remaining contours were ≤ +/- 5.3 mm while the last 3% was ≤ - 6.8 mm error. The left lateral surface, from gonial angle to condyle head, and the vertical posterior edge of the left condylar process exhibited no overlap between those restored and original areas. The medial (interior) surface of the

left oblique ramus and condyle were the most prominent (≤ + 5.3 mm error). The standard deviation was 2.6 mm and the variance therefore was 6.8 mm.

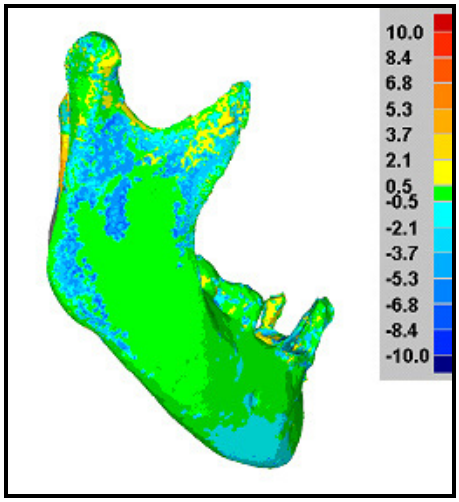

Figure 35: Mandible C lateral right

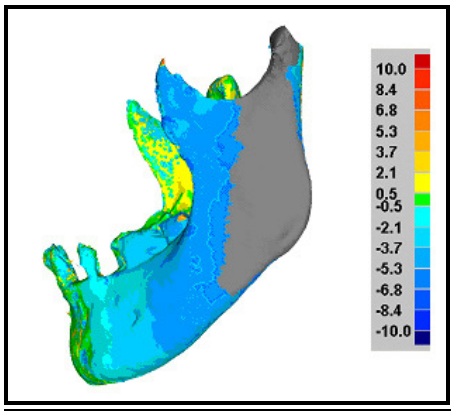

Figure 36: Mandible C lateral left.

.

Superimposition and comparison: Skull C

Cranium C

Cranium's C total of restored area which (in combination) measured greater than or less than the original dimensions was 2.04%. Those differences included a greater width (1.08%), and height (0.96%). There was no discernable difference in cranial length (0%), which is partially supported by the appearance of a close alignment between the superior and inferior orbital edges and the inferior surface of the right mastoid in superimposition.

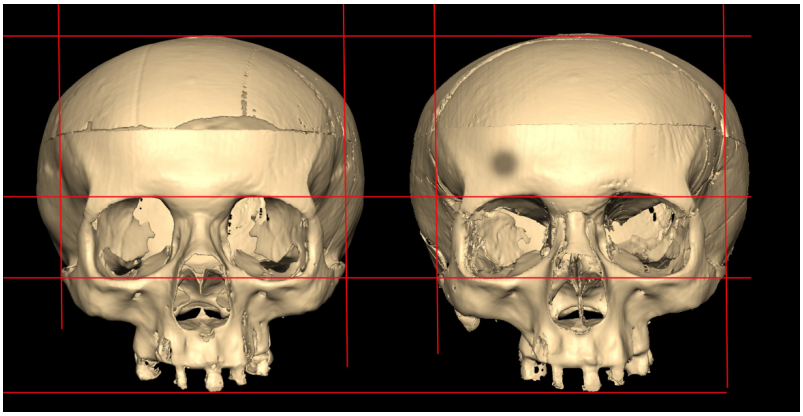

Fig 37: Cranium C - comparison anterior.

Right hand position = after restoration

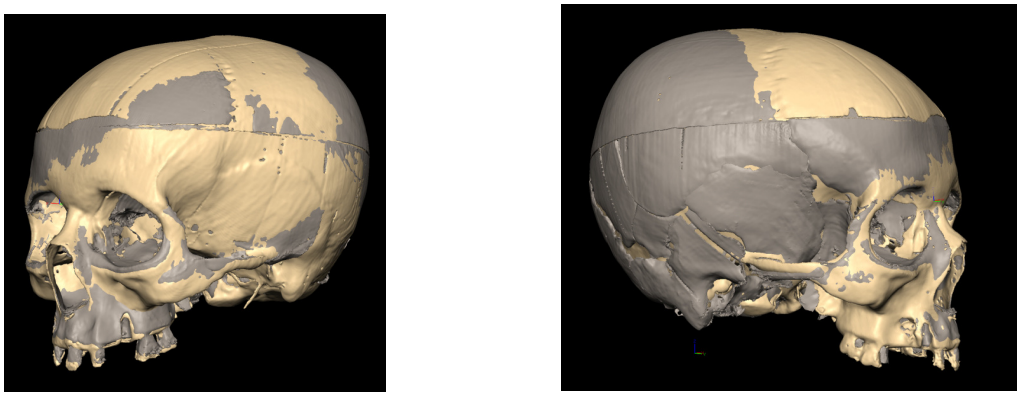

Fig 38: Cranium C - superimposition left and right oblique

Cream = before restoration, grey = after restoration

Mandible C

Restored mandible C had a total of 16.37% which measured greater than or less than the original dimensions. Width (6.34%) and height (3.17%) were both less in restoration than in the original. Length was 6.86% greater. In superimposition, the oblique processes of the body appear angled incorrectly toward the midline.

Fig 39:Mandible C - superimposition posteroinferior.

Cream = before restoration, grey = after restoration

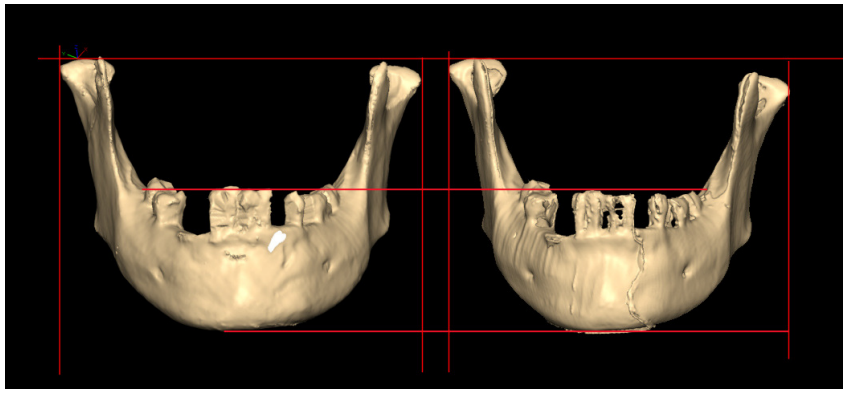

Fig 40: Mandible C - comparison anterior.

Right hand position = after restoration

Shell deviation maps/tables/graphs: skull D

Cranium D

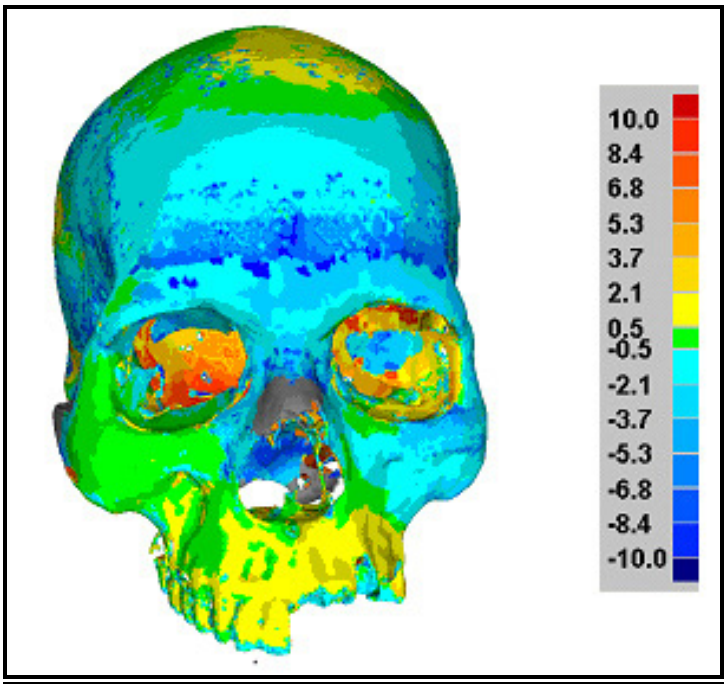

Fig 41: Cranium D anterior.

Green = no significant difference (mm);
lightest yellow = less than or equal to + 0.5 mm error;
lightest blue = less than or equal to – 0.5 mm error

1,020,236 data points were evaluated on cranium D. Areas demonstrating no significant difference between the restored and original cranium were the right upper and lateral maxilla, portions of the anterior and lateral left maxilla, the right zygomatic, and the superior, right lateral cranial vault. The most anterior sections of both maxillae and large patches (anterior to posterior) at the superior vault were more prominent ($\leq$ + 0.5 mm to $\leq$ + 2.1 mm error). Sections of the left and right greater wings of the sphenoid (visible in the back of the eye orbits), reached the upper ranges of prominence ($\leq$ + 5.3 mm to $\leq$ + 8.4 mm).

A horizontal band across the forehead was less prominent, in the range of $\leq$ - 5.3 to $\leq$ -

8.4 mm error, as was the inferior occipital bone at the midline. The right inferior and the posterior occipital, the right inferior temporal bone, both zygomatic archs, the right mastoid, and the most anterior tips of the nasal bones demonstrated no overlap between the restored and original cranium. The total amount of the restored cranium shell ≤ +/- 2.1 mm error was 54%. Of that total, 28% was less prominent (≤ - 2.1 mm), and 26% was more prominent (≤ + 2.1 mm) in relation to the original cranium. 29% of the remaining shell was ≤ +/- 5.3 mm and 17% was ≤ +/- 10.00 mm error. The standard deviation was 4 mm and the variance 16.8 mm.

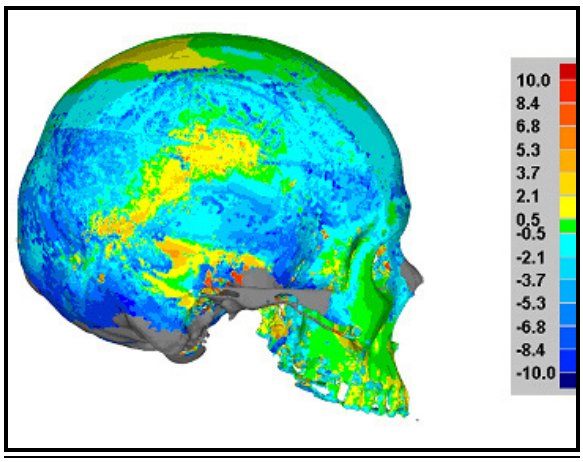

Fig 42: Cranium D lateral right.

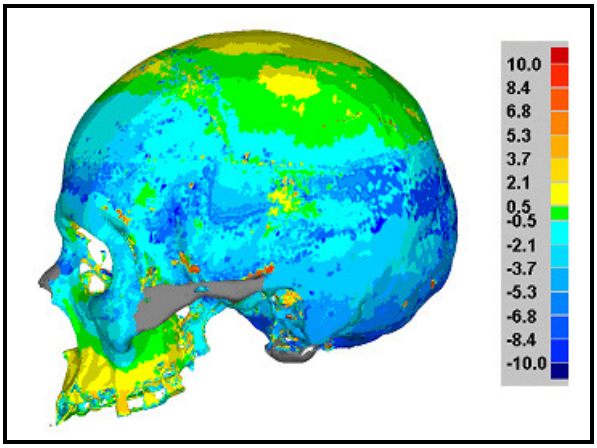

Fig 43: Cranium D lateral left.

Mandible D

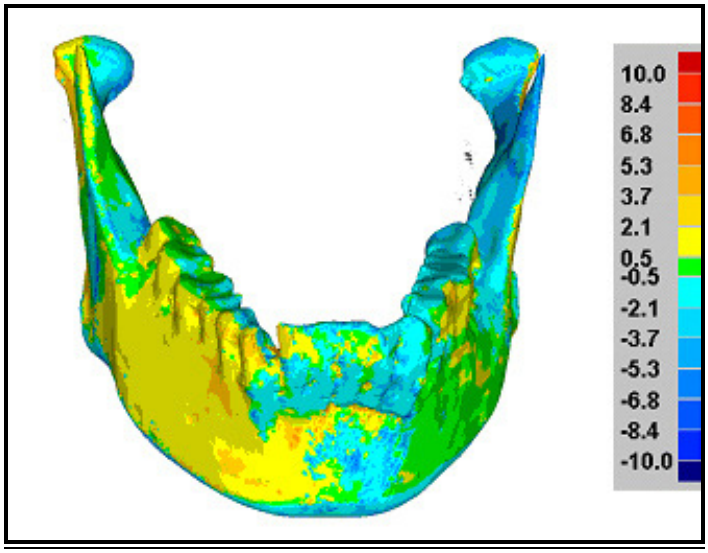

Fig 44:Mandible D anterior.

Green = no significant difference (mm);
lightest yellow = less than or equal to + 0.5 mm error;
lightest blue = less than or equal to – 0.5 mm error

186,879 data points were evaluated on mandible D. The lateral right ramus and posterolateral right condylar porcess were more prominent (≤ +0.5 mm to ≤ + 2.1 mm); the left side of the mandible demonstrated no significant differences through the anterior, oblique body, but was more prominent (≤ + 2.1 mm) on the lateral surface of the left condylar process. Both condyle heads, the inferior oblique lines, and medial surface of the condylar processes were less prominent (≤ -0.5 mm to ≤ - 5.3 mm error), the increments forming a mixed landcape of error.

The total amount of the restored mandible shell which was ≤ +/- 2.1 mm error was 82%. Of that total, 50% was less prominent (≤ - 2.1 mm) and 32% was more prominent (≤ + 2.1 mm) in relation to the oringinal mandible. 17% of the remaining contours were ≤ +/- 5.3 mm and ¾ of a final 1% was ≤ - 6.8 mm error. No part exhibited error > +/- 10 mm. The standard deviation was 2 mm and the variance 4 mm.

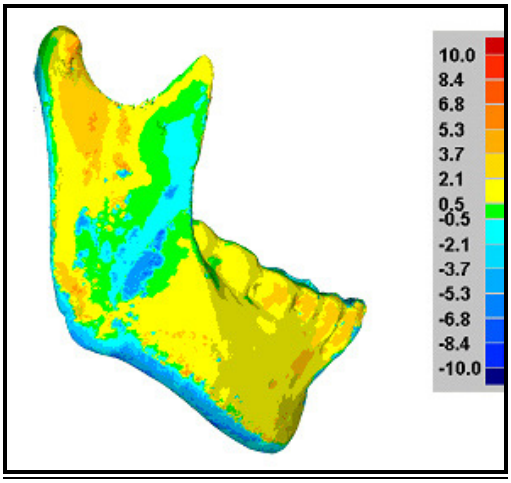

Fig 45: Mandible D lateral right

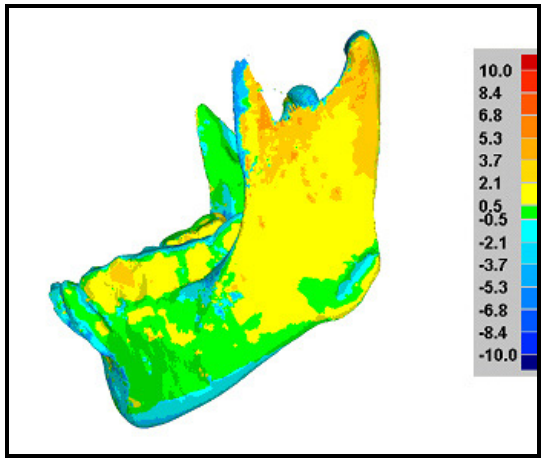

Fig 46: Mandible D lateral left.

Superimposition and comparison: Skull D

Cranium D

Re-assembled, cranium D had the fourth highest total percentage of measured differences - 6.03% of the restoration was less in width (1.32%) and in length (4.46%), and minimally greater in height (0.25%). Superimposition demonstrates a close approximation of the left maxilla, and the inferior edge of the left orbit in the restored cranium to the original.

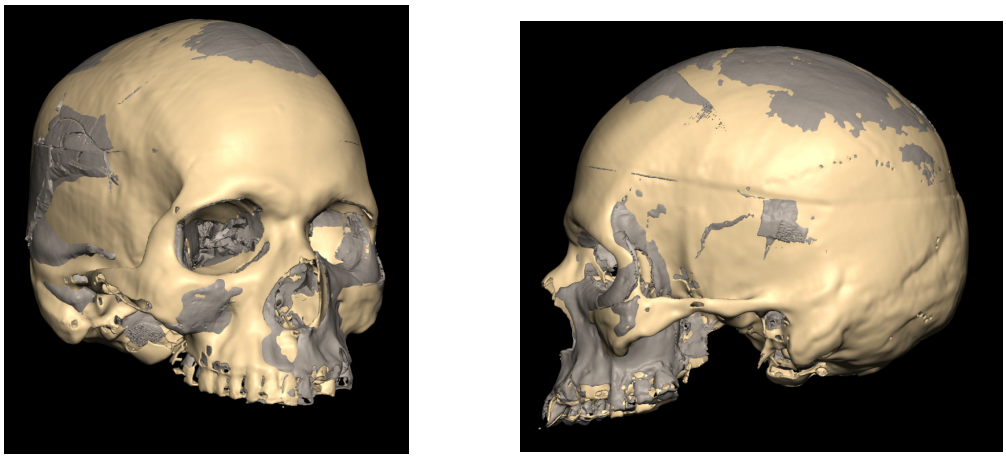

Fig 47: Cranium D - superimposition oblique right and lateral left.

Cream = before restoration; grey = after restoration

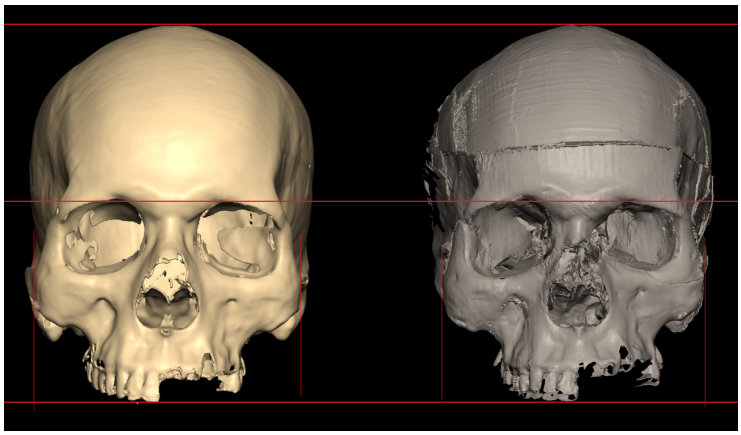

Fig 48: Cranium D - comparison anterior.

Right hand position = after restoration

Mandible D

In contrast to the cranium, mandible D exhibited the best score (4.28%), for the total restored dimensions which were greater than or less than the original. Less in length (3.94%), and height (0.34%), it was ambiguous in width. In superimposition, restored intercondylar width appeared less than that of the original (figure 55); but the measured intergonial angle width (0% difference) ,upon which the comparison measurement was based in this instance, suggests a good approximation (figure 56).

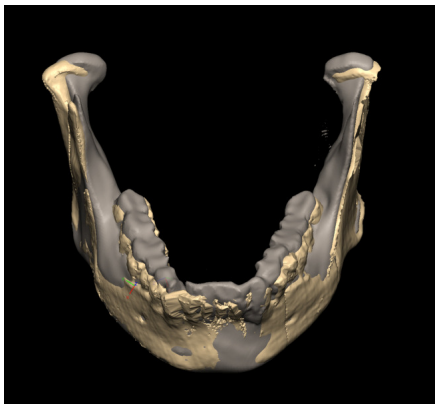

Fig 49:Mandible D - superimposition anterior.

.

Cream = before restoration; grey = after restoration

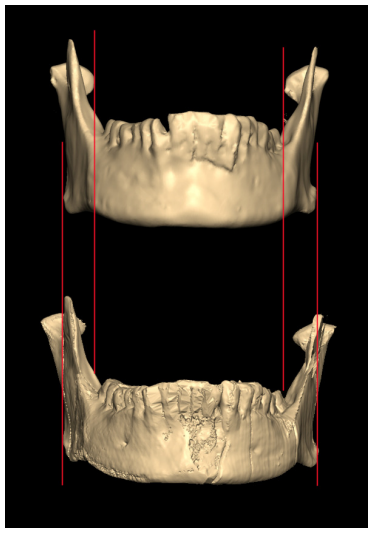

Fig 50: Mandible D - comparison anterior.

Bottom position = after restoration

Shell deviation maps/tables/graphs: skull E

Cranium E

459, 073 data points were evaluated on cranium E. 64% of the points were ≤ +/- 2.1 mm error. Distribution of the contours included in this category (particularly those of no significant difference), were dispersed primarily throughout the middle 1/3 facial area at the orbit edges, the left maxilla, both zygomatics, and in bilateral patches descending inferiorly from the temporal line to include the inferior surface of both zygomatic arches. The anterior dome of the forehead was included in this range, as were the upper palate and portions of the inferior temporal bones. The worst accuracy of least prominence (≤ -5.3 mm to ≤ - 6.8 mm) was restricted to the left and mid-posterior cranial vault and a patch superior and medial to the right orbit. The medial posterior walls of both orbits registered in the range of ≤ + 5.3 mm to ≤ + 8.4 mm error (greater prominence).

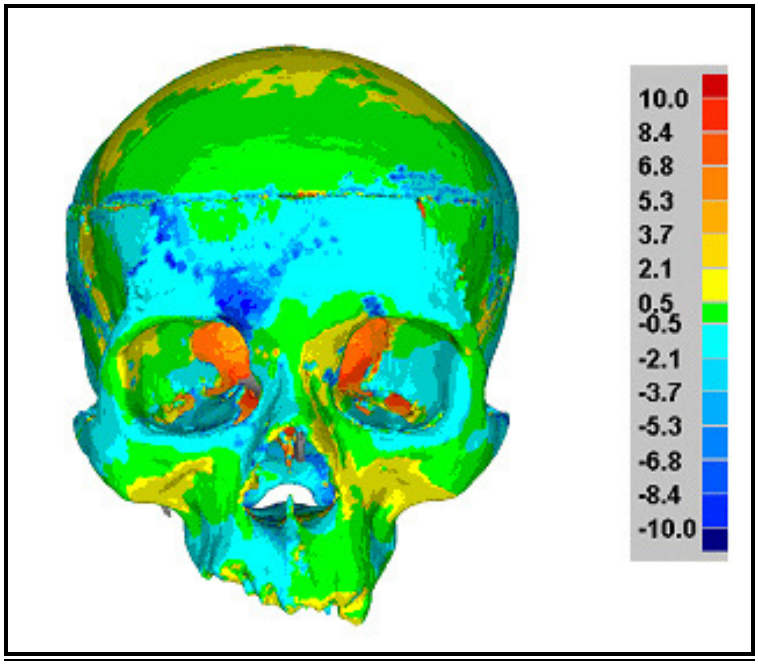

Fig 51: Cranium E anterior.

Green = no significant difference (mm);
lightest yellow = less than or equal to + 0.5 mm error;
lightest blue = less than or equal to – 0.5 mm error

Of the total area ≤ +/- 2.1 mm error, 35% was less prominent (≤ -2.1 mm) and 28% was more prominent (≤ + 2.1 mm) in relation to the original cranium. 26% of the contours remaining were ≤ +/- 5.3 mm and 11% was ≤ +/- 10 mm error. No part fell outside +/- 10 mm. The standard deviation was 3.5 mm and the variance therefore was 12.25 mm.

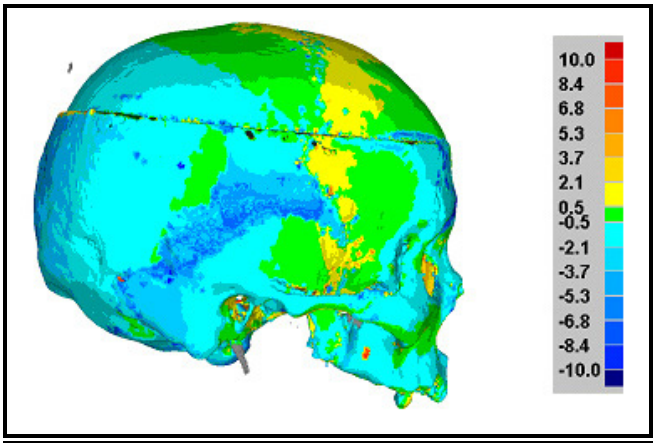

Fig 52: Cranium E lateral right.

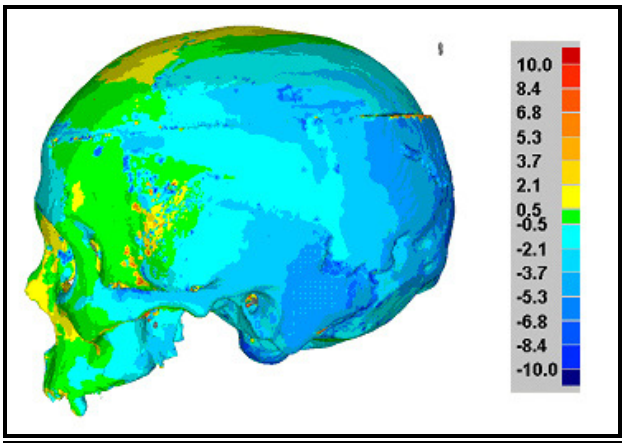

Fig 53: Cranium E lateral left.

Mandible E

248,310 data points were evaluated on mandible E. The most superior and lateral/medial portions of the left condyle and coronoid process exhibited no overlap between the original and restored mandible. The remainder of the posterior surface of the left ramus was less prominent than the original (≤ - 3.7 mm to ≤ - 6.8 mm error). Areas demonstrating no significant error included the anterior, lateral/medial surfaces, and inferior oblique line of the body. The right condyle head and vertical posterior border of the right ramus was ≤ +/- 0.5 mm error.

The total amount of the restored mandible shell ≤ +/- 2. 1 error was 77%. Of that total, 60% was less prominent (≤ -2.1 mm) and slightly less than 18% was more prominent (≤ + 2.1 mm) in relation to the original mandible. 22% of the remaining shell was ≤ +/- 5.3 mm, and less than 1% was ≤ - 6.8 mm error. The standard deviation was 2 mm and the variance therefore was 4 mm.

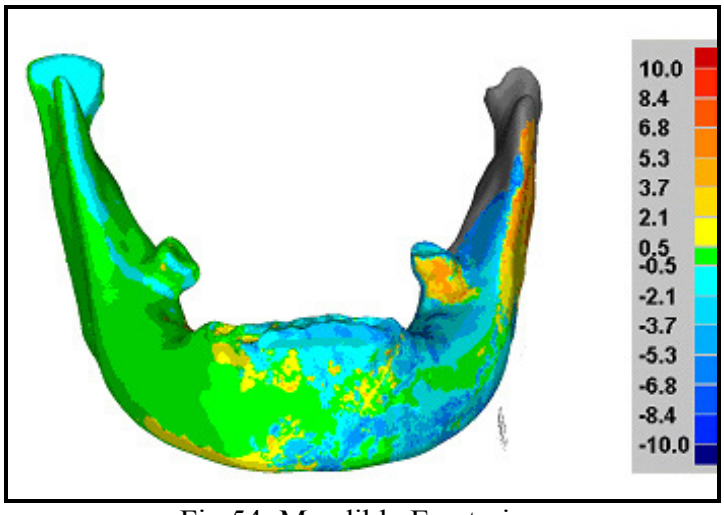

Fig 54: Mandible E anterior.

Green = no significant difference (mm);
lightest yellow = less than or equal to + 0.5 mm error;
lightest blue = less than or equal to – 0.5 mm error

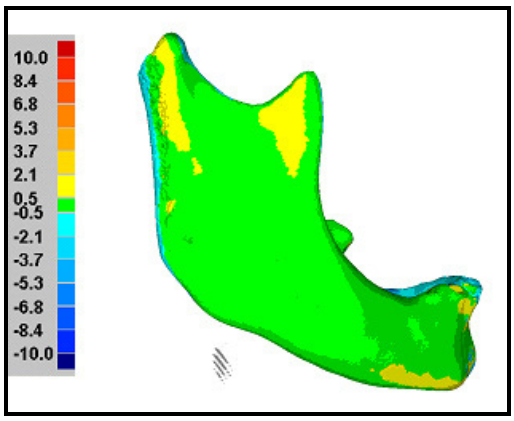

Fig 55: Mandible E lateral right

.

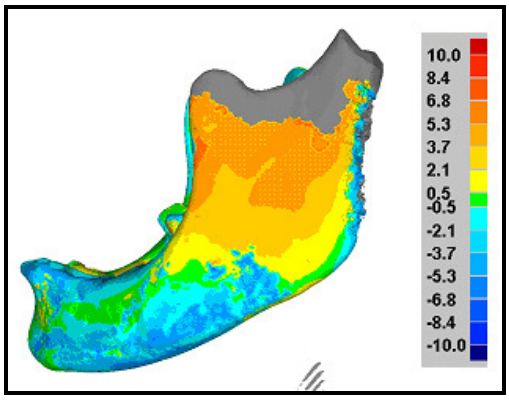

Fig 56: Mandible E lateral left.

Superimposition and comparison: Skull E

Cranium E

The highest total for combined percentage of measured differences in the mandible restorations was found in mandible E at 7.68%. Width (3.13%), length (3.76%), and height (0.79%) were all less than the original. Superimposition confirmed a close approximation between original and restored cranial height at the nasal and zygomatic bones and the inferior edge of the maxillae.

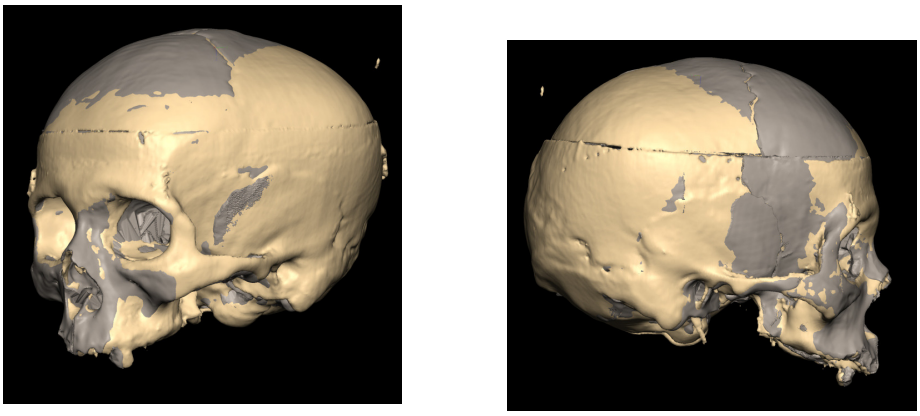

Fig 57: Cranium E - superimposition oblique left and lateral right.

Cream = before restoration; grey = after restoration.

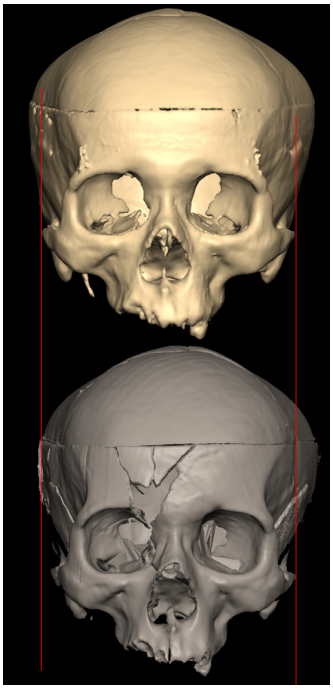

Fig 58: Cranium E - comparison anterior.

Bottom position = after restoration.

Mandible E

14.64% of re-assembled mandible E measured greater than or less than the original dimensions. Measurements of length (4.12%) and height (3.56%) were less than the original; width was 6.96% greater. Condyles appear incorrectly angled toward the midline. Height of the anterior body demonstrates a close approximation in superimposition.

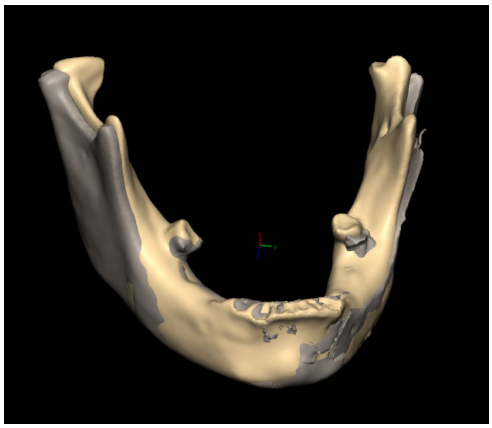

Fig 59: Mandible E - superimpostion anterior oblique right.

Cream = before restoration; grey = after restoration

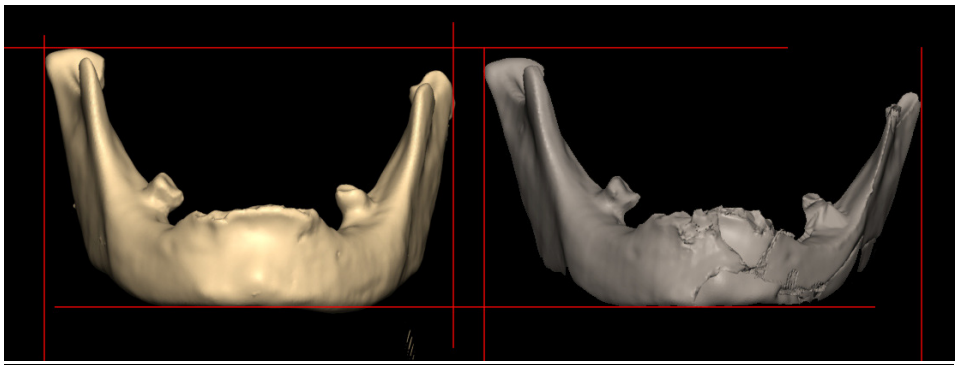

Fig 60: Mandible E - comparison anterior.

Right hand position = after restoration

DISCUSSION

The issue central to this research is the extent to which the surface contour profiles of restored skulls concurred with that of the same skulls prior to fracture and re-assembly. Secondary interests include the level of operator subjectivity involved in computer assisted technique, the time required to perform the restoration (and associated tasks), and a practical assessment of both the difficulties encountered and the skill levels necessary to facilitate re-assembly.

Factors pertaining to the Freeform computer assisted method (in order of priority) and potentially affect the accuracy of the restorations were:

1) The quality of 3D digital models. This must include a consideration of the suitability of the scanner type (automated or hand held) for the capture and processing of models, and more specifically, how the skulls and fragments were scanned – for example, through plexiglass, through regular glass, against a solid background on one side only, or on two surfaces (with subsequent combination in FreeForm modelling).

   While the quality of models appears to lie mostly within the purview of the laser scanner, there is a possibility that some inherent incompatibility between FASTSCAN and FreeForm software contributed to the degraded images.

2) The ability of the operator; to which training and experience contribute.
3) The efficacy of Freeform modelling as a computer program for skull re-assembly. Does the absence of any integrated semi-automatic or automatic accuracy control make Freeform inappropriate for this task? To what degree can operator ability serve to compensate for this absent component?
4) The physical condition and configuration of the skulls: includes the number

of fragments, their availability as a physical reference for re-assembly, and whether the craniums were transected.

General observations and admissions

Operator ability

The author's minimal ability with computers at the beginning of this project affected the speed and success with which the training regime could address a lack of confidence and understanding of programs like FreeForm and FASTSCAN. In retrospect, training should have started earlier, and for that, the author is entirely responsible. The practice and time required to master the computer assisted elements of the project were incorrectly estimated. A more aggressive investigation of the complexities of the hand held laser scanner, new though it was to the operator, might have afforded greater success in realising the optimum range and application of settings for scanning, particularly in regard to the use of the plexiglass and glass surfaces. Currently, an appreciation for the degree of acclimatization to the virtual world and the practise required in computer operations to make full use of such technology is fully apprehended.

Uneasiness with computers must be managed if it is not to interfere with what must be learned. This psychological element is a reality pertinent to the expectation that someone, simply because they have knowledge in physical anthropology and anatomy or ability in sculpture, can expertly command the technology employed to scan images, and re-assemble virtual fragments on computers. Alternately, it should be recognised that anyone who is masterful with computer systems, and wishes to restore or reconstruct skulls, cannot, without knowledge of anatomy (particularly osteology), use

such technology with productive ease.

Initially, re-assembly in computer assisted 3D felt awkward and progress with the first skull (A) was uneven. Intervention from a supervisor experienced in computer re-assembly to correct error propagation was necessary with skulls A to D – repeatedly with skull A, then less so as confidence was gained and skulls C and B were completed. The author spent seven cumulative hours re-assembling skull A before noticing an error of propagation; this occurred in four out of the five skull restorations. Skull A was attempted five times, skull B twice, skull C, three times, skull D twice and E, once.

By 'attempted' what is meant is that re-assembly reached a point where the mal-alignment of fragments and a developing 'skew' of the crania required returning to a former stage in the restoration to correct the error. This was done by temporarily making invisible the parts fitted which suggested a departure from a coherent alignment (Subke, 2005) For this reason, it was advised that 'versions' of ongoing assembly in FreeForm be saved - if an error was judged to have started at a particular point, it could easily be revisited and the process re-directed before the skew was further worsened (Wilkinson, 2007).

Skull A formed the essential manner and method template which was applied to the five skulls - A, C, B, D and E in order of completion. Restoration resumed (incorrectly as it happens) with skull A, by starting again with the foramen magnum 'circle' and the sphenooccipital synchondrosis as they were perceived to relate to an articulation of the temporomandibular joint. Despite caution in the second attempt, it was necessary to stop again, and again, until it was recognised that without restoring the face first, the temporal bones (and mandible) were simply not going to come together properly. A

noted asymmetry in the height of the zygomatic bones in skull A contributed to the level of difficulty (fig 61), since this asymmetry was referred through the alignment of the tempormandibular joint and surrounding articulations. Ignoring the asymmetry inherent to a greater or lesser degree in all skulls, whether consciously or unconsciously, is detrimental to any attempt to restore the original shape and appearance (Fedosyutkin and Nainys, 1993; Wilkinson, 2004).

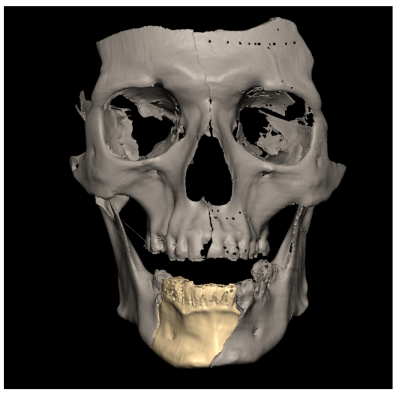

Fig_61: Difference in zygomatic arch height from anterior view.

Subjectivity

Subjectivity it first introduced in tailoring each 3D-DM as it proceeds through FASTSCAN processing – adjustments made to settings, for instance, were dependent on a visual determination of quality on a piece by piece basis. Combining two scans to form one piece in Freeform (as was the case with some cranium C fragments), is an example of an unnecessarily subjective operation (figure 62 and 63). In Freeform each fragment must be positioned and aligned according to the visual perceptions of the operator. Complete elimination of subjectivity in CAD skull re-assembly is impossible – in the instance where portions of fragments are missing or edges are eroded, final restoration dimensions and contours must rely on operator judgement. Ideally, limiting a subjectivity which is a result of poor quality images and no semi-automated accuracy

control during assembly is answered by refining both those mechanisms in tandem. The very nature of the elements which at this stage of technical development make 3D object manipulation in Freeform a useful application for skull re-assembly (weightless, non-material acting models), make the positive, unambiguous articulation of fragments an ambitious aim.

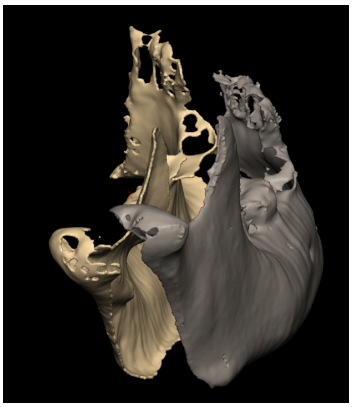

Fig_62: Mandible C fragment – combining.

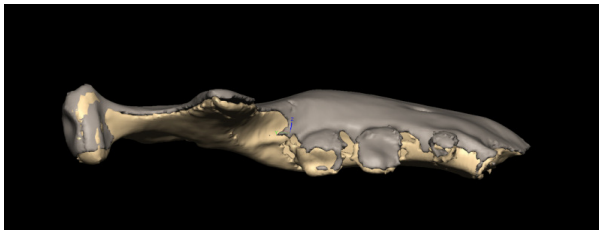

Fig 63: Mandible C fragment – combined.

Shell deviation comparisons

Analysis of the shell deviation results for skulls A-E indicate that skull re-assembly using computer assistance is a technique with potential. Cranium accuracy ratings were less than acceptable in two cases (54 and 56%), acceptable in two (64%), and reasonable in one (70%). Mandible accuracy values demonstrate a wider range of accuracy values - from two at the first level (acceptable at 66%), one in the middle category (reasonable at 77%), and two in the ‘good’ range (82 and 88%).

A compensating factor in the generally poor-to-acceptable accuracy results is the demand (which the purpose of supporting facial reconstruction entails) to assess individual skulls in their own context. What is meant by this is that it is the facial skeleton, and not the cranial vault or basicranium which is important if the restoration is to enable the modelling of a recognisable face. A context driven analysis then, includes working out where the most important facial features are and the weight of the corresponding accuracy level for that area – and how it may compensate or detract from the remaining accuracy 'map' of the face. This approach to analysis may be applied to each of the five skulls (Figure 64).

For example: the 'acceptable' accuracy score for cranium B, with a distribution of 64% (from 'no significant differences' to +/- 2.1 mm error), increases the likelihood that the face, forehead, (as well as the right lateral parietal bone, and vault) could support a facial reconstruction. Areas of worst accuracy may be mirror modelled from the opposite stronger side, and the accuracy for cranium B as a whole improved upon. The right zygomatic bone included patches of no significant difference and patches accurate to within – 0.5 mm error. The frontal and temporal processes of the left zygomatic demonstrated $\leq$ - 2.1 mm and $\leq$ – 3.7 mm error; and the anterior and lateral right maxilla were + 0.5 to + 2.1 mm error. The more accurate circumference of the right eye orbit could, if necessary, be modelled onto the left which is not as accurate. These elements form the central components of the face, (the eyes, nose and mouth) and as such, are primary in facial recognition (Wilkinson, 2004).

The right upper maxilla, right temporal and parietal b-ones of cranium B could also be mirror modelled to the left side to replace less accurate left equivalents. The 'orange' and 'red' zones in the lateral and posterior walls of the left orbital cavity are largely

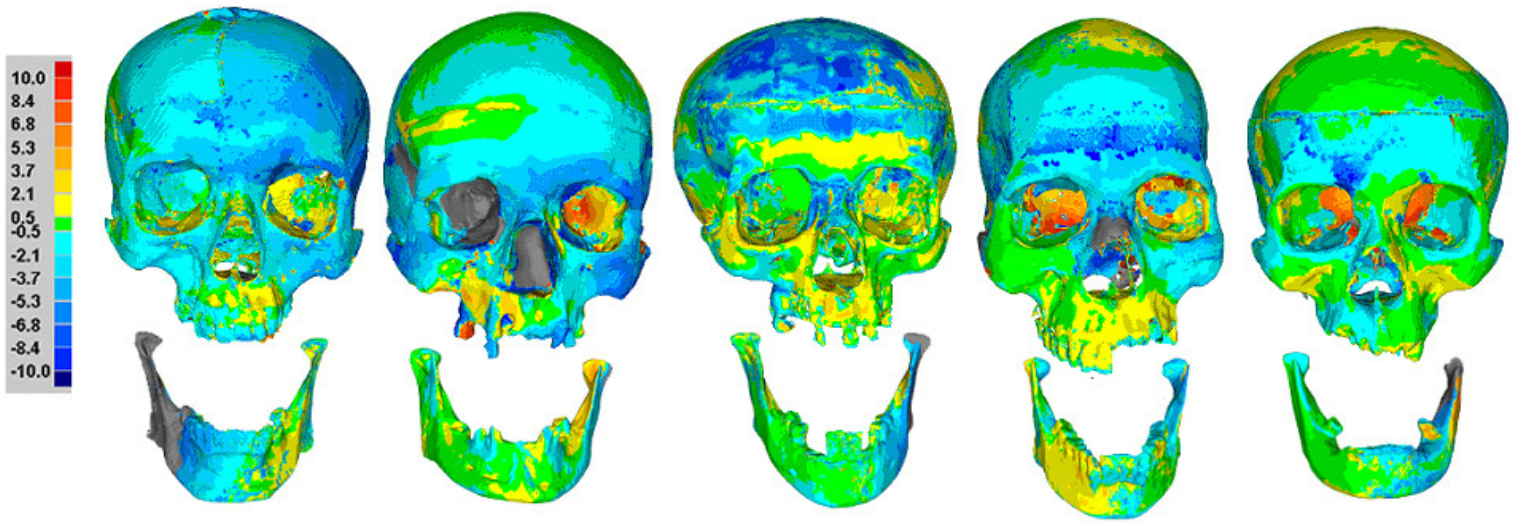

Figure 64: Shell deviation maps for skulls A-E.

irrelevant to the concerns of facial reconstruction because accuracy of bone is less important in these areas. The worst accuracy occurred on the inferior surfaces of the cranium, notably the inferior surface of the left zygotemporal arch, the inferior line of the left zygomatic, the right palatine bone, and most of the sphenoid, where no overlap between the original and the restored cranium were evident. The palatine, posterior maxillae, sphenoid bone and mastoid process are again less significant because they are 'behind' the face.

The acceptable accuracy in the facial area of cranium B is further supported by good accuracy (88% at a level that was $\leq$ +/- 2.1 mm error} in mandible B. Since the mandible forms the lower one third of the face, the presence or absence, and degree of accord between the restored and original mandible can be important to a facial reconstruction. Deriving the biological sex of an individual is easier if the mandible is included in the skull analysis. It is believed that the prominence and rugosity of mandible morphology influence the contours of soft tissues (Wilkinson, 2004).

If one or the other of the vertical or width dimensions are missing in a skull, the absent element can be compensated for – in terms of height, the front of the mandible body is more important for facial reconstruction and the height of the condylar ramus less so. Width of the anterior body can be extrapolated from the height of the ramus but not with complete reliability. The width of the mandible between gonial angles is more critical than the breadth of the anterior chin (Wilkinson, 2007). The comparison of mandible width using an inter-condylar rather than an inter-gonial measurement may also mean that mandible B is more accurate than the width measurement (3.46% less than the original), would indicate.

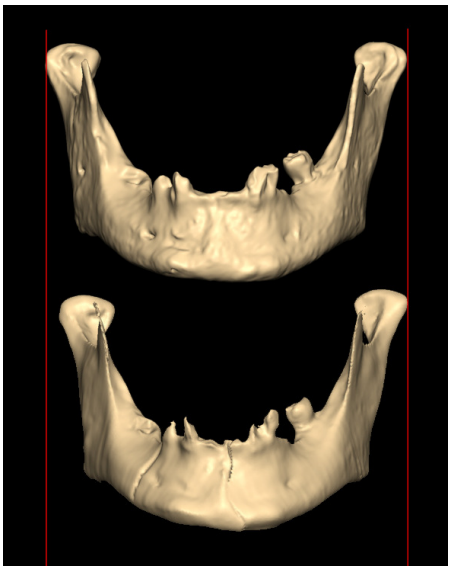

Figure 65: Mandible B comparison.

Lower image = restoration

The individual context approach to analysis may be applied to the remaining skulls. Craniums A and E, for example, were less homogenous in variance of values overall (standard deviations of 3.7 and 3.5 mm). Cranium E did not exhibit any 'no overlap' portions; which in and of itself neither makes or breaks the balance of accuracy quality in the cranium, since it is *where* areas of no overlap are situated more than whether they are present or not that is important. Cranium C registered a reasonable 70% which was ≤ +/- 2.1 mm error, and was more homogenous in variance of values overall (standard deviation of 3 mm). It appears less suitable for supporting a facial reconstruction than either cranium A or E, because the concentration and dispersal of higher accuracy categories, (no significant differences and < - 0.5 mm error), are better placed in A and E crania – meaning there is substantial coverage of the central facial region. The greater the homogeneity of values in the facial complex (meaning the lower the variance, or standard deviation), the greater is the likelihood of a closer approximation. If heterogeneous (high variance) contour profiles are found in areas other than the face,

they may not negatively affect the accuracy rating.

Assessment of mandibles is complex because their value to the skull re-assembly is interdependent with the score of the cranium with which it is paired. For instance: the fact that mandible C was an acceptable 66%, and E a reasonable 77% (≤ +/- 2.1 mm error) does not necessarily make mandible E the 'better' facial reconstruction candidate. Apart from the left condyle head which exhibits no overlap between the restored and original specimen, the greater portion of the external anterior body and right ramus of mandible C reflect no significant differences or, on the left exterior ramus and codylar process, an accuracy which was ≤ - 2.1 mm to ≤ - 3.7 mm error. Again, the right condyle could mirror a substitute for the small amount of the left condyle head which shows no overlap between original and restoration.

The second increment level of accuracy (% of restored area which is > +/- 2.1 mm but ≤ +/- 5.3 mm error) can support the accuracy rating of crania and mandibles, especially when it is in an area strategically effective at increasing the likelihood that the facial region will endorse soft tissue reconstruction – meaning that it is situated immediately adjacent to sections which are strong in accuracy or occupies an area of secondary importance, like the forehead or superior and lateral cranial vault . For the crania most percentages at this level were in the mid to high twenties, ranging from 24% to 31.5%. For the mandibles, the range was more variable, from 12% to 31%. The combining of ≤ +/- 3.7 mm and ≤ +/- 5.3 mm error into one category for simplification of results was inappropriate for the purposes of analysis because the balance of the dispersal of differently 'weighted' accuracy levels is so pertinent to determining the quality (usefulness) of a skull restoration. It is useful to know the proportion of contour profiles which are as *close* as possible to the accuracy category of primary importance – in this

case that was ≤ +/- 2.1 mm error - the *next* most important increment was therefore ≤ +/- 3.7 mm error. Reducing the increment of next importance to the narrowest practical margin fine tunes the diagnostic assessment process.

Deciding what is more crucial in an accurate representation of an original skull - morphology or morphometry – can affect the interpretation of error tolerances. The illustrated relationship between facial bone shape and the soft tissues of the face is established (Iscan and Helmer, 1993; Schimmler, *et al*., 1993). If a mandible, zygomatic, or maxilla bone is acceptably true in reproduction to its original morphology, how much does it matter if the length, width or height of the pieces assembled *in toto* is less or more than the pre-restoration skull dimensions? And what degree of 'less' or 'more' is permissible without incurring distortions that make a reconstructed face unequal to the task of familiar recognition? This question arose out of studying the images of the reconstituted skulls – as individuals and as part of a group. Each re-assembled crania and mandible, as mentioned previously, were *so* immediately recognisable relative to their pre-fracture images that the author and observers began to question this balance of morphology to morphometry as criteria for accuracy.

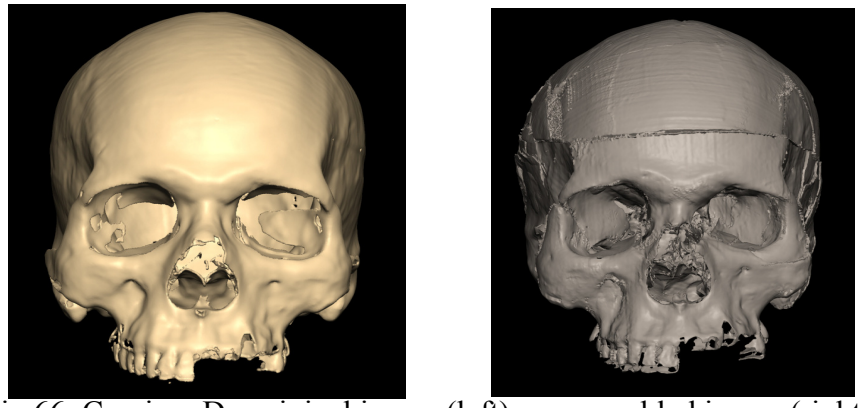

Fig 66: Cranium D - original image (left); re-assembled image (right).

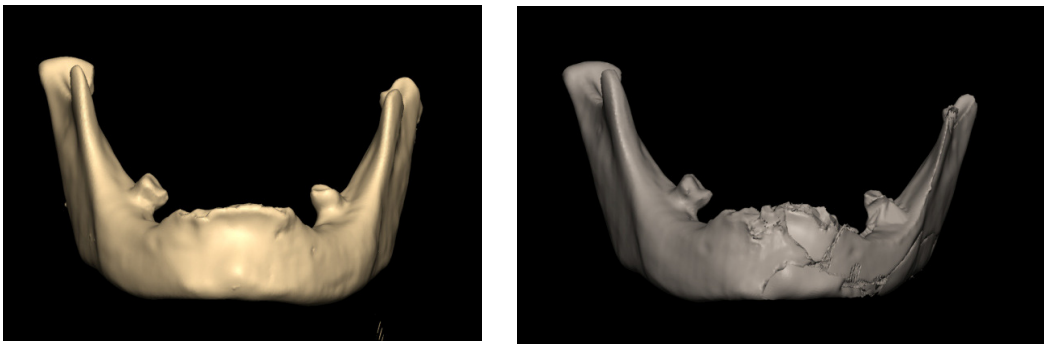

Fig 67: Mandible E – original image (left) re-assembled image (right).

Despite the distortions which fracturing and reconstitution entail, both cranium D and mandible E images (fig 73 and 74) are clearly discernable as reproductions of their originals. The rugged concavities of the zygomaxillary area, the relatively large mastoid processes, the outline of the nasal opening, and the orbital margin shape should impart specific and individual characteristics to a facial reconstruction. The resorption of the anterior body resulting form reduced dentition and the non symmetry of mandible E's condyles would create a unique appearance and articulation of the chin.

Scanning - image production

The Scorpion hand-held scanner is very portable and only costs 15,840 pounds sterling (£), but may not be the most appropriate tool when the aim is efficient and accurate skull re-assembly. Because a laser scanner captures images by a reflective method, the supporting surface on which the object rests must be filtered out of the point cloud which orchestrates the final image. A point cloud is a set or coordinates of x,y,and z – the Cartesian reference system of virtual 3D. The repression of the cloud point creates a "superimposition error, which can [and does] affect the next processing phases" (Galantucci, *et al*., 2006).

Interestingly, Park *et al*. (2006), found in a comparison between direct measuring on skulls and craniometry using the FASTSCAN Cobra laser scanner (one camera as opposed to two in the Scorpion), that laser scans done with point localization (for craniometric measurements) had good reliability, both in terms of inter- and intra-

examiner performance, and were accurate enough to replace conventional measurement methods using osteometric board, craniophore, and calipers. Additionally, the reliability of stationary automated laser scanners for measuring living soft tissue facial morphology over time in growth or treatment changes studies has been verified (Kau, *et al.*, 2005). In light of the difficulties in producing clear, recognisable images of small bone fragments, or even accurate edges on larger fragments with the Scorpion scanner in this research, it is important to ask why the hand held laser generated image of an intact skull is of sufficient quality to permit accurate morphometric analysis, but scans of fragments performed with the same type of scanner inadequately support 3D computer re-assembly (because the reproduction of fragment edges was both inconsistent and poor).

Subke (2005) describes two automated laser systems used to digitize skull fragments in preparation for restoration: both are multi-camera techniques, capable of producing detailed bone images (with natural surface colour) in 3D images and local resolution of surface morphology better than 1 mm, which is crucial if fragments are to fit as precisely as possible. The complexity and sophistication of the combined technologies used to capture fragment images in this way is costly, and require a considerable amount of dedicated set-up space (Subke, 2005). As such it contrasts with the relative in-expense and simplicity of the hand held scanner.

Unfortunately, variation in the distance between the Scorpion wand and object can affect resolution (0.5 mm per 200 millimetre range), and accuracy (1 mm per 200 mm range) (Park, *et al.*, 2006). Potential resolution and accuracy therefore, are adversely affected by hesitation or tremor in wand (hand held) movements, and by unintended departures from an ideal distance or threshold for resolution between object and wand.

Hence, the operator must exercise care in planning the minimum number of sweeps which will collect the maximum detail without covering one area repeatedly. By necessity, some areas of bone require multiple passes from different angles because the laser may not record enough detail on initial or even subsequent sweeps. The greater the number of passes over the same path, the harder it is for FASTSCAN to smoothly integrate image details using functions called “register sweeps” and “basic formatting” (Polhemus, 2007), whilst maintaining morphological continuity (especially edge integrity) of the image. Registry of sweeps is designed to correct poorly aligned triangulated data. Mal-aligned sweeps equate with poor image production. Increasing the number of alignments the processing unit must manage contributes to 'noise' (figures 68; 69; 71; 72).

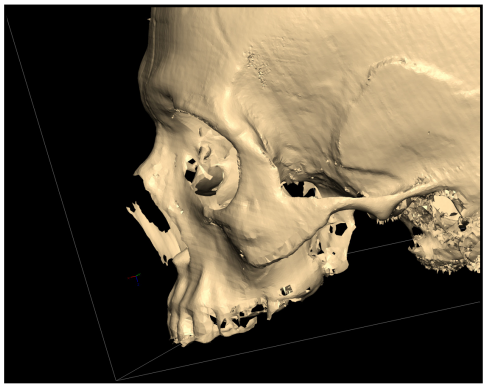

Fig_68: Cranium A - spurious projection of maxilla.

This artefact projecting inferior and anterior to the nasal cavity did not exist in physical reality.

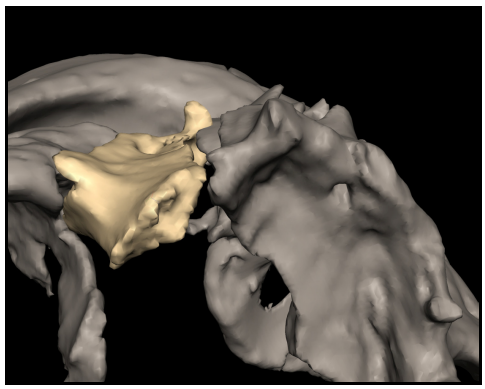

Fig 69: Cranium B - spurious projection.

The lump jutting from the infraobital edge of the right orbit did not exist in physical specimen.

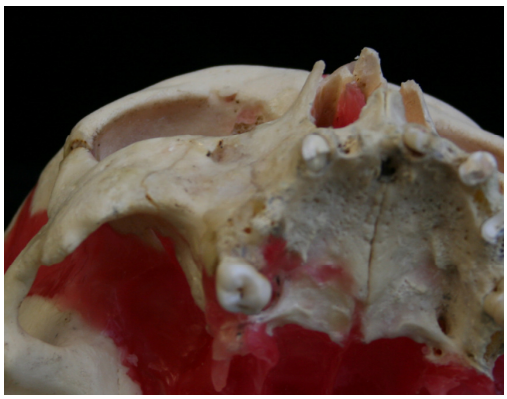

Fig 70: Cranium B – physical specimen.

Physical cranium B viewed from same angle as in figure 75 – no projection beneath right orbit.

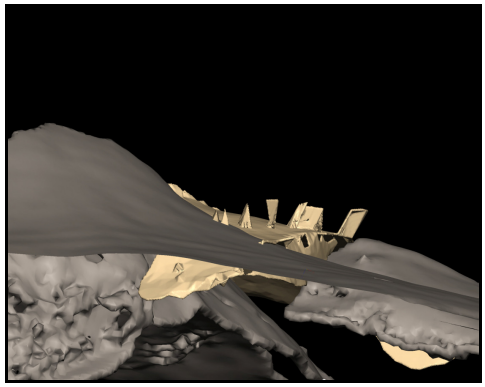

Fig 71: Cranium C - non-existent ‘spikes’.

Rectangular and triangular projections from superior surface are spurious artefacts.

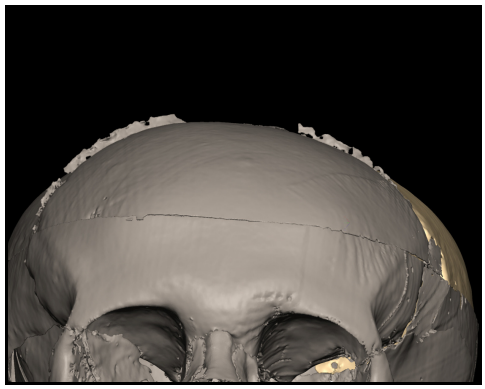

Fig_72: Cranium C – 'frill'.

Perpendicular projections from vault surface did not exist in physical specimen.

Missing aspects such as a foramen, sulcus, or process, make fitting less certain because the fragment is harder to identify in the first place (figure 73). False and incomplete edges (figure 74) increase error in fitting fracture lines – this conclusion is consistent with a potential limitation in the process as noted by Subke (2005). A process which depends on the precise fitting of one fragment with another to accurately (≤ +/- 2 mm error) reproduce the original dimensions of an object before fracture, but adds to or subtracts falsely from image surfaces representing those fragments, reduces quantifiable assessments into approximations with less value than would be the case if the image production were more reliable.

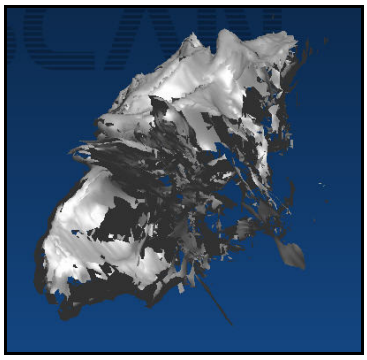

Fig_73: Cranium D – sphenoid with partial pterygoid in FASTSCAN image.

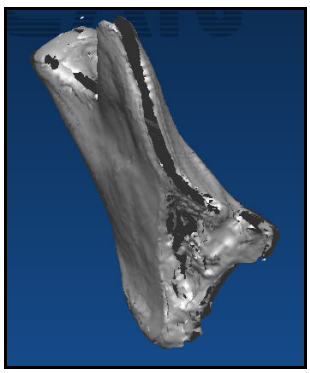

Fig_74: Mandible D – FASTSCAN image.

Information is missing along vertical edge of coronoid process.

The laser works best on simple, flat surfaces with no shadow and few angles. The morphology of trabecular bone, competing angles producing shadow, foraminae, styloid processes, minor concavities, minor convexities, or the projecting 'fingers' of sutures, do not translate into clear images generally, and interfere with the production of accurate edges. The most difficult bones to scan were the mandible, the sphenoid and small, thin fragments. The easiest to scan were large pieces of vault.

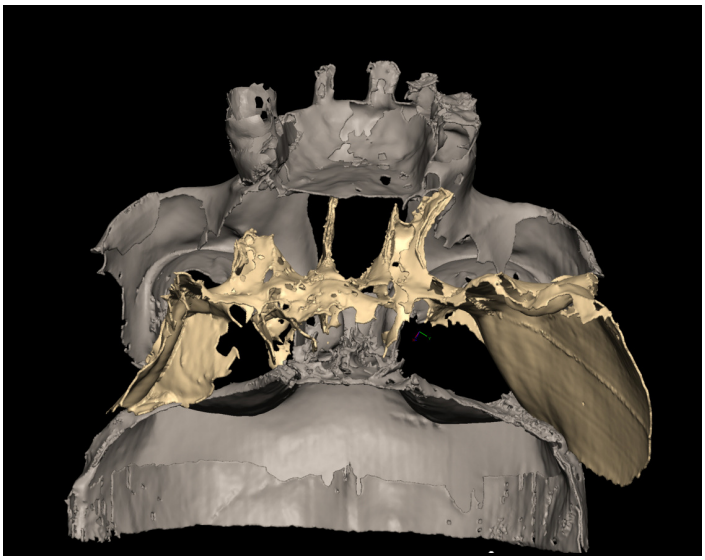

Fig_75: Cranium C – virtual sphenoid placement.

Fig 76: Cranium C physical fragments.

Photograph of physical sphenoid, maxillae and frontal bone manually articulated. Note clarity of edges and morphology in comparison to virtual equivalent in fig 81.

The plexiglass stand (provided by the engineering department at the University of Dundee) through which skull A and D were scanned, initially was used because it was assumed the "through glass" (Polhemus, 2007) component of the scanner software was present in the package installed on the laptop. This was not the case. When fragment scans of skull A proved to be poor (figure 77), the process of scanning through the plexiglass was deemed a significant barrier, and skull A fragments were re-scanned against the background of black synthetic felt.

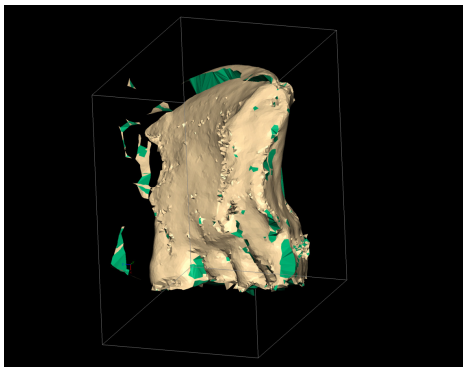

Fig_77: Mandible A fragment – scanner noise.

Floating and extruded pieces are artefacts from laser scanning through plexiglass.

Scanning pieces through the plexiglass effected edge density and clarity. The spaces between scanned sides were void (fig 78). The laser cannot capture an edge which is angled inferiorly away from the beam, or sitting on the plexiglass surface against which, or through which, it is scanned.

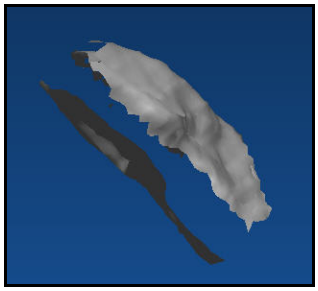

Fig 78: Cranium D fragment.

Another (incorrect) assumption made was that plexiglass can be scanned through in the same way in which regular non-plexiglass might scan, or for that matter, tempered glass, or glass of different thicknesses. The scanner manual does not stipulate the type of glass which should be used for through-scanning. The author was at first unaware of the laser's lack of affinity for plexiglass and continued to be ignorant of the refractive settings possible while scanning skull D. The use of the plexiglass was tried again at that point because of the inadequacies of scanning fragments on one side only. Increasing the value of smoothing from 1.00 to 1.50 improved overall image qualities but meant more morphological detail was lost, especially on edges and small fragments.

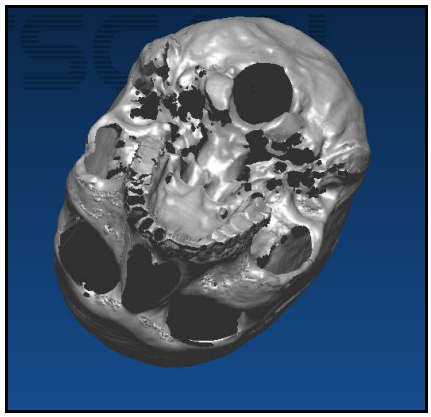

Fig_79: Cranium D inferior in FASTSCAN.

.STL file after registered sweeps and basic formatting; the black areas posterior and medial to the temporal fossae, nose and eye orbits represent lost information.

Fig 80: Cranium D inferior – physical specimen.

Note the detail available on physical specimen in comparison to figure 85.

Skull C, (both intact and fragmented) had been scanned using the one-side-only method on black felt. Scanning only one side of a fragment created two problems: first, as with the plexiglass method, the full dimension of the edge immediately adjacent to the surface upon which the piece rests is not entirely captured. Aligning fragments, some of which have partial thickness dimension and some which do not, challenges estimation of an appropriate edge-to-edge angle at which edges conjoin. When assembling the curved cranial vault or the plane of the facial bones to the vault, the degree of angle on which one fragment 'hinges' with another can affect substantially whether all fragments will fit together eventually as a contiguous whole. Secondly, interior detail important for identifying the position of whole bone or their fragments is lost. An example is the passages for the meningeal vessels on the interior parietal bones (fig 81). These affects are exaggerated when temporal, sphenoid, or maxillae fragment images are missing interior (relative to the skull).

Fig 81: Photograph of internal morphology – physical parietal bone.

Skull E was the only specimen to be scanned through regular glass (with appropriate setting for glass refraction and glass thickness). Again, it was necessary to set the smoothing parameter higher (1.5 or 2.0) depending on the individual piece, to compensate for reflective noise. Knowing and setting the correct parameters for glass thickness and refraction correction did address distortion to some extent.

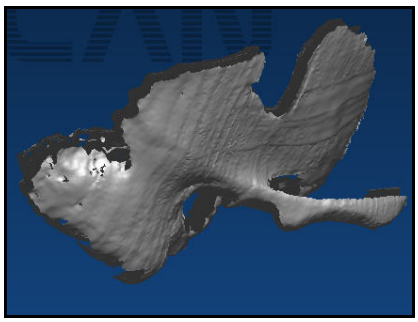

Fig 82 Cranium E – FASTSCAN image.

Note incomplete edges and concavities on exterior temporal bone surface

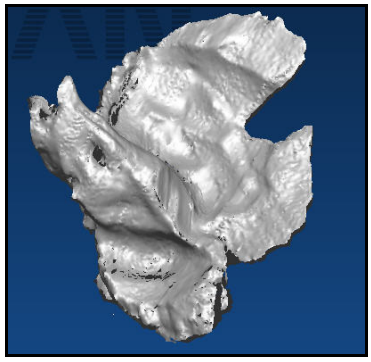

Fig_83 Cranium E – FASTSCAN image.

Interior temporal bone image displays good detail in contrast to the exterior in figure __.

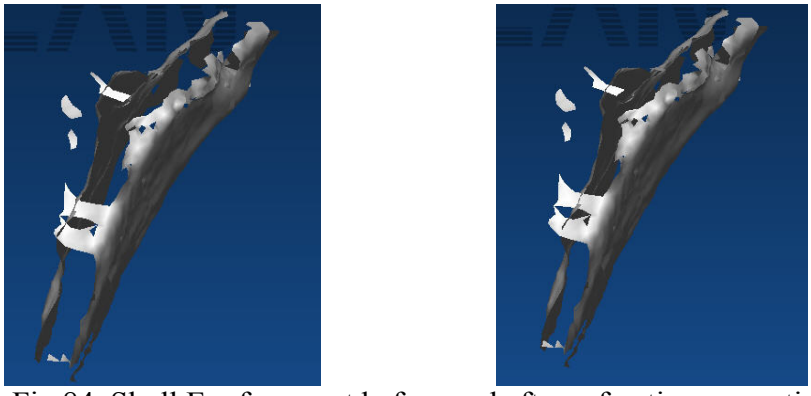

Fig 84 Skull E – fragment before and after refraction correction.

Note the two 'sides' are pulled together, but the edge is still partially void.

CT scans

The price of a portable CT unit weighing 336 kilograms is now £123,000, as opposed to a machine with special climate controlled housing requirements, weighing 7,000 kilograms, and costing £740,000. Apart from the recent appearance of portable CT units like the CereTom (NeuroLogica Corporation, 2007), CT scanners have been stationary. The cost of automated laser scanning systems as stipulated by Subke (2005) may approach the cost of a portable CT machine.

The strength of CT scans for analysis and restoration of fractured bone - and hence it's extensive use in maxillofacial surgery - lies in the clarity of detail generated by the ability to render internal morphologies as well as exterior surfaces (Galantucci, *et al*., 2006). CT scans penetrate through an object with x-ray, providing a single volumetric presentation without the interference of unwanted coordinate repression. CT scans have proven their accuracy as morphometric tools in paleoanthropology and in model replication (Zollikofer, *et al*., 1998). The reconstruction of an archaeological skull provides an example of how CT scans can be used to control accuracy *during* the rebuilding process. An industrial CT unit scanned the petrosal portion of the Le Moustier 1 temporal bones, producing 0.5 mm slices with a resolution of 0.1 mm within each slice. The preserved semicircular canals were then oriented to an angle +/- 45 degrees relative to the sagittal plane, correctly positioning the temporal bones in their lateral inclination and controlling the breadth of the cranial base and the upper cranial vault (Ponce de Leon and Zollikofer, 1999).

Determining the lateral inclination of the temporal bones in 3D is difficult because without the maximum and minimum ‘lock’ affect (perceived by eye and hand) which is provided by physical fragments as they are manipulated one against the other, the

temporal bone's many articulations (if misaligned) can change the appearance (width primarily) of the cheek, the upper jaw, the temporal, and upper cranial vault area. When the posterior elements of the sphenoid or the anterior, oblique, and inferior elements of the occipital bone were absent or degraded in the image, the author found positioning temporal bone fragments without some other source of alignment (such as the interior semicircular canals) tended to be a prime source of error propagation, and that their incorrect lateral inclination within the restoration was a common cause of having to backtrack and start afresh.

Using the scanner

Scanning action was trial and error. A scanning movement which facilitated a reasonable translation of the morphology of one fragment failed to work on another piece very similar in shape and size. With practice, the angles at which the laser was less likely to generate incorrect information became easier to anticipate; the laser's tolerance for perspective was difficult to predict however. It is difficult to reconcile the needs and likes of the laser with maintaining consistency of arm speed and body position. In contrast, stationary laser units with rotating platforms and automated arms ensuring continuous speed and smooth movement of the light beam traversing an object do not produce inconsistencies inherent in human hand-eye coordination (Galantucci, *et al*., 2006).

A second method of generating images with the hand held laser is possible; a small receiver (approximately 23 x 29 x 15 mm) is attached to the object to be scanned, allowing the object to be moved in between sweeps (Polhemus, 2007). The freedom to move the object means it can be scanned from all sides, which is not possible using the

larger receiver. The small receiver must be attached securely to the object so that it does not move when the object is turned or inverted. This can be done with a rubber band, tightly applied, or by squeezing a temporary adhesive between box and bone. Evidence of the small receiver itself can be erased by ticking a specific command on a subsequent sweep. Any evidence of the rubber band or adhesive material cannot be erased in the compensatory sweep, and must either be left in the image or removed ('scrubbed') from the image in FreeForm. The smaller the fragments, the more difficult the placement of the receiver on the bone – successful attachment is therefore variable. If the fragment is smaller than the receiver, this technique is not possible.

Computer aided re-assembly

Core elements which make FreeForm modelling useful for virtual skull re-assembly - the freedom to move pieces without gravity, to re-start a restoration without time wasted separating and re-adhering pieces, to 'handle' objects virtually thus avoiding damaging specimens, to dematerialise fragments temporarily for visual access to inspect formerly joined fractures – all work well. But the wizardry of 3D virtual mechanics is not in itself sufficient. Good representations of the corresponding physical pieces to be re-assembled are critical. Degraded or distorted models impair re-assembly accuracy, and this is why an analysis of the efficacy of 3D computer assisted restoration is impossible to separate from the discussion about the 3D-DM produced in laser scanning.

The landscape observed while navigating the interior image of a skull under restoration in FreeForm is more like the twisted and melted girders of a bombed building than the meticulous detailed morphology of a cranium (fig 85).

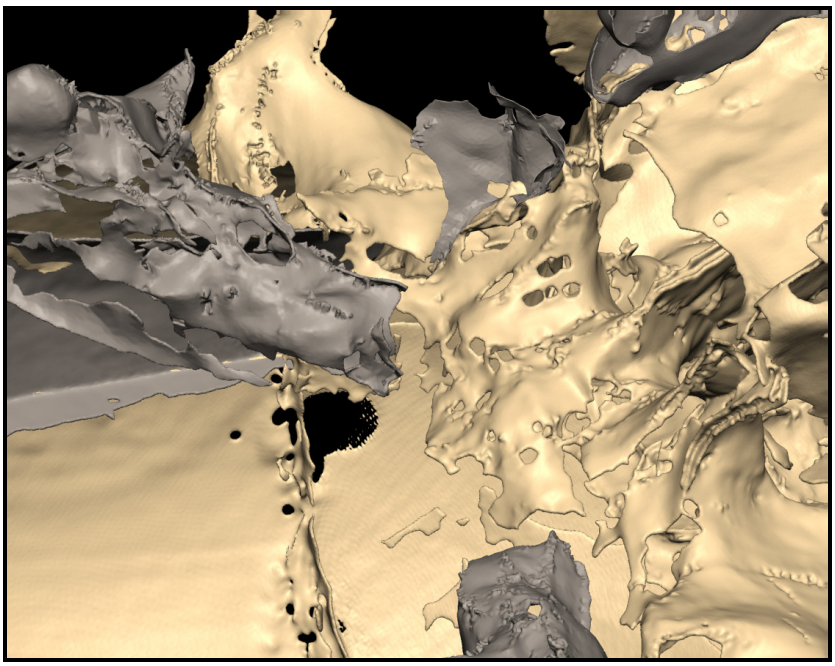

Figure 85: Interior view of cranium in Freeform.

Structures normally recognised (even fragmented) in physical reality become unrecognizable. Swooping through a zygomatic arch like a miniaturised intergalactic pilot is exhilarating as one becomes aware this is a unique view afforded by a new technology. But novelty quickly turns to frustration as it becomes obvious that neither the laser scanner nor Freeform, which acts as a transducer of scanner images, 'see' in the same way human eyes see.

The appearance of the 3D models as they manifest in Freeform may indicate a conflict between software programs – at least as far as the continuity of model integrity is concerned (Wilkinson, 2007). The quality of the Cranium B fragments generated by the stationary automated Minolta laser (figure 86) was not much better than the quality of scans completed with the hand-held Scorpion. When viewed in Freeform prior to processing, large pieces were identifiable but smaller fragments were indistinct in outline and reminiscent of melted glass (figure 87) - in fact the majority of the smallest

pieces were so difficult to identify they were left out of the final restoration. In an attempt to improve quality, the images were repeatedly re-imported and the functions of "fill holes" or "thicken" (Freeform Users Guide) altered during processing to see which level and type of formatting would produce more discernable detail. B fragments were eventually transformed into .cly flies at 30% resolution using the fill holes category (figure 93).

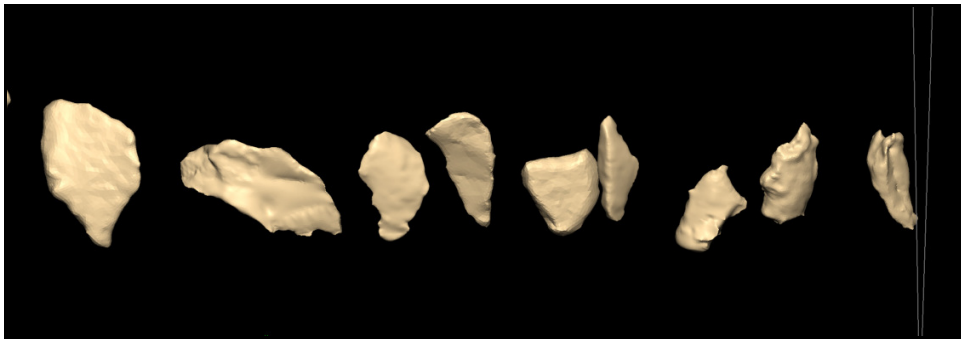

Fig 86: Cranium B small fragments prior to Freeform processing.

Automated scan images

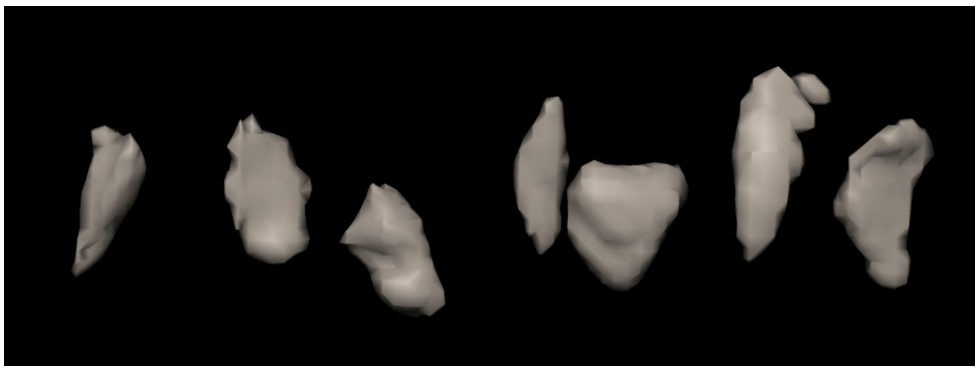

Fig 87: Cranium B small fragments after Freeform processing.

Automated scan images imported to FreeForm at 30% resolution.

30% resolution was a compromise which facilitated manipulation of the 3D-DM in Freeform; other levels of resolution presented different effects in fragments appearance – none of which were as good as the already poor quality B fragment models in

Freeform before conversion to .cly format. This was unexpected – after the difficulties procuring decent scans of fragments sets for skull A and C, it was suspected that the quality of the automated scan images would be an improvement. That this was not the case may be supported by the low accuracy score cranium B exhibited (64 % was $\leq$ +/- 2.1 mm error), *in spite* of having the lowest standard deviation, *and* the fact that the operator had acquired some skill with skulls A and C.

The poor quality of 3D-DM images in this research raises the question whether there are particular combinations of software which are not conducive to 3D model production for the purpose of computer assisted skull re-assembly - of which the pairing of FASTSCAN and Freeform is one. Until further research pairing specific scan processing and re-assembly systems are evaluated, multi-stage processing of laser scans will be trial and error for each restoration attempted. While it is feasible that the Scorpion scanner and FreeForm modelling may work together better than has been demonstrated (limited trials were performed before beginning specimen scanning, this is a weakness of the method employed in this study), it is also true that Freeform was not designed for skull re-assembly – instead the software serves as an adaptation to the purpose.

Subke (2005) argues "the control of the precision of a fit of two digitally adjoining surfaces is the crucial procedure in the process of the digital reconstruction". Imageware, a CAD software program (Unigraphics Solutions, Germany) provides objective quantitative quality control throughout assembly by means of algorithmic functions manually or semi-automatically applied as each piece is fitted. The Imageware program is partnered with either a one projector/two cameras, or four projector/four cameras automated SLT (optical surface measuring) scanning system of

more sophistication than the hand held Scorpion. The digitalised models it produces are therefore presumably of a quality commensurate with Imageware itself. Manual measurement of distance between fracture edges is achieved by choosing points on two fragments and measuring the single distance between the two points by algorithmic calculation. Semiautomatic measurement involves a geometrical matching algorithm of two surface areas whereby the average distance is optimized until the figure reaches a minimum. Subke (2005) admits the results of this constant accuracy control are subject to the nature of the shape of the interacting surface shapes – the more specific the shape, the higher the chances of a precise fit.

So, although in theory an algorithmic 'docking' function is ideal for the purpose of generating the best accuracy in restoration as possible, there are still two problems. The first is the dependence on surface morphology – presumably fragments of the sphenoid, edges made of suture projections, or any bone with detailed convexities, concavities, and complex angles is going to be less suitable for the algorithmic calculations upon which the method relies. A second problem is the difficulty assessing overlap of fragment edges which determines the angle at which fracture edges meet (Wilkinson, 2007). In the mandible, this factor is perhaps the cause of the greatest margin of error in restoration – and highlights one of the acknowledged advantages of the classical manual method of re-assembly using physical specimens – an angle of true articulation can be *felt* as well as seen, thereby avoiding the inaccuracies seen in the mandible widths in this research.

No statistics on accuracy comparisons are documented by Subke in regard to validating the technology advocated. Certainly any function that effectively monitors accuracy of re-assembly during the process is likely to offer an improvement over a system that has

none. The accuracy of restoration in FreeForm is assessed by submitting the final product to another program. How much efficiency and accuracy is lost by not having an edge-to-edge detection feature operating continuously during re-assembly? (Subke, 2005).

Measurement in Photoshop

Mandible width could have been measured between gonial angles, *and* condyle heads, providing additional comparative data. Only mandible D was measured between gonial angles It is suspected the correct width between gonial angles is more important (and realistic) to a successful facial reconstruction than a width between condyles. The appearance of the lower third of a face is more likely to be guided by re-assembling the inter-condylar width to correspond with the width of the temporal bone fossae, rather than the other way about. The restored height of the mandible anterior body could also have been measured in addition to that of the condyle heads.

Cranial length was measured from the most anterior point on the forehead to the occipital protuberance, which disregards the additional length of the facial complex, (particularly variance in the degree of prognathism). Again, a measure of length from which ever point was most anterior (rhinion or subnasale), would have provided a skull as well as a cranial length.

Timing

To a large extent this project served as a training program. The progressive improvement in the time required to restore is indicative of skills acquired in the process, but does not explain why the accuracy scores for the skulls did not also improve. The decrease in the number of times each skull was attempted (from five for skull A to once only for skull E), did not have a positive effect on the accuracy of the last two skulls. What the author perceived as a reduction in the difficulty of restoration (particularly skulls D and E), appears to have had no discernable (and expected) correlate improvement on accuracy.

There is no relationship between the number of fragments and time invested in re-assembly. Skull A with 30 fragments had a completion time of approximately 50 hours. Skull D had 34 fragments, but took only 6.5 approximate hours to complete. The difference between 50 hours for skull A and 6 hours for the last skull (E), suggests that a true test of the time it takes to use computer assistance for skull re-assembly is possible only when the operator has demonstrated a more than adequate ability and speed prior to the timed performance

Time allocated for handling computer processing (which in this case included the initial naming and classifying, transferring, importing, second processing, renaming, and cataloguing of image files), should be incorporated into, and accounted for, in projections on the efficacy of computer aided processes (Wilkinson, 2005). Without the investiture of time spent doing these tasks, computer assisted processes are not possible. A more thorough treatment of time estimation in this study would have included a breakdown of time spent on necessary procedures associated with, but not directly related to the 3D restoration itself.

Fragmentation

The aim in fracturing was to produce enough pieces to sustain a reasonable test of computer-assisted re-assembly processes, not to create so many pieces as to make the task excessively labour intensive. There is no discernable relationship between the number of fragments and the accuracy results, except perhaps in regard to the mandibles, although it is suspected that it is *where* in the mandible fractures occur as much as the *number* of fragments which may affect levels of restoration accuracy. This is because the morphology of the posterosuperior portion of the mandible incorporates multiple contradictory angles in close proximity to one another. This is bourn out by the consistency with which the condylar process and the condyle mandible heads were outside the bounds of deviation tolerances or demonstrate poor alignment scores. It is further supported by the operator's experience that the intact mandible is also one of the most difficult bones to scan.

The degree to which the facial bones of the four skulls resisted fracture (and were therefore easier to articulate with the vault and basicranium), was a positive contributing factor to restoration. Although the only cranium without a transection line (A) had the second lowest accuracy score (56% $\leq$ +/- 2.1 mm error), it is felt the effect of transection created an instrumental guide to the placement of vault fragments, superiorly, laterally, and posteriorly, which may have been greater than if the cranium had *not* been transected. The semi-straight line incised by the stryker saw during autopsy provided a clear orientation of 'up' and 'down' for those pieces superior and inferior to the transection (parietal, frontal, and occipital bone).

CONCLUSIONS

These results demonstrate that computer assisted skull re-assembly techniques can produce acceptable and reasonable degrees of accuracy. Results are predicated upon the veracity of images captured and processed by surface laser scanners, the ability of the operator and the efficacy of the Freeform modelling program itself.

Maximization of CAD potential in the context of the research aims relied on the appropriate pairing of computer hardware and software programs; it may only be fully realised by the adoption (and continued development) of two complementary and current, but not most commonly used technologies:

1) multi-camera, multi-laser, stationary automated laser scanners (optical surface measuring) or computed tomography (radiology) for image production;
2) a program specifically created for skull re-assembly which incorporates some function of a constant determination of the distance either between two localised surface points or between two neighbouring sectors of surfaces as is offered in some CAD surfacing software. Such algorithmic 'docking' may quantifiably support the visual control which initiates assembly.

Several things are also surmised indirectly from the results:

1) operator ability may compensate (though not to a known amount) for a lack of 3D-DM clarity and the absence of a semi-automated edge-to-edge control mechanism during restoration in the case of experienced practitioners.
2) Complete removal of subjectivity in impossible in computer aided techniques, the implementation of the technology itemised above may effectively reduce the unnecessary subjectivity arising from poor image quality, possible processing conflicts, and the absence of intra-assembly accuracy control.

3) Novice training in hand held laser scanning should consist of 50-100 hours, and training in CAD re-assembly in the range of 250 hours. This experientially based estimate multiplies the approximate 50 hours spent on the first skull re-assembled in the research by 5 (skulls).
4) Approximations made on the time required to complete CAD skull re-assembly is inconclusive – because the sample size is too small and because the level of training in computer processes was insufficient for testing of time parameters.

The practical aims as outlined – laser scanning, computer aided re-assembly, quantification of restoration accuracy, a secondary assessment using superimposition, and proportional comparison measurements in Photoshop, and a qualification of productivity in computer assisted image capture and skull re-assembly were achieved.

The strongest implication which arises from this work is that more thorough and far reaching research is required to adequately test the accuracy of computer assisted skull re-assembly. The pairing of software processing is particularly important to investigate, as are comparisons of CAD skull re-assembly using images created by CT, with re-assembly with images produced by stationary, automated lasers and hand held laser scanners. The relationship between image quality and programs used for 3D manipulation must be clearly delineated and compared relative to the quantified accuracy of the final product of those combined technologies.

The contribution to the field of human identification by this research is modest. It does serve to highlight techniques employed in skull restoration which are underwritten by computers, software, and instruments which purport to deliver an objectivity and efficacy which is to date, largely untested. Though affected by myriad changes in

scanning methods and inconsistencies in aspects of proportional measurements, the exploration of parameters for the hand held laser, and an experiential account of novice training are more than has been previously documented.

Directions for Further research should include:

1) using an automated multi-camera, multi-laser system for image capture to the same end of quantified skull restoration;
2) employing CT scans for the same exercise;
3) testing for compatibility and comparability between program software;
4) testing CAD programs like Imageware in comparable methods and manner.

The suggested modifications to repetition of this research include:

1) a larger sample size – minimum of 20 skulls;
2) if the same type of hand held laser was to be used, setting up the laser equipment per the recommendation of the manual so that no metal was within three feet of the operating unit;
3) ensure software and hardware are appropriately matched;
4) prepare for re-assembly by following recommended guidelines and running pre-research trials on general and specific ability levels;
5) complete facial reconstructions on a minimum of half the total sample size in order to imitate the forensic circumstances which normally accompany the need for and use of skull re-assembly;
6) establish sound secondary assessment processes (set relevant and consistent protocols for craniometry points for example).

References

Bass, W.M. (1995) *Human Osteology A Laboratory and Field Manual*. 4th ed. USA, Missouri Archaeological Society Inc.

Clement, J.G. and Marks, M.K. eds. (2005) *Computer-Graphic Facial Reconstruction.* Amsterdam, USA, Elsevier Ltd.

Colledge, H. (1996) *Loss of Face? The effect on the outcome of craniofacial reconstruction when part of the skull is missing.* MSc. thesis, University of Manchester.

Conway, G.C., Vannier, M.W. (1984) Noninvasive Three-Dimensional Computer Imaging of Matrix-Filled Fossil Skulls by High-Resolution Computed Tomography. *Science.* 226, pp. 456-458.

Davy, S.L., Gilbert, T., Schofield, D., Evison, M.P. (2005) Forensic Facial Reconstruction Using Computer Modeling Software. Chapter 10 in: *Computer-Graphic Facial Reconstruction.* Clement, J.G. and Marks, M.K. Eds. Amsterdam, Elsevier Ltd., pp. 183-196.

De Greef, S., Willems, G. (2005) Three-dimensional Cranio-Facial Reconstruction in Forensic Identification: Latest Progress and New Tendencies in the 21st century. *Journal of Forensic Science.* 50 (1), pp.6.

Dyer, G.S.M., Thorndike, M.E.L. (2000) *Quidne Mortui Vivos Docent ?* The Evolving Purpose of Human Dissection in Medical Education. *Academic Medicine.* 75(10), pp. 969-979.

Fedosyutkin, B.A., Nainys, J.V. (1993) The Relationship of Skull Morphology to Facial Features. Chapter 15 in: Iscan, M.Y., Helmer, R.P. Eds. *Forensic Analysis of the Skull: craniofacial analysis, reconstruction and identification.* New York, Wiley-Liss. pp.199-213.

FreeForm Feel the Difference: FreeForm Users Guide. Woburn, MA., USA, SensAble technologies.

Galantucci, L.M., Percoco, G., Angelelli, G., Lopez, C., Introna, F., Liuzzi, C., De Donno, A. (2006) Reverse engineering techniques applied to a human skull, for CAD 3D reconstruction and physical replication by rapid prototyping. *Journal of Medical Engineering & Technology*. 30 (2), March/April, pp.102-111.

Galloway, A., ed. (1999) *Broken Bones: Anthropological Analysis of Blunt Force Trauma.* USA, Charles C. Thomas Publishers.

Geomagic (2007*) Geomagic Inc*. [Internet]. North Carolina, USA, Available from: http://www.geomagic.com/en/products/qualify/ [Accessed 01 November 2007].

Helmer, R.P., Buzug, T.M., Hering, P. (2003). *Plastic facial reconstruction on the skull – a transition in Germany from a conventional technique to a new one* -. From: International Conference on Reconstruction of Soft Facial Parts. Potsdam/DE, (2003). Germany, BundeskRiminalment.

HyperFocal (2006) *HyperFocal Ltd*. [Internet]. UK, Available from: < http://www.hyperfocal.biz/hyperfocal/index.html > [Accessed 09 September 2007].

Iscan, M.Y., Helmer, R.P., eds. (1993) *Forensic Analysis of the Skull: craniofacial analysis, reconstruction and identification.* New York, Wiley-Liss.

Kau, C.H., Richmond, S., Zhirov, A.I., Knox, J., Chestnutt, I., Hartles, F., Playle, R. (2005) Reliability of measuring facial morphology with a 3-dimensional laser scanning system. *American Journal of Othodontics and Dentofacial Orthopedics.* 128 (4), pp. 424-430.

Klempt, A., Infantosi, A.F.C. (1992) Thee-Dimensional Reconstruction of the Human Skull using a Microcomputer. *Automedica* 15, pp. 53-161

Knott, S. (2002) *Reconstruction of Skeletal Remains: A New Technique*.

Matshes, E. , Burbridge, B. , Sher, B. Mohamed, A. , Juurlink, B. , Allen, C. (2005) *Human Osteology and Skeletal Radiology: An Atlas and Guide.* Boca Raton, CRC Press.

Mckenna, T. (1993) *History Ends in Green.* Part 6. USA, Mystic Fire Audio, [audio cassette].

Neave, R. (1986) *The reconstruction of skulls of facial reconstruction using radiographic techniques.* From: Science in Egyptology Symposia. Manchester University Press.

NeuroLogica Corporation (2007) *NeuroLogica :Inovations for a healthier world*. [Internet]. USA, Available from: <µhttp://www.neurologica.com/§> [Accessed 13 August 2007].

Park, HK., Chung, JW., Kho, HS. (2006) Use of hand-held laser scanning in the assessment of craniometry. *Forensic Science Interantional.* 160. pp. 200-206.

Polhemus (2007) *FASTCAN Cobra and Scorpion Handheld Laser Scanner User Manual.* USA.

Ponce de Leon, M.S., Zollikofer, C.P.E. (1999) New Evidence from Le Moustier 1: Computer-Assisted Reconstruction and Morphometry of the Skull. *The Anatomical Record.* 254, pp.254-474.

Prag, J., Neave, R. (1997) *Making Faces: Using forensic and archaeological evidence.* England, British Museum Press.

Quigley, C. (2001) *Skulls and Skeletons: Human Bone Collections and Accumulations*. UK, McFarland & Company Inc.

Recheis, W., Weber, G.W., Schafer, K., Knapp, R., Seidler, H., Neddon, zur Nedden, D. (1999) Virtual reality and anthropology. *European Journal of Radiology*. 31, pp.88-96.

Richmond, S. (2007) Personal communication.

Rynn, C., Wilkinson, C. (2006) Appraisal of Traditional and Recently Proposed Relationships Between the Hard and Soft Dimensions of the Nose in Profile. *American Journal of Physical Anthropology.* 130, pp. 364-373.

Scheuer, L., Black, S. (2000) *Developmental Juvenile Osteology.* UK, Elsevier Academic Press.

Schimmler, J.B., Helmer, R.P., Rieger, J. (1993) Craniometric Individuality of Human Skulls. Chapter 7 in: Iscan, M.Y., Helmer, R.P. eds. *Forensic Analysis of the Skull: Craniofacial Analysis, Reconstruction and Identification.* New York, Wiley-Liss, Inc., pp. 89-96.

Seeley, R.R., Stephens, T.D., Tate, P. (2006) *Anatomy and Physiology.*7th ed. USA, McGraw-Hill

SensAble technologies (2007) *Products and Services.*[Internet]. USA, Available from: <http://www.sensable.com/freeform-system-requirements.htm> [Accessed 18 August 2007].

Sherman, W.R., Craig, A.B. (2003) *Understanding Virtual Reality Interface, Application, and Design*. San Francisco, Morgan Kaufmann Publishers.

Subke, J. (2005) Digital 3D reconstruction of skulls from fragments using SLT and CAD/CAM tools. Chapter 9 in: Clement, J.G. And Marks, M.K., eds. *Computer-Graphic Facial Reconstruction*. Amsterdam, Elsevier Academic Press, pp.163-182.

Subke, J., Wittke, M. Germany, Kreartive Konzepte. (2005) *CAD Enhanced Soft Tissue Reconstruction in Forensics with Phantom 3D Touch – An Electronic Modelling Tool with Haptic Feedback.* From: International Conference on Reconstruction of Soft Facial Parts (2nd). Remagen.

Taylor, J.H. (2004) *Mummy: the inside story.* UK, British Museum Press.

Vanezis, P., Blowes, R.W., Linney, A.D., Tan, A.C., Richards, R., Neave, R. (1989) Application of 3-D computer graphics for facial reconstruction and comparison with sculpting techniques. *Forensic Science International.* 42, pp. 69-84.

Verhoff, M.A., Ramsthaler, F., Krahahn, J., Deml, U., Gille, R.J., Grabherr, S., Thale, M.J., Kreutz, K. (2007) Digital forensic osteology – Possibilities in cooperation with the Virtopsy project. *Forensic Science International.* Article in press.

Vialet, A., Li, T., Grimaud-Herve, D., de Lumley, MA., Liao, M., Feng, X. (2005) Proposition de reconstitution du deuxieme crane d'*Homo erectus* de Yunxian (Chine). *Comptes Rendus Palevol.* 2, pp. 265-274

Virtopsy. (2007) *University of Bern* [Internet]. Switzerland, Available from: <µhttp://www.virtopsy.com/§> [Accessed 09 September 2007].

White, T., Folkens, P.A. (2000) *Human Osteology*. 2nd ed. USA, Academic Press.

Wilson, I. (2001) *Past Lives: unlocking the secrets of our ancestors.* UK, Cassell and Company.

Wilkinson, C., Neave, R. (2001) Skull re-assembly and the implications for forensic facial reconstruction. *Science & Justice*. 41 (3), pp.5-6.

Wilkinson, C. and Whittaker, D.K. (2002) *Juvenile Forensic Facial Reconstruction: a detailed accuracy study*. From: Proceedings of the 10th meeting of IACI. Italy, Universita degli studi di bari. Pp. 98-110.

Wilkinson, C. (2004) *Forensic Facial Reconstruction*. UK, Cambridge University Press.

Wilkinson, C. (2005) Computerized Forensic Facial Reconstruction A review of Current Systems. *Forensic Science, Medicine and Pathology.* 1(3), pp. 173-177.

Wilkinson, C., Rynn, C., Peters, H., Taister, M., Kau, C.H., Richmond, S. (2006) A Blind Accuracy Assessment of Computer-Modeled Forensic Facial Reconstruction Using Computed Tomography Data From Live Subjects. *Forensic Science, Medicine and Pathology.* 2 (3), pp.179-187.

Wilkinson, C. (2007) Personal Communication.

Wind, J. (1984) Computerized X-ray Tomography of Fossil Hominid Skulls. *American Journal of Physical Anthropology.* 63, pp. 265-282.

Zollikofer, C.P.E., Ponce de Leon, M.S., Martin, R.D., Stuckl, P. (1995) Neanderthal computer skulls. *Nature.* 375, pp. 283-285

Zollikofer, C.P.E., Ponce de Leon, M.S., Martin, R.D. (1998) Computer-Assisted Paleoanthropology. *Evolutionary Anthropology*. 6(2), pp.41-54.

Zollikofer, C.P.E. (2002) A Computational Approach to Paleoanthropology. *Evolutionary Anthropology.* Supplemental 1, pp. 64-67

Zollikofer, C.P.E., Ponce de Leon, M.S. (2005) *Virtual Reconstruction: A Primer in Computer-Assisted Paleontology and Biomedicine*. USA, John Wiley & Sons, Inc.

Zollikofer, C.P.E., Ponce de Leon, M.S., Lieberman, D.E., Guy, F., Pilbeam, D., Liklus, A., Mackaye, H.T., Bignaud, P., Brunet, M. (2005) Virtual cranial reconstruction of *Sahelanthropus tchadensis*. *Nature* 434, pp.755-759.

Bibliography

Berryman, H.G., Symes, S.A. (1998) Recognizing Gunshot and Blunt Cranial Trauma through Fracture Interpretation. In: Reiches, K.J. ed. *Forensic Osteology: Advances in the Identification of Human Remains.* 2nd ed. USA, Charles C. Thomas Publishers Ltd, pp. 333-352.

Catteneo, C. (2007) Forensic anthropology: developments of a classical discipline in the new millennium. *Forensic Science International.* 165, pp. 185-193.

Cullinane, D.M., Einhorn, T.A. (2002) Biomechanics of Bone. In: Belezikean, J.P., Raisz, L.G., Rodan, G.A. Eds. *Principles of Bone Biology* 2nd ed. Academic Press. pp. 17-32.

De Greef, S., Willems, G. (2005) Three-dimensional Cranio-Facial Reconstruction in Forensic Identification: Latest Progress and New Tendencies in the 21st century. *Journal of Forensic Science.* 50 (1), pp.6.

DiMaio, V.J. and DiMaio, D. (2001) *Forensic Pathology.* 2nd ed. Boca Raton, CRC Press.

Donaldson, R.R. (2004) *An Introductory Course In Forensic Human Osteology.* 3rd ed. Canada, University of Victoria.

Fenton, T.W., Stefan, V.H., Wood, L.A., Sauer, N.J. (2005) Symmetrical Fracturing of the Skull from Midline Contact Gunshot Wounds: Reconstruction of Individual Death Histories from Skeletonized Human Remains. *Journal of Forensic Science.* 50 (2), pp. 1-12.

Galloway, A. (1999) Fracture Patterns And Skeletal Morphology: Introduction And The Skull. In: Galloway, A. ed. *Broken Bones: Anthropological Analysis of Blunt Force Trauma.* USA, Charles C. Thomas Publishers Ltd, pp. 63-80.

Galloway, A. (1999) The Biomechanics Of Fracture Production. In: Galloway, A. ed. *Broken Bones: Anthropological Analysis of Blunt Force Trauma.* USA, Charles C. Thomas Publishers Ltd, pp. 35-62.

Gurdjian, E.S. And Lissner, H.R. (1946) Deformations of the skull in head injury studied by the "stresscoat" technique, quantitative determinations. *Surgery, gynecology and obstetrics.* 83 July-December, pp.219-233.

Gurdjian, E.S. And Lissner, H.R. (1947) Deformations of the skull in head injury as studied by the "stresscoat" technic. *The American Journal of Surgery.* January-June, pp. 269-281.

Gurdjian, E.S., Webster, J.E., Lissner, H.R. (1953) Observations on Prediction of Fracture Site in Head Injury. *Radiology.* 60 January-June, pp. 226-235.

Gurdjian, E.S. (1975) *Impact Head Injury: Mechanistic, clinical and preventive correlations.* USA, Charles C. Thomas.

Guo, X.E. (2001) Mechanical Properties of Cortical Bone and Cancellous Bone Tissue. In: Cowin, S.C. ed. *Bone Mechanics Handbook*. 2nd ed. USA, CRC Press, pp. 10/1-10/5.

Iscan, M.Y. (2002) Global forensic anthropology in the 21st century. *Forensic Science International.* 117, pp. 1-6.

Jepsen, K.J., Davy, D.T. Akkus, O. (2001) Observation of Damage in Bone. In: Cowin, S.C. ed. (2001) *Bone Mechanics Handbook*. 2nd ed. USA, CRC Press, pp. 17/1-17/9.

Klempt, A., Infantosi, A.F.C. (1992) Thee-Dimensional Reconstruction of the Human Skull using a Microcomputer. *Automedica* 15, pp. 53-161.

Knight, B. (1996) *Forensic Pathology.* 2nd ed. London, Oxford University Press.

Kroman, A.M. (2004). *Experimental Study of Fracture Propagation in the Human Skull: A Re-Testing of Popular Theories*. Dallas, Texas. American Academy of Forensic Sciences.

Lakes, R. (2001) Viscoelastic Properties of Cortical Bone. In: Cowin, S.C. ed. *Bone Mechanics Handbook*. 2nd ed. USA, CRC Press, pp. 11/1-11/15.

LeCount, E.R., Apfelbach, C.W. (1920) Pathologic Anatomy of Traumatic Fractures of Cranial Bones. *Journal of American Medical Association.* 74(8), pp. 501-511.

Luchinetti, E. (2001) Composite Models of Bone Properties. In: Cowin, S.C. ed. *Bone Mechanics Handbook*. 2nd ed. USA, CRC Press, pp. 12/14-12/15.

Lynnerup, N., Hjalgrim, H., Nielsen, L.R., Gregersen, H., Thuesen, I. (1997) Non-invasive Archaeology of Skeletal Material by CT Scanning and Three-dimensional Reconstruction. *International Journal of Osteoarchaeology.* 7. pp.91-94.

Mehta, B.V., Marinescu, R. (2002) *Comparison of image generation and processing techniques for 3D reconstruction of the human skull.* From: International Mechanical Engineering Congress & Exposition, New Orleans, Louisiana.

Moss, J.P., Linney, A.D. Grindrod, S.R., Arridge, S.R., Clifton, J.S. (1987) Three-dimensional visualization of the face and skull using computerized tomography and laser scanning techniques. *European Journal of Orthodontics.* 9,pp. 247-253.

Rogers, L.F. ed. (2002) Radiology of Skeletal Trauma. 3rd ed. Vol. 1. USA, Churchill Livingstone.

Science Photo Library (2004) *Inside the body: fantastic Images from Beneath the Skin.* UK, Cassell Illustrated.

Seeley, R.R., Stephens, T.D., Tate, P. (2006) *Anatomy and Physiology.*7th ed. USA, McGraw-Hill.

Stephan, C.N., Henneberg, M. (2001) Building Faces from Dry Skulls: Are They Recognized Above Chance Rates ? *Journal of Forensic Science.* 46, pp. 432-440.

Stephan, C.N. (2003) Anthropological facial 'reconstruction' – recognizing the fallacies, 'unembracing' the errors, and realizing method limits. *Science and Justice*. 43 (4), pp. 193-200.

Stephan, C.N., Henneberg, M. (2006) Recognition by forensic facial approximation: Case specific examples and empirical tests. *Forensic Science International.* 156, pp. 182-191.

Tubbs, R.S., Salter, E.G., Oakes, W.J. (2006) Artificial Deformation of the Human Skull: A review. *Clinical Anatomy.*19, pp. 372-377.

Turner, C.H. and Burr, D.B. (2001) Experimental Techniques for Bone Mechanics. In: Cowin, S.C. ed. *Bone Mechanics Handbook*. 2nd ed. USA, CRC Press, pp. 17/1-17/5.

Wilkinson, C. (2003) "Virtual Sculpture" as a method of computerized reconstruction. *International Conference on Reconstruction of Soft Facial Parts.* Potsdam, European Commission-Directorate General Justice and Home Affairs.

Appendix 1

Measured differences between original and re-assembled cranium images in Photoshop comparisons (with percentages).

crania	original			re-assembled			difference			percentage			% totals		
	width	length	height	width	length	height	width	length	height	width	length	height	<	>	< & >
A	9.03	18.97	16.76	9.03	18.60	16.76	0	0.37<	0	0	1.95<	0	1.95	0	1.95
B	15.45	19.10	15.59	15.08	18.79	15.65	0.37<	0.31<	0.06>	2.39<	1.62<	0.38>	4.01	0.38	4.39
C	14.76	18.35	18.64	14.92	18.35	18.82	0.16>	0	0.18>	1.08>	0	0.96>	0	2.04	2.04
D	16.62	25.33	23.44	16.40	24.20	23.50	0.22<	1.13<	0.06>	1.32<	4.46<	0.25>	5.78	0.25	6.03
E	15.01	20.99	18.87	14.54	20.20	18.72	0.47<	0.79<	0.15<	3.13<	3.76<	0.79<	7.68	0	7.68

Distance measurements are in centimetres; **<** means the distance (or percentage) figure is that much **less** than the original;
> means the distance (or percentage) figure is that much **more** than the original

Measured differences between original and re-assembled mandible images in Photoshop comparisons (with percentages).

Mandible	**original**			**re-assembled**			**difference**			**percentages**			**% totals**		
	width	length	height	width	length	height	width	length	height	width	length	height	<	>	< & >
A	19.60	11.99	14.46	18.68	12.45	13.90	0.92<	0.46>	0.56<	4.69<	3.83>	3.87<	8.56	3.83	12.39
B	16.74	17.46	10.95	16.16	18.09	10.69	0.58<	0.63>	0.26<	3.46<	3.60>	2.37<	5.83	3.60	9.43
C	15.93	10.05	11.66	14.92	10.74	11.29	1.01<	0.69>	0.37<	6.34<	6.86>	3.17<	9.51	6.86	16.37
D	14.80	14.71	8.76	14.80	14.13	8.73	0	0.58<	0.03<	0	3.94<	0.34<	4.28	0	4.28
E	16.79	13.58	10.65	17.96	13.02	10.27	1.17>	0.56<	0.38<	6.96>	4.12<	3.56<	7.68	6.96	14.64

Distance measurements are in centimetres; < means the distance (or percentage) figure is that much **less** than the original;
> means the distance (or percentage) figure is that much **more** than the original

Appendix 2

Summary of shell deviations for craniums A-E.

cranium	A	B	C	D	E
average +/- deviation (mm)	+3 /-2.8	+1.4/ -2.6	+2.3/ -2	3.5 /-2.9	3 /-2.3
standard deviation (mm)	3.7	2.8	3	4	3.5
% within +/- 2.1 mm	56	64	70	54	64
% between +/- 2.1 and +/- 5.3 mm	31.5	24	23.5	29	25
% between +/- 5.3 and +/- 10 mm	12	11.5	6	17	11
% outside maximum and minimum tolerance	0	0	0	0	0

Summary of shell deviations for mandibles A-E.

mandible	A	B	C	D	E
average +/- deviation (mm)	1.3 / - 2.5	+1 /-1	1.7 / -2.3	1.4 /-1.6	1 /-1.8
standard deviation (mm)	2.4	1.6	2.6	2	2
% within +/- 2.1 mm	66	88	66	82	77
% between +/- 2.1 and +/- 5.3 mm	31	12	31	17	22
% between +/- 5.3 and +/- 10 mm	3	0.2	3	1	1
% outside maximum and minimum tolerance	0	0	0	0	0

(Numbers are rounded to the nearest decimal)

Appendix 3

Cranium A shell deviation tables.

Reference Model	skull A cranium
Test Model	# skull A
# Data Points	560927

Tolerances	mm
Max Tol +	10.000
Min Tol +	0.500
Min Tol -	-0.500
Max Tol -	-10.000

Deviation	mm
Max Dev +	9.200
Max Dev -	-9.200
Average +/-	3.153 / -2.765
Std Dev	3.715

Percentage Deviations

>=Min	<Max	# Points	%
-10.000	-8.417	4037	0.720
-8.417	-6.833	12574	2.242
-6.833	-5.250	26560	4.735
-5.250	-3.667	37723	6.725
-3.667	-2.083	52293	9.323
-2.083	-0.500	98413	17.545
-0.500	0.500	62750	11.187
0.500	2.083	90091	16.061
2.083	3.667	64489	11.497
3.667	5.250	54927	9.792
5.250	6.833	31827	5.674
6.833	8.417	18676	3.329
8.417	10.000	6567	1.171

Out of Max Tol +	0	0.000
Out of Max Tol -	0	0.000

Standard Deviations

Distribution ()	# Points	%
-6 * Std Dev	0	0.000
-5 * Std Dev	0	0.000
-4 * Std Dev	0	0.000
-3 * Std Dev	0	0.000
-2 * Std Dev	35732	6.370
-1 * Std Dev	107703	19.201
1 * Std Dev	229779	40.964
2 * Std Dev	138541	24.699
3 * Std Dev	49172	8.766
4 * Std Dev	0	0.000
5 * Std Dev	0	0.000
6 * Std Dev	0	0.000

Cranium A shell deviation maps

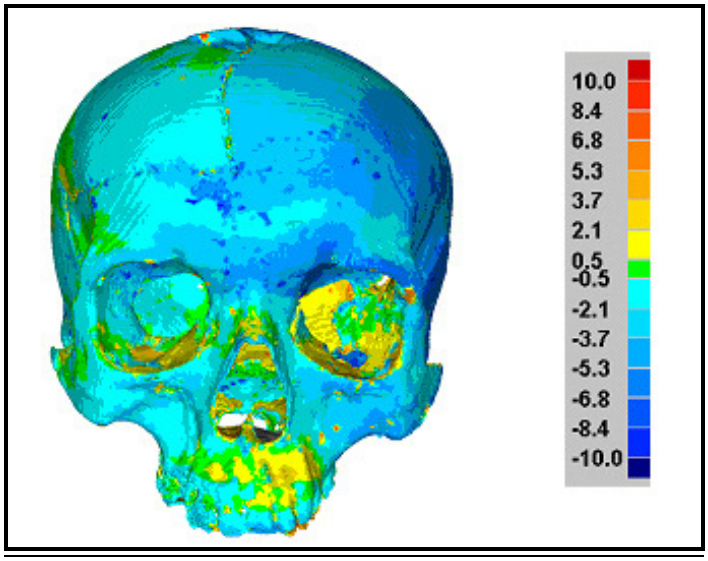

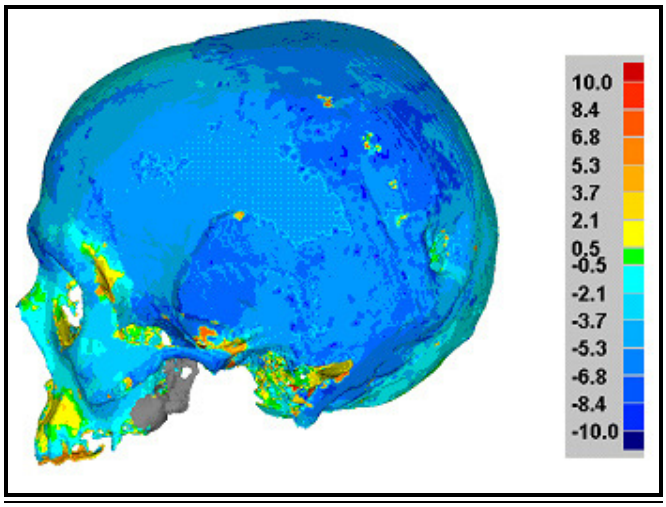

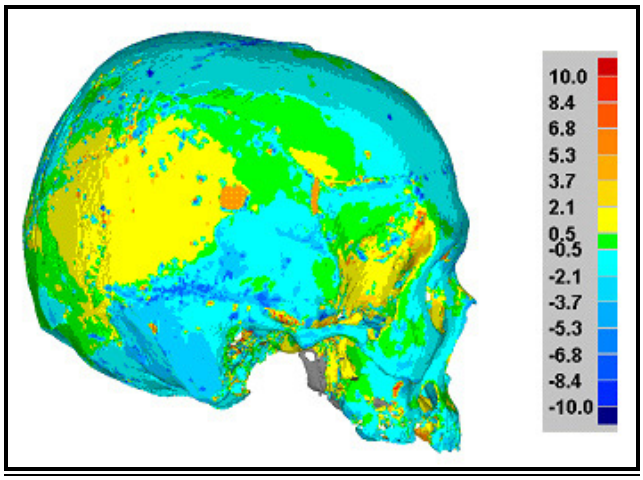
10.0
8.4
6.8
5.3
3.7
2.1
0.5
-0.5
-2.1
-3.7
-5.3
-6.8
-8.4
-10.0

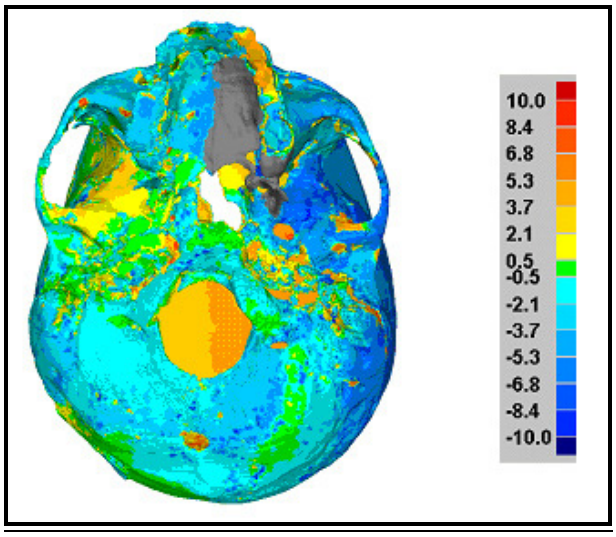
10.0
8.4
6.8
5.3
3.7
2.1
0.5
-0.5
-2.1
-3.7
-5.3
-6.8
-8.4
-10.0

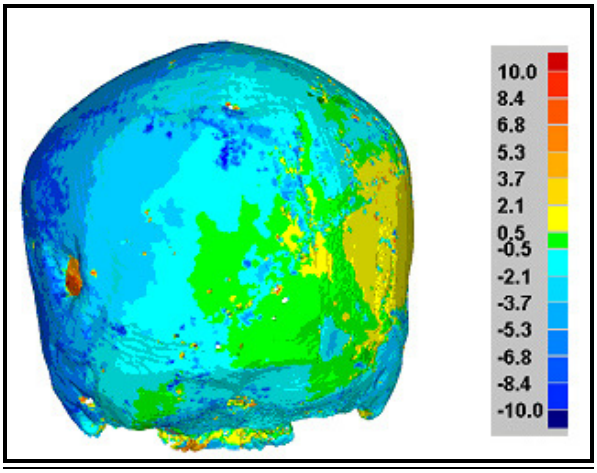
10.0
8.4
6.8
5.3
3.7
2.1
0.5
-0.5
-2.1
-3.7
-5.3
-6.8
-8.4
-10.0

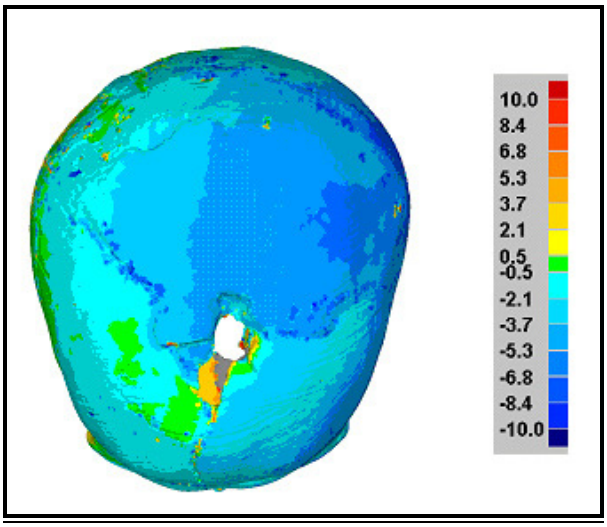
10.0
8.4
6.8
5.3
3.7
2.1
0.5
-0.5
-2.1
-3.7
-5.3
-6.8
-8.4
-10.0

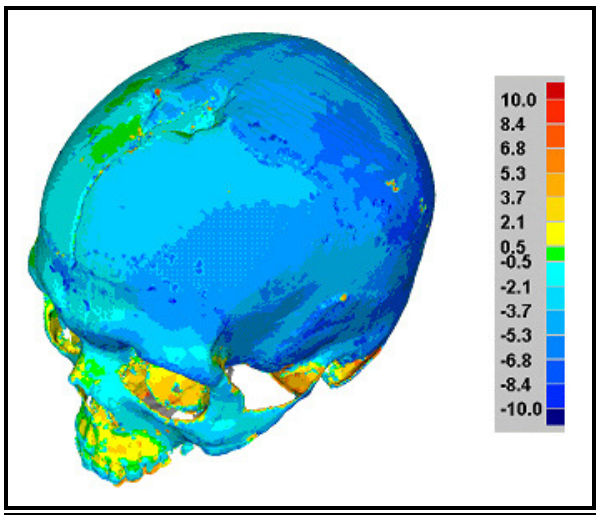

Cranium A standard deviations

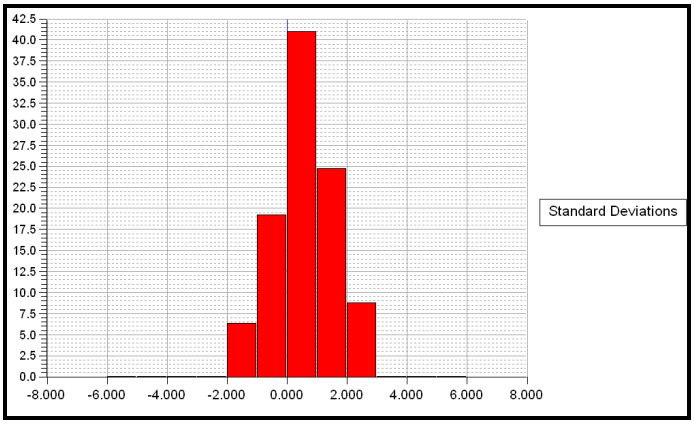

Cranium A deviation distribution.

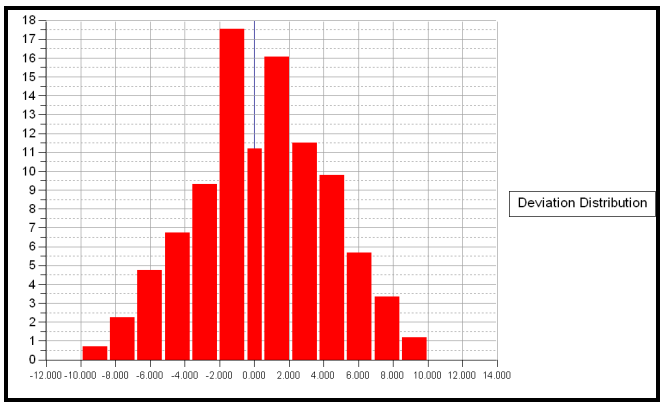

Vertical axis = percentage;
horizontal axis = millimetres

Cranium A annotated map and table.

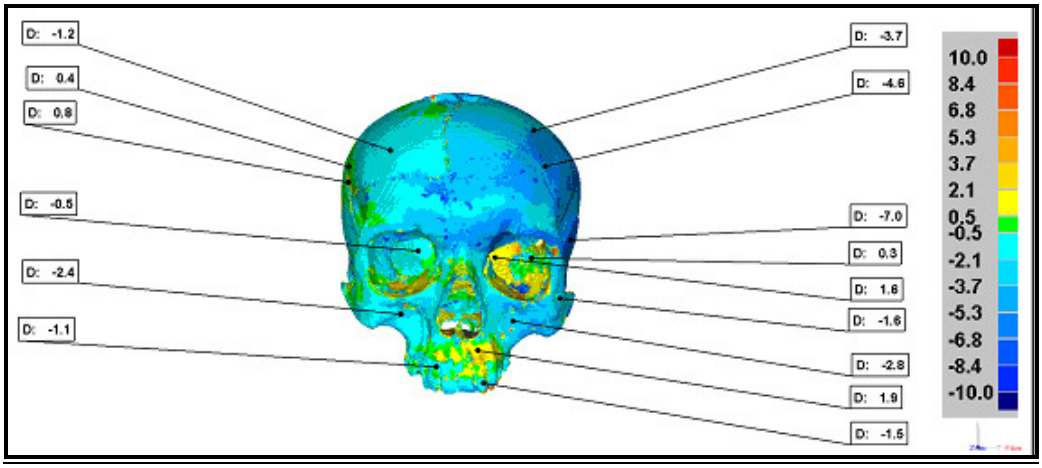

Name	Dev	Ref X	Ref Y	Ref Z	Dev Radius	Dev X	Dev Y	Dev Z	Test X	Test Y	Test Z
A001	-4.566	44.864	67.839	-12.504	1.000	-3.484	-1.568	-2.501	41.381	66.271	-15.005
A002	-7.006	64.117	27.854	-61.974	1.000	-6.216	2.217	-2.353	57.901	30.071	-64.328
A003	-1.577	53.380	-3.060	-17.370	1.000	-1.430	-0.359	-0.559	51.949	-3.419	-17.929
A004	-2.771	27.649	-14.352	-8.004	1.000	-0.500	1.079	-2.502	27.149	-13.274	-10.507
A005	-1.499	11.543	-44.341	9.765	1.000	-0.624	-0.044	-1.363	10.919	-44.386	8.403
A006	1.935	8.767	-28.421	3.675	1.000	0.618	0.859	1.620	9.385	-27.562	5.295
A007	1.562	23.391	14.711	-156.845	1.000	-0.607	0.471	1.360	22.783	15.182	-155.486
A008	0.283	38.756	18.413	-26.546	1.000	-0.175	0.015	0.222	38.580	18.428	-26.324
A009	-3.690	40.236	88.758	-28.749	1.000	-1.999	-2.628	-1.646	38.237	86.129	-30.395
A010	-1.153	-37.142	75.799	-6.072	1.000	0.692	-0.658	-0.646	-36.450	75.141	-6.718
A011	0.397	-64.725	70.431	-52.469	1.000	-0.383	0.063	0.084	-65.108	70.494	-52.385
A012	0.766	-65.095	61.360	-52.731	1.000	-0.734	-0.043	0.214	-65.829	61.317	-52.517
A013	-0.455	-29.553	19.339	-154.224	1.000	-0.157	-0.151	-0.399	-29.710	19.188	-154.624
A014	-2.390	-31.589	-10.465	-5.812	1.000	-0.524	1.370	-1.887	-32.113	-9.095	-7.699
A015	-1.057	-12.522	-36.011	9.379	1.000	0.363	0.137	-0.984	-12.159	-35.875	8.395

Units: mm

Mandible A shell deviation tables.

Reference Model	skull A mand
Test Model	# mand
# Data Points	146726

Tolerances	mm
Max Tol +	10.000
Min Tol +	0.500
Min Tol -	-0.500
Max Tol -	-10.000

Deviation	mm
Max Dev +	5.700
Max Dev -	-5.700
Average +/-	1.316 / -2.497
Std Dev	2.446

Percentage Deviations

>=Min	<Max	# Points	%
-10.000	-8.417	0	0.000
-8.417	-6.833	0	0.000
-6.833	-5.250	4875	3.323
-5.250	-3.667	17946	12.231
-3.667	-2.083	20526	13.989
-2.083	-0.500	23337	15.905
-0.500	0.500	33334	22.719
0.500	2.083	32902	22.424
2.083	3.667	7335	4.999
3.667	5.250	5271	3.592
5.250	6.833	1200	0.818
6.833	8.417	0	0.000
8.417	10.000	0	0.000

Out of Max Tol +	0	0.000
Out of Max Tol -	0	0.000

Standard Deviations

Distribution ()	# Points	%
-6 * Std Dev	0	0.000
-5 * Std Dev	0	0.000
-4 * Std Dev	0	0.000
-3 * Std Dev	0	0.000
-2 * Std Dev	22807	15.544
-1 * Std Dev	32880	22.409
1 * Std Dev	69013	47.035
2 * Std Dev	15565	10.608
3 * Std Dev	6461	4.403
4 * Std Dev	0	0.000
5 * Std Dev	0	0.000
6 * Std Dev	0	0.000

Mandible A shell deviation maps.

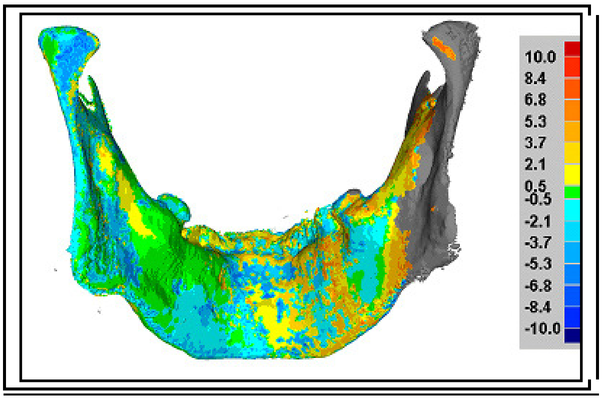

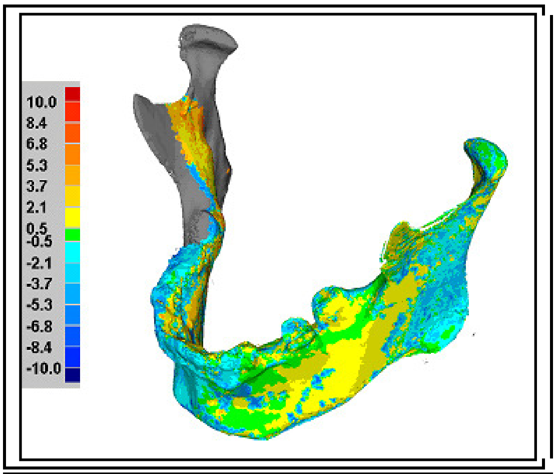

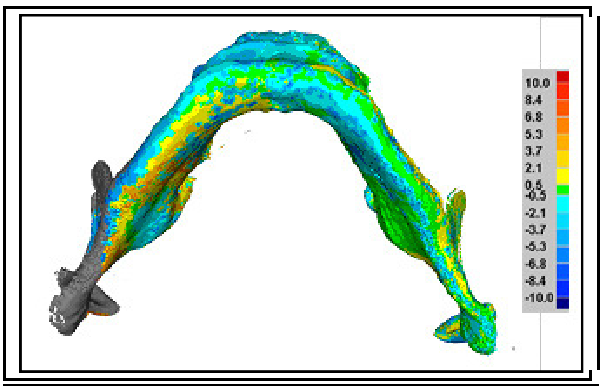

Mandible A annotated map and deviation table.

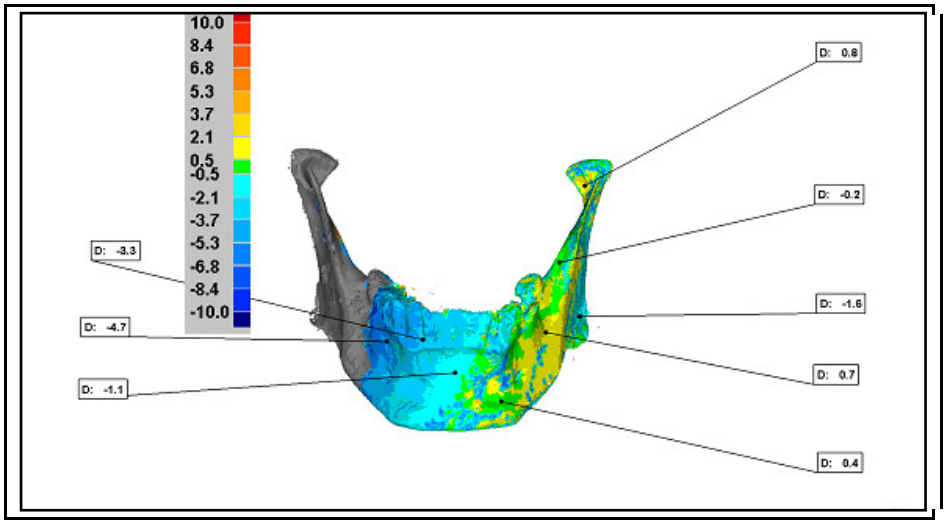

Name	Dev	Ref X	Ref Y	Ref Z	Dev Radius	Dev X	Dev Y	Dev Z	Test X	Test Y	Test Z
A001	0.758	45.472	-11.623	-69.093	1.000	-0.326	0.042	0.683	45.146	-11.581	-68.409
A002	-0.161	33.868	-39.581	-45.398	1.000	0.068	-0.038	-0.141	33.936	-39.619	-45.539
A003	-1.640	43.104	-58.427	-64.729	1.000	-1.490	-0.290	-0.620	41.613	-58.717	-65.349
A004	0.660	28.322	-62.555	-33.854	1.000	0.505	0.087	0.415	28.827	-62.468	-33.438
A005	0.353	13.055	-82.851	-14.363	1.000	0.166	0.155	0.270	13.221	-82.697	-14.093
A006	-1.129	-1.079	-73.418	-7.498	1.000	0.100	0.179	-1.111	-0.979	-73.238	-8.608
A007	-4.690	-22.160	-64.628	-17.867	1.000	3.506	1.100	-2.914	-18.654	-63.529	-20.781
A008	-3.261	-10.670	-63.243	-4.016	1.000	1.867	-0.473	-2.632	-8.803	-63.716	-6.648

Units: mm.

Mandible A standard deviations

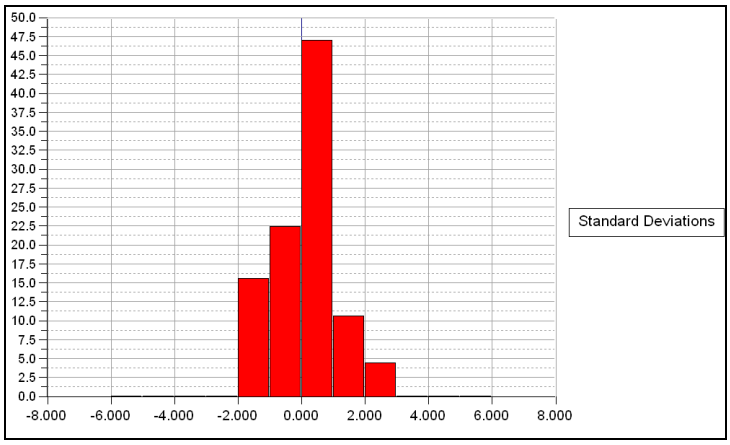

Mandible A deviation distribution

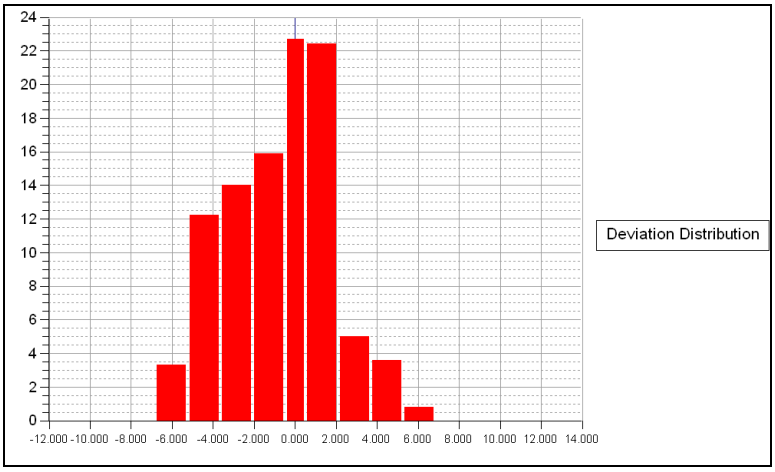

.

Vertical axis = percentage;
horizontal axis = millimetres

Skull A comparison and superimposition.

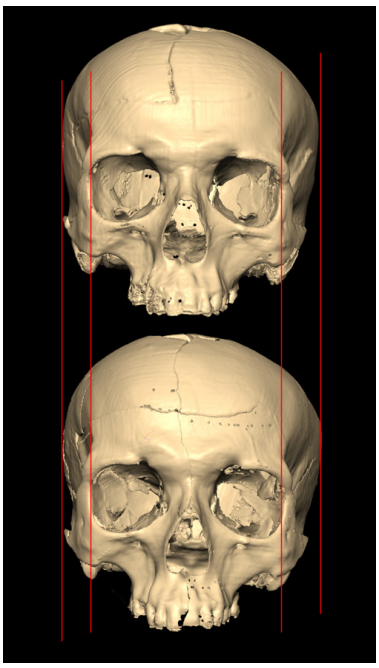

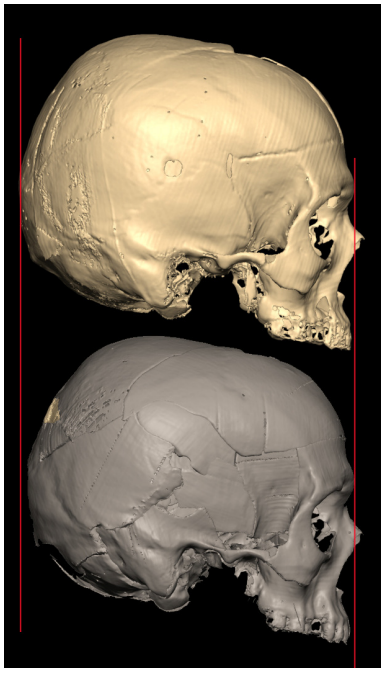

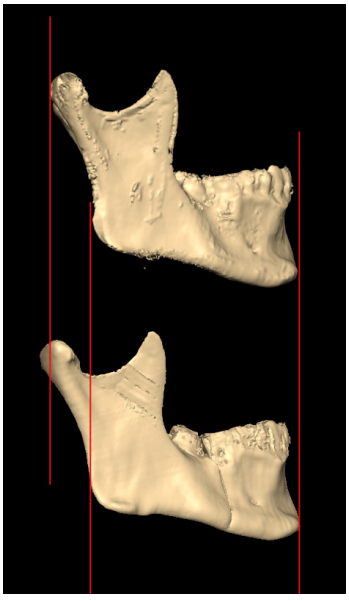

Lower image = after restoration

Appendix 4

Cranium B shell deviation tables.

Reference Model	skull B cranium
Test Model	# skull B cranium
# Data Points	146542

Tolerances	mm
Max Tol +	10.000
Min Tol +	0.500
Min Tol -	-0.500
Max Tol -	-10.000

Deviation	mm
Max Dev +	9.291
Max Dev -	-9.300
Average +/-	1.431 / -2.572
Std Dev	2.842

Percentage Deviations

>=Min	<Max	# Points	%
-10.000	-8.417	2495	1.703
-8.417	-6.833	5630	3.842
-6.833	-5.250	7556	5.156
-5.250	-3.667	13269	9.055
-3.667	-2.083	18683	12.749
-2.083	-0.500	37014	25.258
-0.500	0.500	37939	25.890
0.500	2.083	14772	10.080
2.083	3.667	4433	3.025
3.667	5.250	2261	1.543
5.250	6.833	1292	0.882
6.833	8.417	856	0.584
8.417	10.000	342	0.233

Out of Max Tol +	0	0.000
Out of Max Tol -	0	0.000

Standard Deviations

Distribution ()	# Points	%
-6 * Std Dev	0	0.000
-5 * Std Dev	0	0.000
-4 * Std Dev	0	0.000
-3 * Std Dev	7133	4.868
-2 * Std Dev	15536	10.602
-1 * Std Dev	36805	25.116
1 * Std Dev	75053	51.216
2 * Std Dev	8264	5.639
3 * Std Dev	2710	1.849
4 * Std Dev	1041	0.710
5 * Std Dev	0	0.000
6 * Std Dev	0	0.000

Cranium B shell deviation maps.

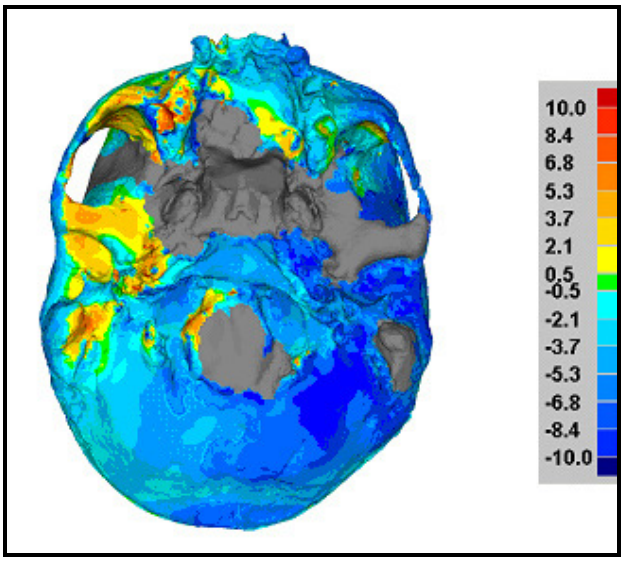

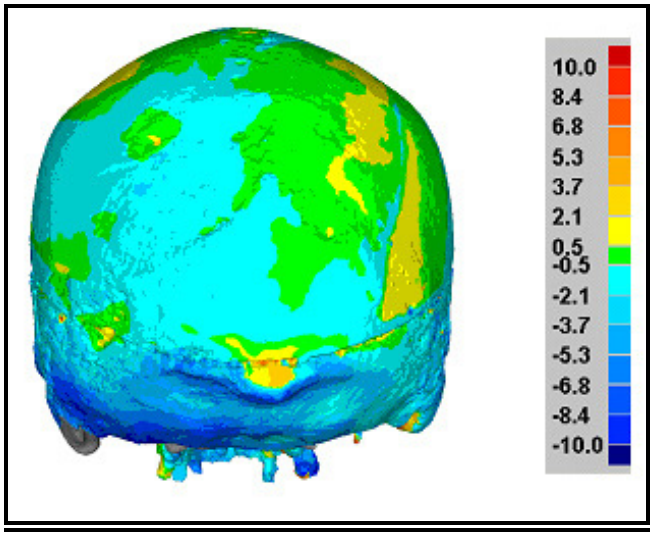

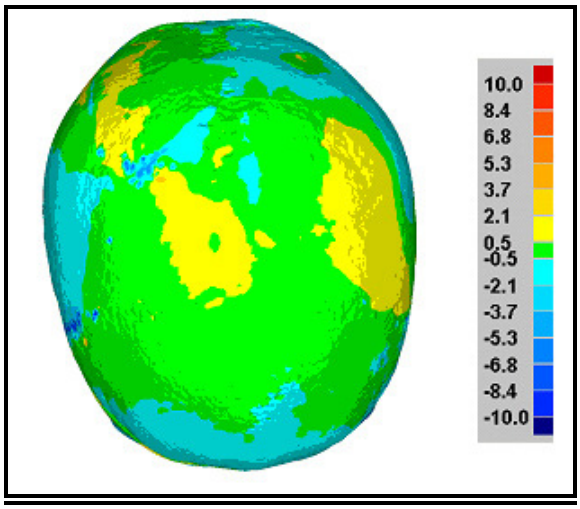
10.0
8.4
6.8
5.3
3.7
2.1
0.5
-0.5
-2.1
-3.7
-5.3
-6.8
-8.4
-10.0

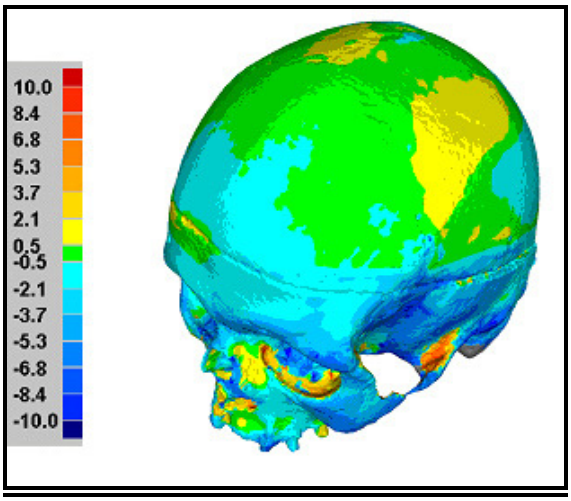
10.0
8.4
6.8
5.3
3.7
2.1
0.5
-0.5
-2.1
-3.7
-5.3
-6.8
-8.4
-10.0

Cranium B annotated map and deviation table

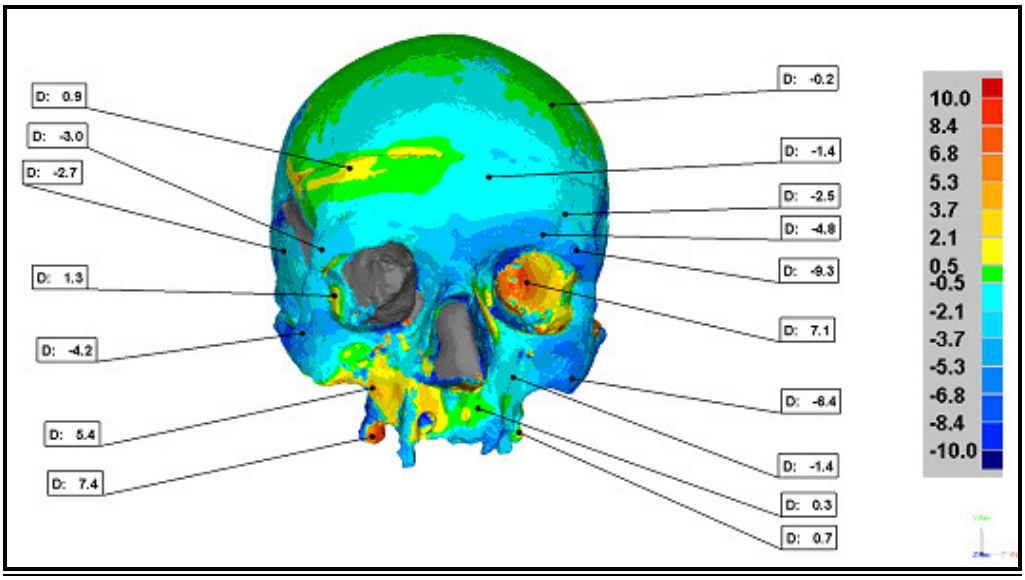

Name	Dev	Ref X	Ref Y	Ref Z	Dev Radius	Dev X	Dev Y	Dev Z	Test X	Test Y	Test Z
A001	-1.366	17.888	53.407	-4.885	1.000	-0.232	0.136	-1.339	17.656	53.543	-6.225
A002	-2.540	47.239	39.694	-14.760	1.000	-1.607	-0.375	-1.931	45.631	39.319	-16.691
A003	-4.821	38.301	31.893	-8.078	1.000	-1.613	1.919	-4.118	36.688	33.812	-12.196
A004	-9.274	51.604	25.718	-14.505	1.000	-5.018	-1.466	-7.661	46.586	24.252	-22.166
A005	7.120	34.946	12.352	-47.650	1.000	-4.851	1.533	4.981	30.096	13.885	-42.668
A006	-6.412	51.130	-24.591	-27.105	1.000	-4.224	1.363	-4.627	46.905	-23.227	-31.731
A007	-1.356	27.740	-23.123	-19.378	1.000	-0.916	0.139	-0.991	26.824	-22.984	-20.369
A008	0.735	30.884	-46.749	-34.019	1.000	0.450	-0.116	0.570	31.334	-46.865	-33.449
A009	0.266	13.946	-33.983	-10.230	1.000	0.116	0.038	0.237	14.063	-33.945	-9.993
A010	-0.219	43.783	83.224	-31.980	1.000	-0.132	-0.135	-0.110	43.651	83.090	-32.090
A011	0.879	-34.634	57.108	-11.807	1.000	-0.469	0.082	0.739	-35.102	57.190	-11.068
A012	-2.738	-66.426	24.922	-67.617	1.000	2.492	0.340	-1.082	-63.934	25.263	-68.699
A013	-3.015	-45.212	26.138	-12.453	1.000	1.602	-0.120	-2.551	-43.611	26.018	-15.004
A014	-4.183	-54.277	-6.879	-28.486	1.000	3.121	-0.528	-2.735	-51.156	-7.407	-31.221
A015	5.356	-26.678	-27.783	-22.956	1.000	-2.568	-2.280	4.110	-29.246	-30.063	-18.846
A016	7.366	-27.015	-47.691	-29.451	1.000	1.622	-1.213	7.082	-25.393	-48.904	-22.368
A017	1.277	-41.696	7.937	-27.816	1.000	1.138	0.225	0.534	-40.558	8.163	-27.283

Units = mm.

Cranium B standard deviations

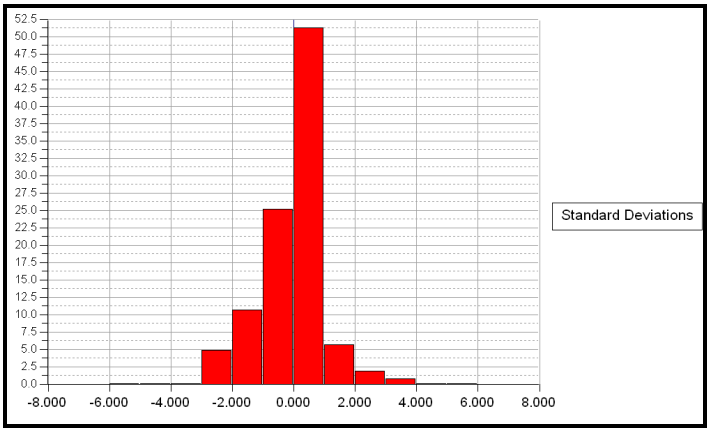

Cranium B deviation distribution.

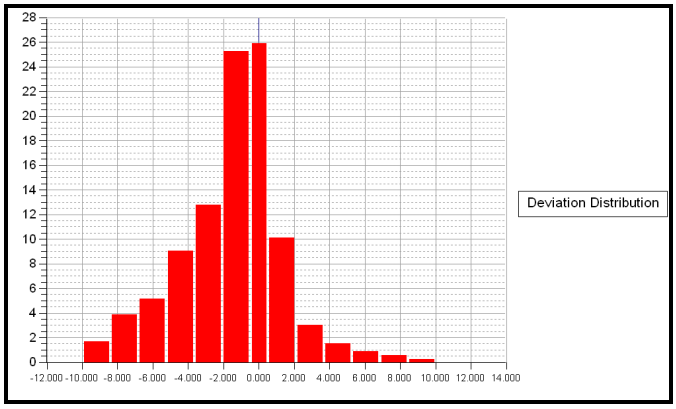

Vertical axis = percentage;
horizontal axis = millimetres

Mandible B shell deviation tables.

Reference Model	skull B mand
Test Model	# skull b mandible
# Data Points	41905

Tolerances	mm
Max Tol +	10.000
Min Tol +	0.500
Min Tol -	-0.500
Max Tol -	-10.000

Deviation	mm
Max Dev +	5.831
Max Dev -	-6.299
Average +/-	0.971 / -1.158
Std Dev	1.617

Percentage Deviations

>=Min	<Max	# Points	%
-10.000	-8.417	0	0.000
-8.417	-6.833	0	0.000
-6.833	-5.250	82	0.196
-5.250	-3.667	1022	2.439
-3.667	-2.083	3107	7.414
-2.083	-0.500	5529	13.194
-0.500	0.500	21975	52.440
0.500	2.083	5923	14.134
2.083	3.667	3315	7.911
3.667	5.250	910	2.172
5.250	6.833	42	0.100
6.833	8.417	0	0.000
8.417	10.000	0	0.000

Out of Max Tol +	0	0.000
Out of Max Tol -	0	0.000

Standard Deviations

Distribution ()	# Points	%
-6 * Std Dev	0	0.000
-5 * Std Dev	0	0.000
-4 * Std Dev	51	0.122
-3 * Std Dev	584	1.394
-2 * Std Dev	2891	6.899
-1 * Std Dev	4276	10.204
1 * Std Dev	26191	62.501
2 * Std Dev	4369	10.426
3 * Std Dev	3090	7.374
4 * Std Dev	447	1.067
5 * Std Dev	6	0.014
6 * Std Dev	0	0.000

Mandible B shell deviation maps.

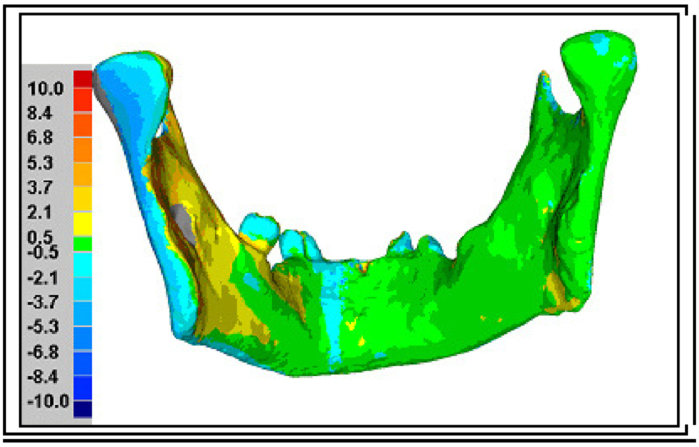

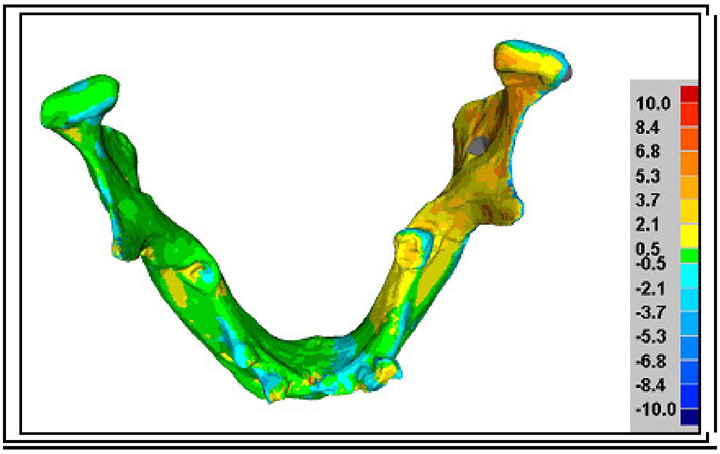

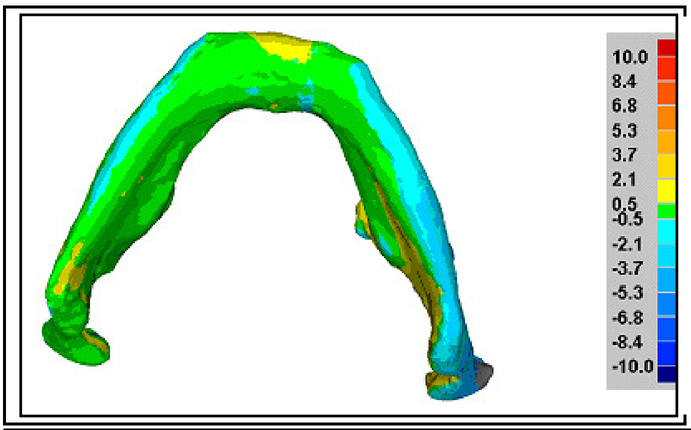

Mandible B annotated map and deviation table.

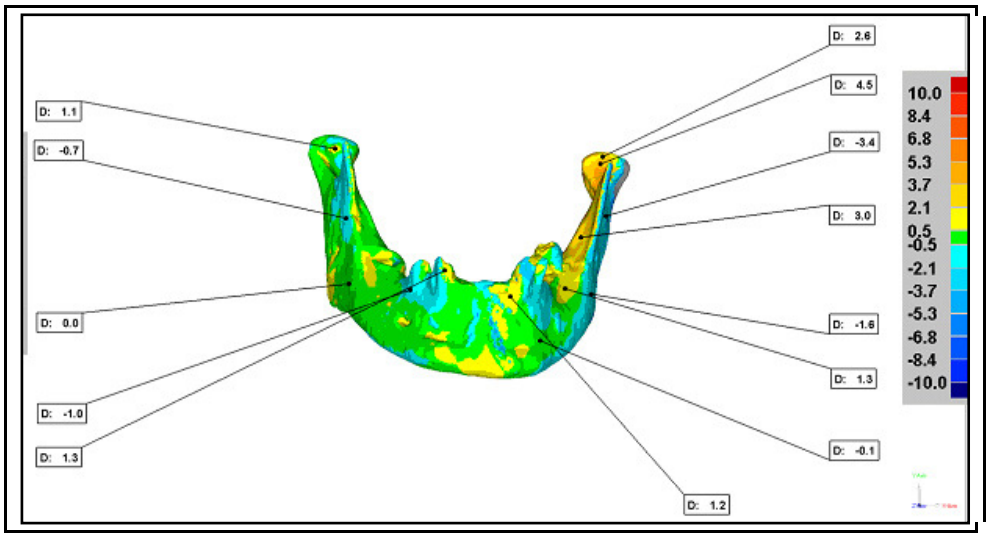

Name	Dev	Ref X	Ref Y	Ref Z	Dev Radius	Dev X	Dev Y	Dev Z	Test X	Test Y	Test Z
A001	3.011	38.865	-47.402	-52.261	1.000	-1.175	1.478	2.346	37.691	-45.924	-49.915
A002	2.572	50.719	-14.956	-83.043	1.000	-0.253	0.507	2.508	50.466	-14.448	-80.535
A003	-3.384	49.582	-39.182	-63.883	1.000	-3.118	0.011	-1.315	46.464	-39.171	-65.198
A004	-1.569	41.536	-67.990	-43.357	1.000	-1.485	-0.101	-0.498	40.052	-68.091	-43.855
A005	1.290	31.480	-65.642	-34.994	1.000	0.485	0.990	0.669	31.965	-64.652	-34.325
A006	-0.108	21.194	-81.845	-11.020	1.000	-0.076	-0.023	-0.074	21.118	-81.868	-11.094
A007	1.224	11.190	-67.016	-5.203	1.000	0.431	-0.447	1.055	11.621	-67.463	-4.148
A008	1.321	-9.770	-58.397	-1.977	1.000	0.398	0.166	1.248	-9.373	-58.230	-0.729
A009	-0.961	-21.520	-65.239	-14.128	1.000	0.756	-0.090	-0.586	-20.764	-65.330	-14.714
A010	0.006	-44.173	-63.981	-35.060	1.000	-0.006	0.001	0.002	-44.179	-63.980	-35.058
A011	-0.693	-46.232	-40.568	-43.280	1.000	0.538	-0.007	-0.437	-45.694	-40.575	-43.717
A012	1.098	-54.073	-12.625	-73.609	1.000	-0.169	-0.295	1.044	-54.241	-12.920	-72.565
A013	4.472	49.901	-17.791	-83.583	1.000	0.020	-1.664	4.151	49.920	-19.454	-79.432

Units: mm

Mandible B standard deviations

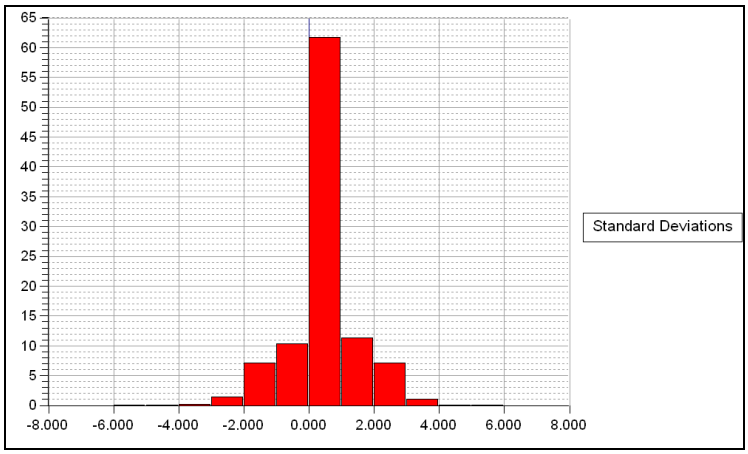

.

Mandible B deviation distribution.

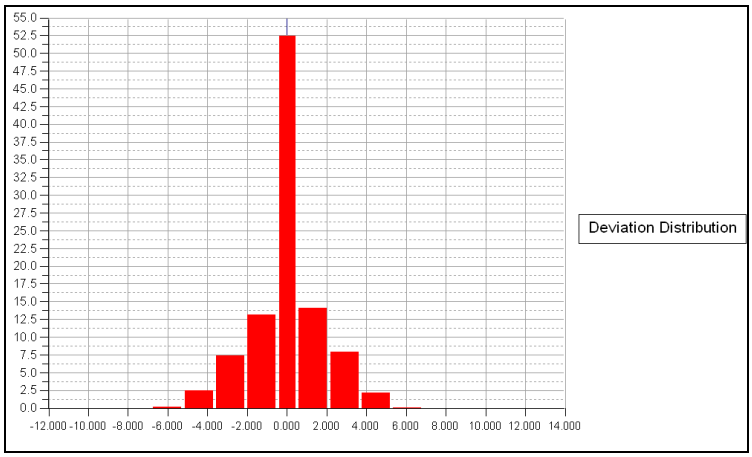

Vertical axis = percentage;
horizontal = millimetres

Skull B comparison and superimposition.

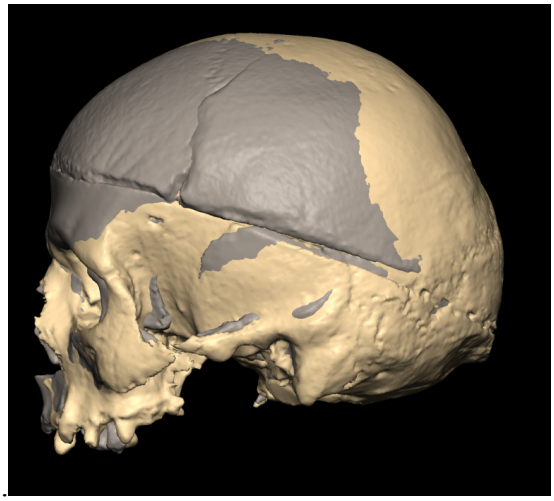

Cream = before restoration; grey = after restoration

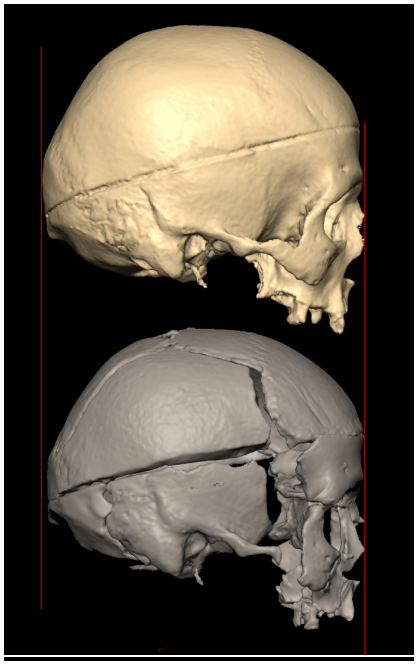

Bottom position = after restoration

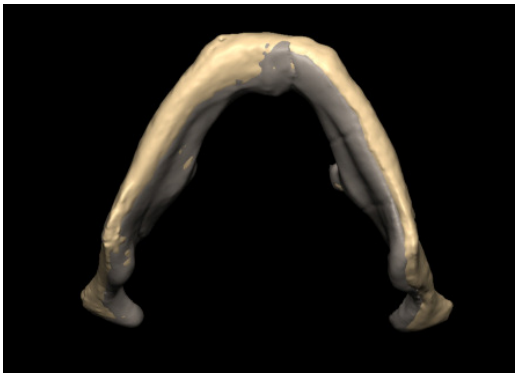

Cream = before restoration; grey = after restoration

Appendix 5

Cranium C shell deviation tables

Reference Model	skull C cranium 10
Test Model	#SkelC
# Data Points	537325

Tolerances	mm
Max Tol +	10.000
Min Tol +	0.500
Min Tol -	-0.500
Max Tol -	-10.000

Deviation	mm
Max Dev +	8.500
Max Dev -	-8.500
Average +/-	2.334 / -2.050
Std Dev	2.916

Percentage Deviations

>=Min	<Max	# Points	%
-10.000	-8.417	300	0.056
-8.417	-6.833	8084	1.504
-6.833	-5.250	14503	2.699
-5.250	-3.667	24315	4.525
-3.667	-2.083	53524	9.961
-2.083	-0.500	123631	23.009
-0.500	0.500	97135	18.078
0.500	2.083	102396	19.057
2.083	3.667	54605	10.162
3.667	5.250	29811	5.548
5.250	6.833	18442	3.432
6.833	8.417	10172	1.893
8.417	10.000	407	0.076

Out of Max Tol +	0	0.000
Out of Max Tol -	0	0.000

Standard Deviations

Distribution ()	# Points	%
-6 * Std Dev	0	0.000
-5 * Std Dev	0	0.000
-4 * Std Dev	0	0.000
-3 * Std Dev	5522	1.028
-2 * Std Dev	28921	5.382
-1 * Std Dev	103465	19.256
1 * Std Dev	253893	47.251
2 * Std Dev	101877	18.960
3 * Std Dev	36659	6.823
4 * Std Dev	6988	1.301
5 * Std Dev	0	0.000
6 * Std Dev	0	0.000

Cranium C shell deviation maps.

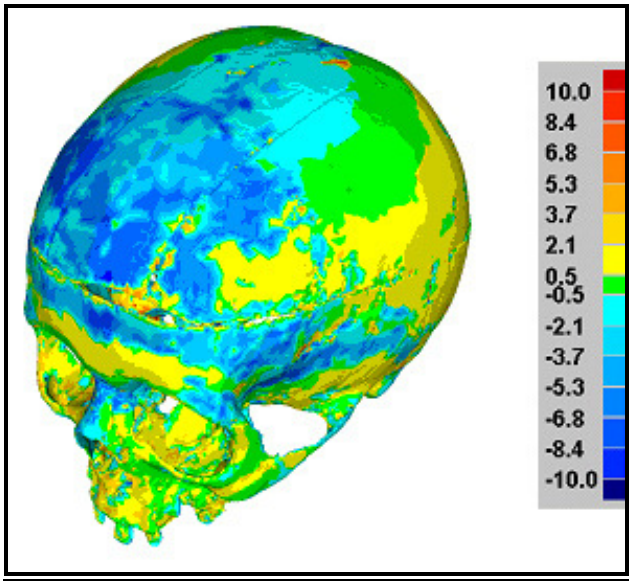

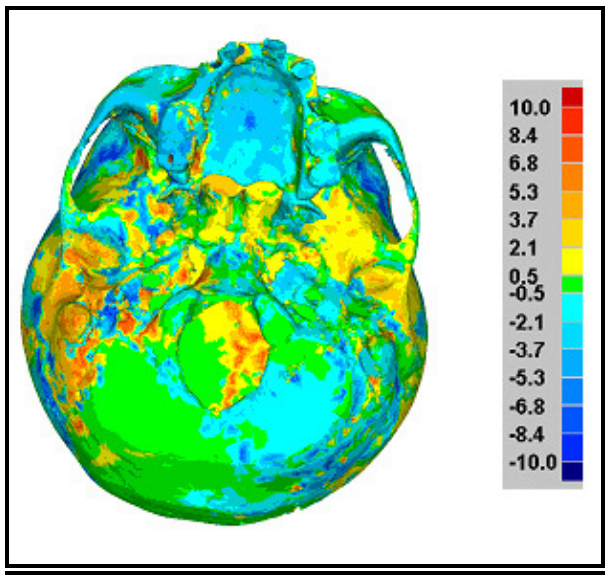

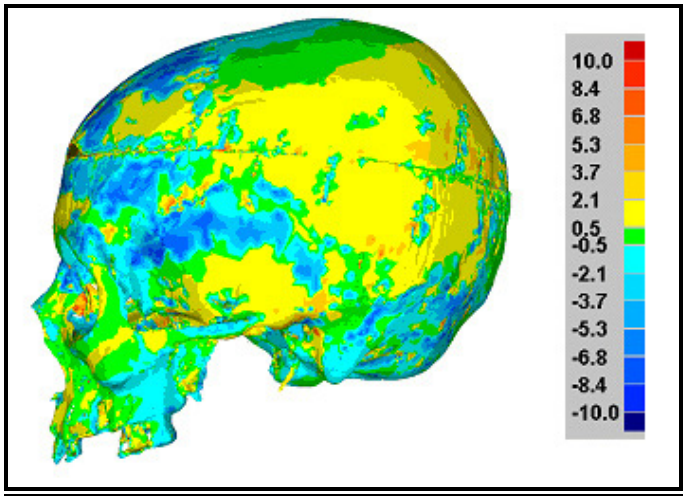
10.0
8.4
6.8
5.3
3.7
2.1
0.5
-0.5
-2.1
-3.7
-5.3
-6.8
-8.4
-10.0

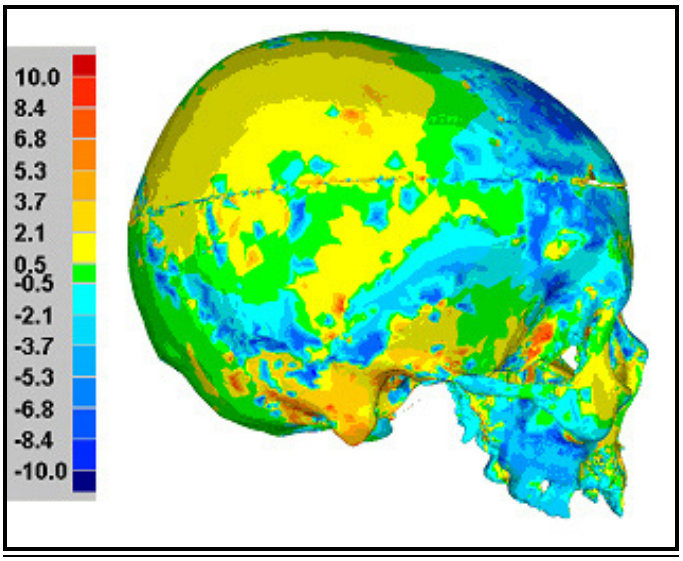
10.0
8.4
6.8
5.3
3.7
2.1
0.5
-0.5
-2.1
-3.7
-5.3
-6.8
-8.4
-10.0

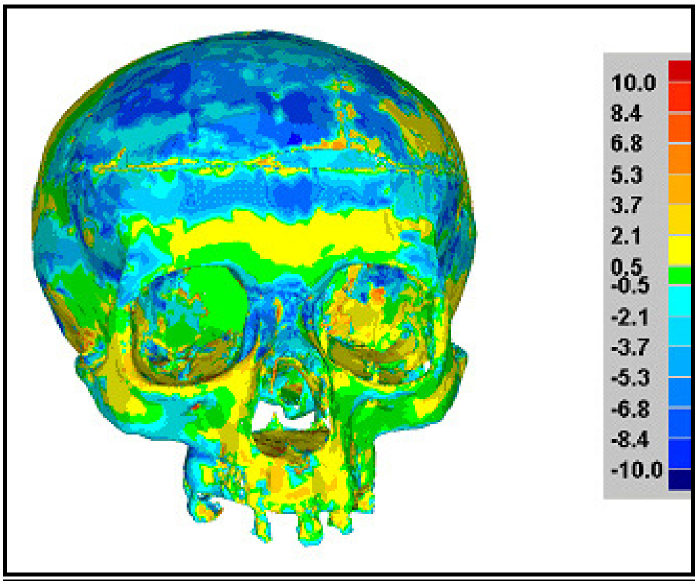
10.0
8.4
6.8
5.3
3.7
2.1
0.5
-0.5
-2.1
-3.7
-5.3
-6.8
-8.4
-10.0

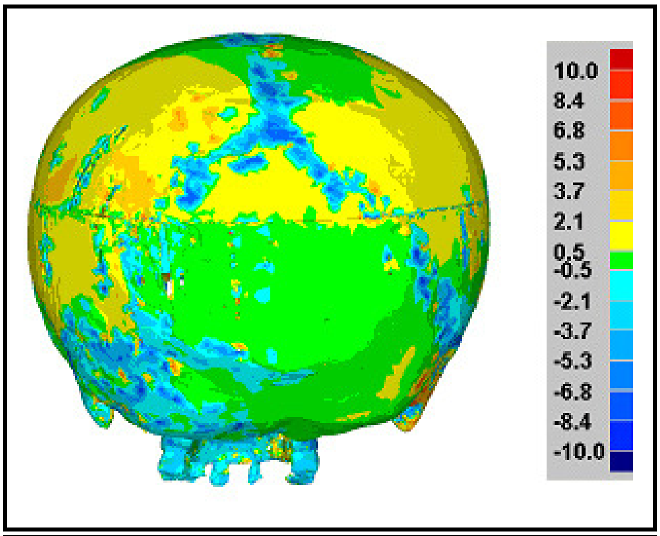
10.0
8.4
6.8
5.3
3.7
2.1
0.5
-0.5
-2.1
-3.7
-5.3
-6.8
-8.4
-10.0

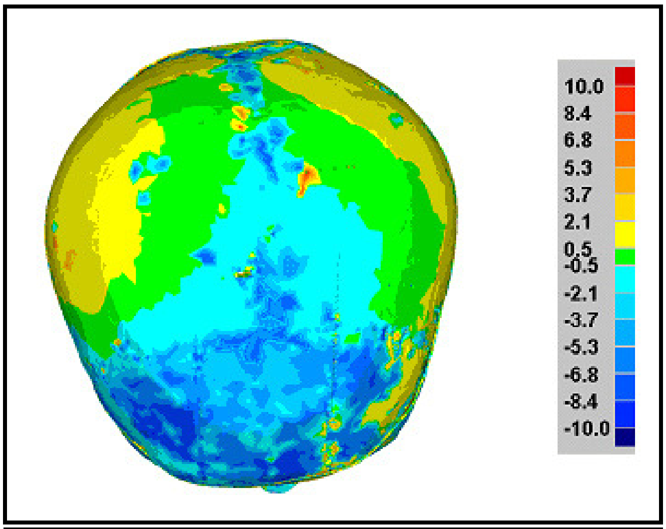
10.0
8.4
6.8
5.3
3.7
2.1
0.5
-0.5
-2.1
-3.7
-5.3
-6.8
-8.4
-10.0

Cranium C standard deviations.

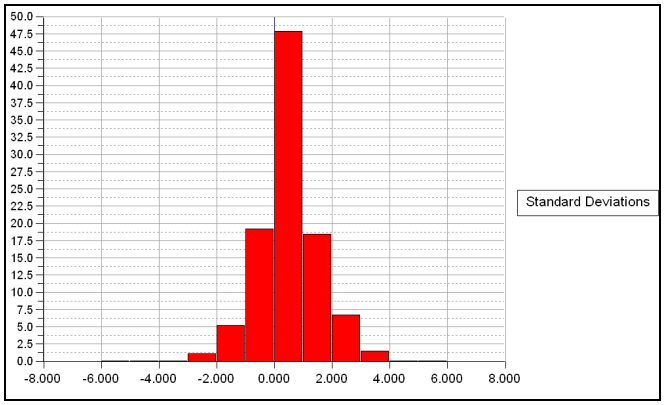

Cranium C deviation distribution.

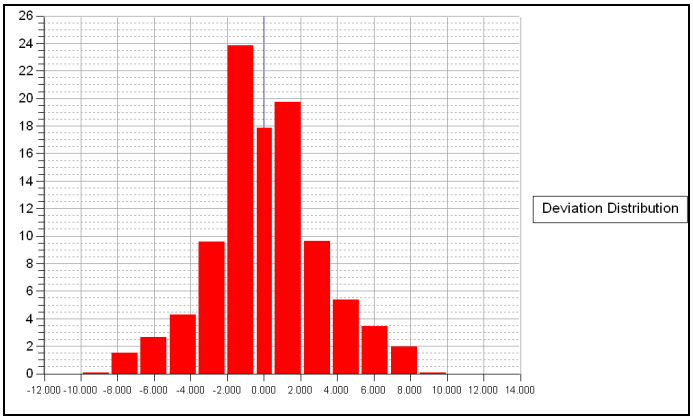

Vertical axis = percentage;
horizontal axis = millimetres

Mandible C shell deviation tables.

Reference Model	skull C mand
Test Model	# mand C
# Data Points	85267

Tolerances	mm
Max Tol +	10.000
Min Tol +	0.500
Min Tol -	-0.500
Max Tol -	-10.000

Deviation	mm
Max Dev +	5.797
Max Dev -	-5.799
Average +/-	1.673 / -2.286
Std Dev	2.640

Percentage Deviations

>=Min	<Max	# Points	%
-10.000	-8.417	0	0.000
-8.417	-6.833	0	0.000
-6.833	-5.250	2753	3.229
-5.250	-3.667	9243	10.840
-3.667	-2.083	9754	11.439
-2.083	-0.500	10948	12.840
-0.500	0.500	25181	29.532
0.500	2.083	13839	16.230
2.083	3.667	6025	7.066
3.667	5.250	6072	7.121
5.250	6.833	1452	1.703
6.833	8.417	0	0.000
8.417	10.000	0	0.000

Out of Max Tol +	0	0.000
Out of Max Tol -	0	0.000

Standard Deviations

Distribution ()	# Points	%
-6 * Std Dev	0	0.000
-5 * Std Dev	0	0.000
-4 * Std Dev	0	0.000
-3 * Std Dev	0	0.000
-2 * Std Dev	10214	11.979
-1 * Std Dev	15659	18.365
1 * Std Dev	42747	50.133
2 * Std Dev	10266	12.040
3 * Std Dev	6381	7.484
4 * Std Dev	0	0.000
5 * Std Dev	0	0.000
6 * Std Dev	0	0.000

Mandible C shell deviation maps.

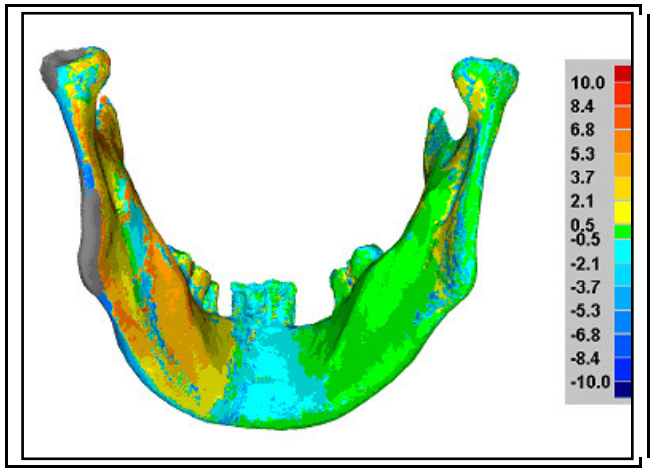

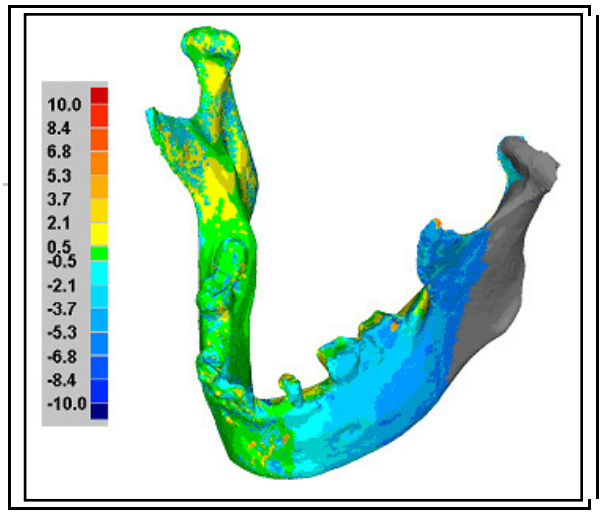

Mandible C annotated map and deviation table

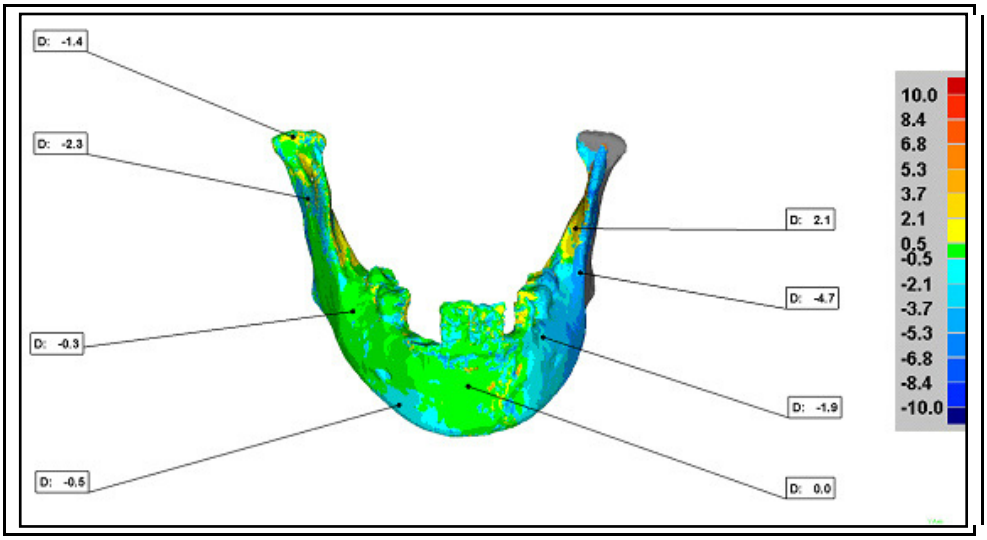

Name	Dev	Ref X	Ref Y	Ref Z	Dev Radius	Dev X	Dev Y	Dev Z	Test X	Test Y	Test Z
A001	0.035	4.176	-70.654	-8.409	1.000	-0.009	0.004	0.033	4.168	-70.650	-8.376
A002	-1.898	26.191	-57.447	-21.045	1.000	-1.417	-0.139	-1.254	24.774	-57.586	-22.299
A003	-4.706	39.441	-38.530	-41.611	1.000	-1.692	-0.910	-4.296	37.749	-39.441	-45.907
A004	2.051	38.263	-24.523	-44.494	1.000	-1.869	0.281	0.796	36.394	-24.242	-43.699
A005	-0.489	-15.807	-77.322	-20.019	1.000	0.349	0.115	-0.322	-15.457	-77.207	-20.341
A006	-0.345	-30.150	-50.187	-29.979	1.000	0.083	-0.116	-0.314	-30.067	-50.303	-30.293
A007	-2.335	-45.394	-15.226	-43.302	1.000	2.041	-0.039	-1.135	-43.353	-15.264	-44.437
A008	-1.441	-50.958	4.973	-50.045	1.000	-0.216	-0.668	-1.258	-51.174	4.305	-51.303

Units: mm.

Mandible C standard deviations.

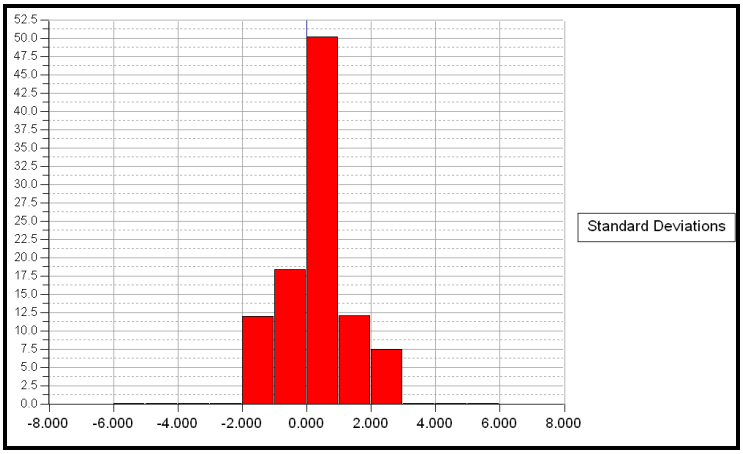

Mandible C deviation distribution

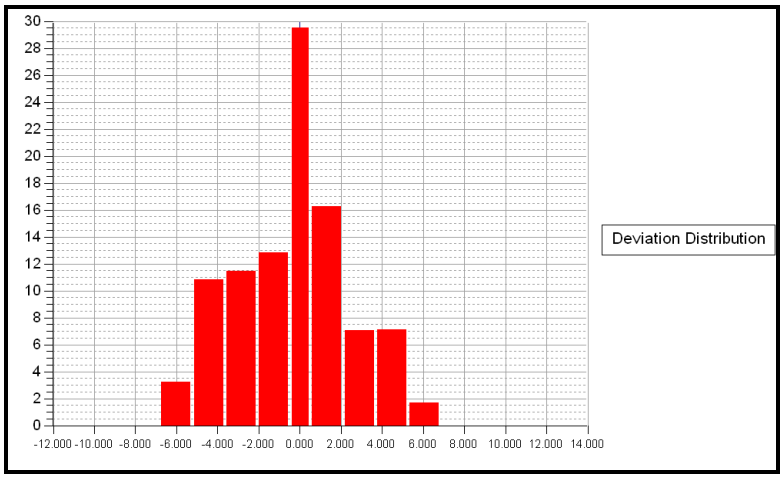

.

Vertical axis = percentage;
horizontal axis = millimetres

Skull C comparison and superimposition.

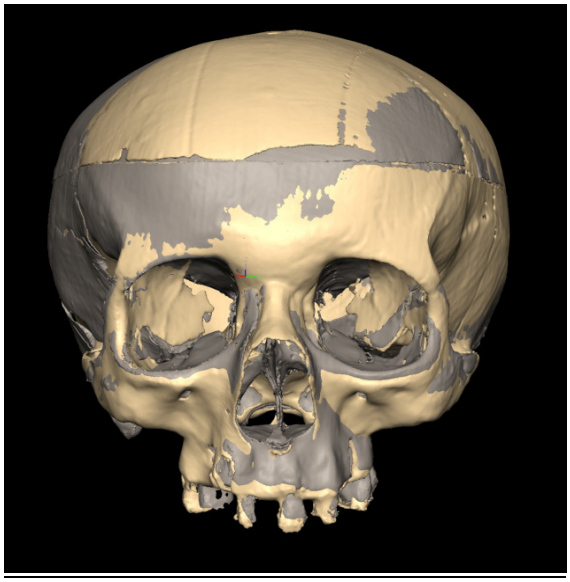

Cream = before restoration; grey = after restoration.

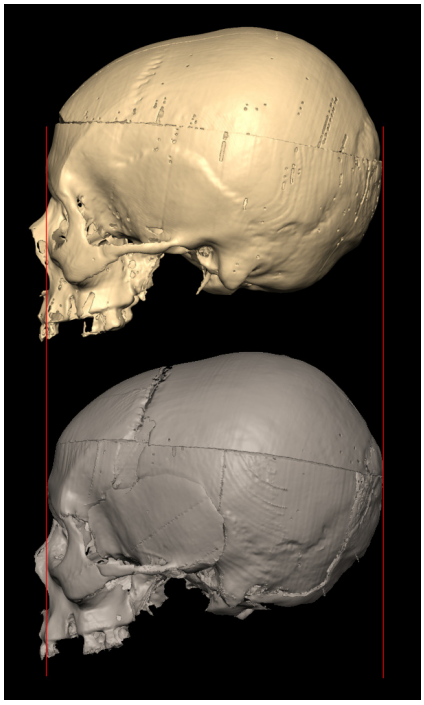

Lower image = after restoration

Cream = before restoration; grey = after restoration

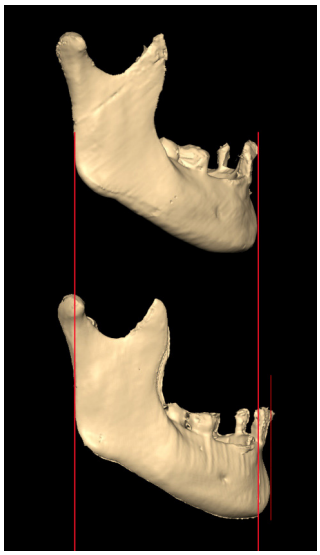

Bottom position = after restoration

Appendix 6

Cranium D shell deviation tables

Reference Model	skull D cranium
Test Model	# Skull D cranium
# Data Points	1020236

Tolerances	mm
Max Tol +	10.000
Min Tol +	0.500
Min Tol -	-0.500
Max Tol -	-10.000

Deviation	mm
Max Dev +	9.400
Max Dev -	-9.400
Average +/-	3.544 / -2.940
Std Dev	4.119

Percentage Deviations

>=Min	<Max	# Points	%
-10.000	-8.417	19606	1.922
-8.417	-6.833	29914	2.932
-6.833	-5.250	40876	4.007
-5.250	-3.667	58193	5.704
-3.667	-2.083	84127	8.246
-2.083	-0.500	161006	15.781
-0.500	0.500	123282	12.084
0.500	2.083	151458	14.845
2.083	3.667	113622	11.137
3.667	5.250	87766	8.603
5.250	6.833	67260	6.593
6.833	8.417	53217	5.216
8.417	10.000	29909	2.932

Out of Max Tol +	0	0.000
COut of Max Tol -	0	0.000

Standard Deviations

Distribution ()	# Points	%
-6 * Std Dev	0	0.000
-5 * Std Dev	0	0.000
-4 * Std Dev	0	0.000
-3 * Std Dev	0	0.000
-2 * Std Dev	63988	6.272
-1 * Std Dev	170358	16.698
1 * Std Dev	432064	42.349
2 * Std Dev	244400	23.955
3 * Std Dev	109426	10.726
4 * Std Dev	0	0.000
5 * Std Dev	0	0.000
6 * Std Dev	0	0.000

Cranium D shell deviation maps.

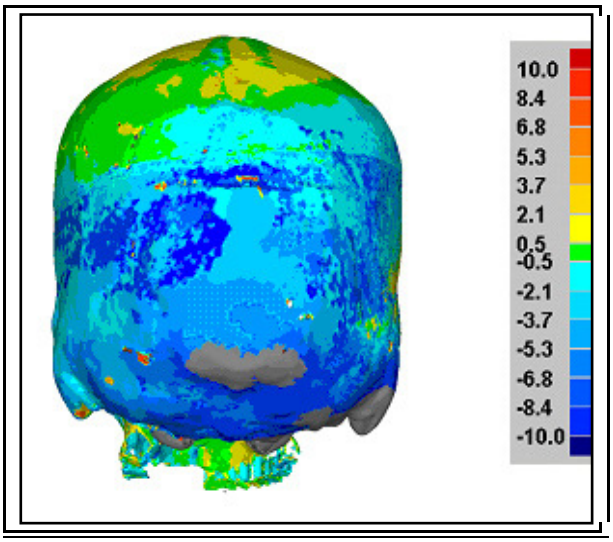

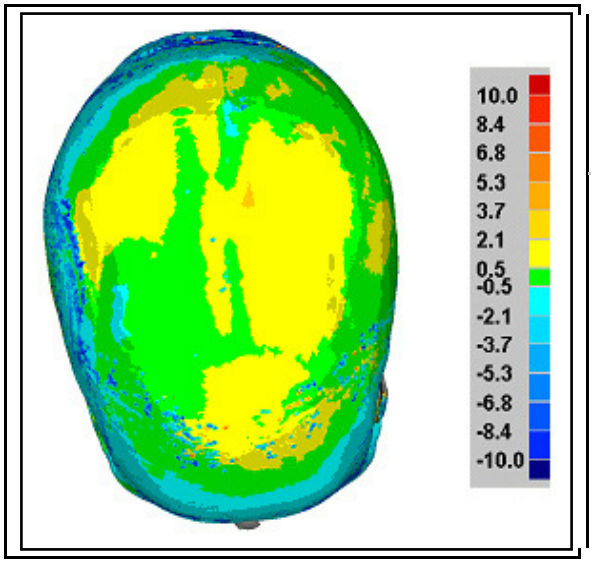

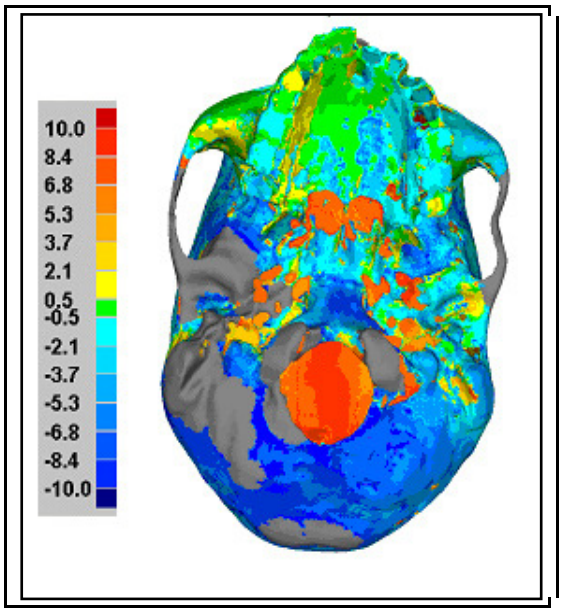
10.0
8.4
6.8
5.3
3.7
2.1
0.5
-0.5
-2.1
-3.7
-5.3
-6.8
-8.4
-10.0

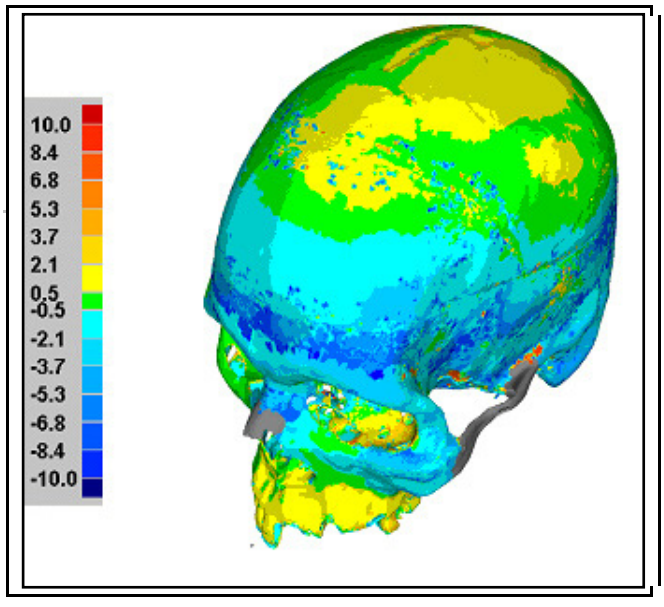
10.0
8.4
6.8
5.3
3.7
2.1
0.5
-0.5
-2.1
-3.7
-5.3
-6.8
-8.4
-10.0

Cranium D annotated map and deviation table.

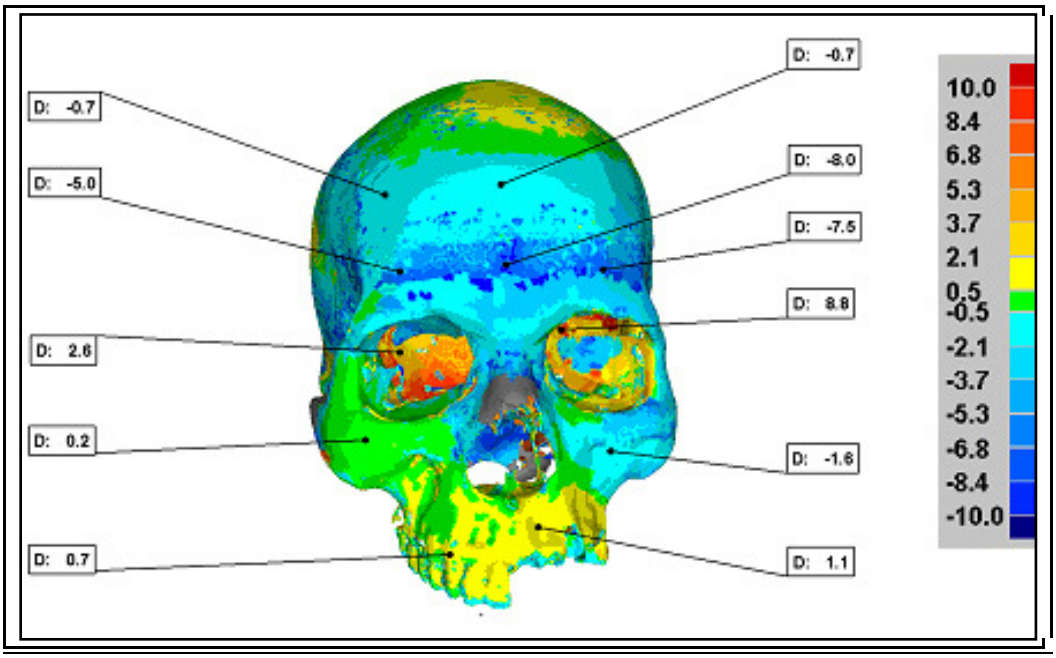

Name	Dev	Ref X	Ref Y	Ref Z	Dev Radius	Dev X	Dev Y	Dev Z	Test X	Test Y	Test Z
A001	-0.707	-2.295	73.230	5.134	1.000	0.007	-0.323	-0.629	-2.288	72.907	4.505
A002	-7.995	-0.826	47.609	10.937	1.000	-0.316	-0.556	-7.969	-1.141	47.052	2.968
A003	-7.507	30.209	46.351	3.398	1.000	-4.144	-1.807	-5.993	26.065	44.544	-2.596
A004	8.775	24.464	26.889	-150.649	1.000	-6.184	0.129	6.224	18.280	27.018	-144.425
A005	-1.576	33.503	-12.178	-8.293	1.000	-0.342	0.783	-1.324	33.161	-11.396	-9.617
A006	1.092	9.566	-35.260	4.078	1.000	0.441	0.441	0.896	10.007	-34.819	4.975
A007	0.208	-45.668	-8.114	-1.831	1.000	-0.070	-0.070	0.183	-45.738	-8.184	-1.648
A008	2.630	-42.888	17.399	-152.202	1.000	1.908	0.694	1.671	-40.980	18.093	-150.531
A009	-4.973	-34.282	45.709	5.040	1.000	2.532	-1.003	-4.161	-31.750	44.707	0.879
A010	-0.709	-39.790	71.072	-8.262	1.000	0.479	-0.286	-0.438	-39.311	70.786	-8.700
A011	0.664	-18.321	-43.428	7.936	1.000	-0.434	-0.100	0.492	-18.755	-43.528	8.428

Units: mm.

Cranium D standard deviations.

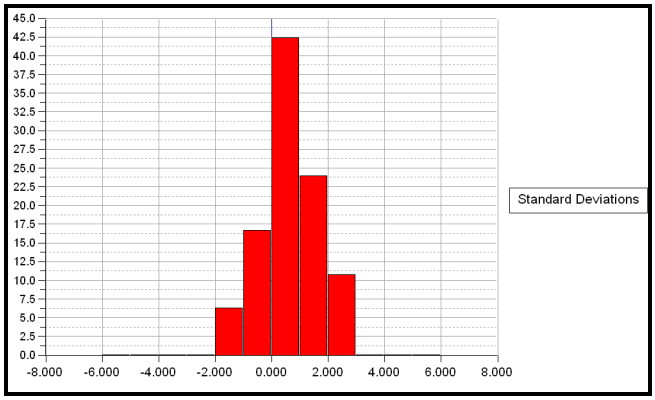

Cranium D deviation distribution.

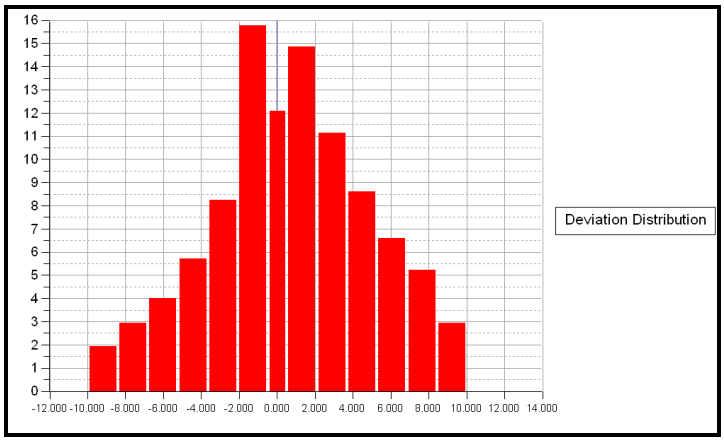

Vertical axis = percentage;
horizontal axis = millimetres.

Mandible D shell deviation tables.

Reference Model	skull D mand
Test Model	# skull D-final mandible
# Data Points	186879

Tolerances	mm
Max Tol +	10.000
Min Tol +	0.500
Min Tol -	-0.500
Max Tol -	-10.000

Deviation	mm
Max Dev +	5.498
Max Dev -	-5.500
Average +/-	1.393 / -1.607
Std Dev	1.992

Percentage Deviations

>=Min	<Max	# Points	%
-10.000	-8.417	0	0.000
-8.417	-6.833	0	0.000
-6.833	-5.250	1401	0.750
-5.250	-3.667	10438	5.585
-3.667	-2.083	15353	8.215
-2.083	-0.500	48918	26.176
-0.500	0.500	44138	23.618
0.500	2.083	47196	25.255
2.083	3.667	12626	6.756
3.667	5.250	6506	3.481
5.250	6.833	303	0.162
6.833	8.417	0	0.000
8.417	10.000	0	0.000

Out of Max Tol +	0	0.000
Out of Max Tol -	0	0.000

Standard Deviations

Distribution ()	# Points	%
-6 * Std Dev	0	0.000
-5 * Std Dev	0	0.000
-4 * Std Dev	0	0.000
-3 * Std Dev	3144	1.682
-2 * Std Dev	13955	7.467
-1 * Std Dev	35873	19.196
1 * Std Dev	87388	46.762
2 * Std Dev	34891	18.670
3 * Std Dev	10790	5.774
4 * Std Dev	838	0.448
5 * Std Dev	0	0.000
6 * Std Dev	0	0.000

Mandible D shell deviation maps.

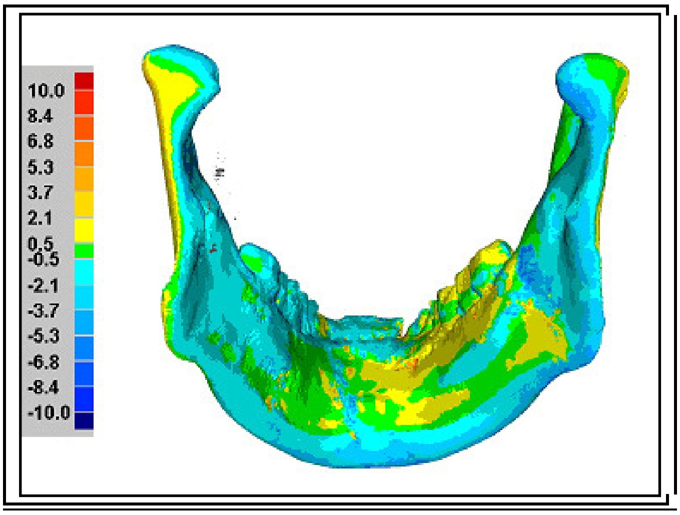

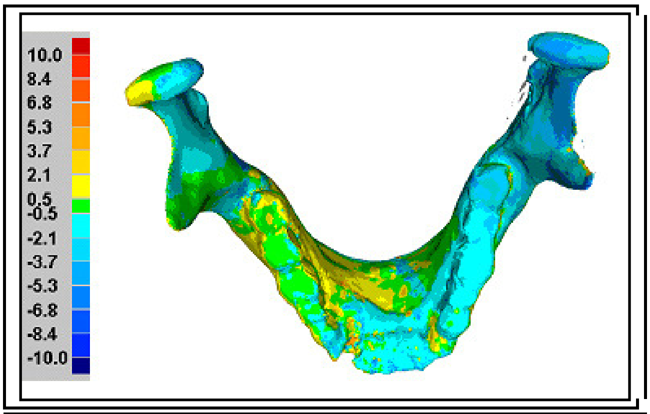

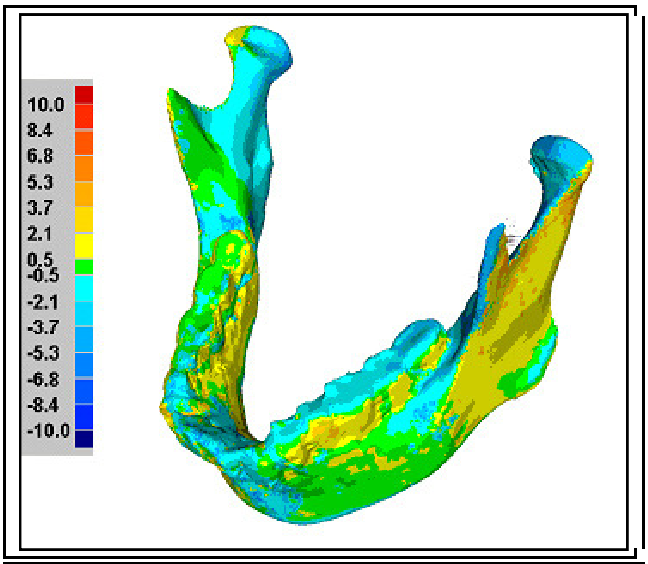

Mandible D annotated map and deviation table

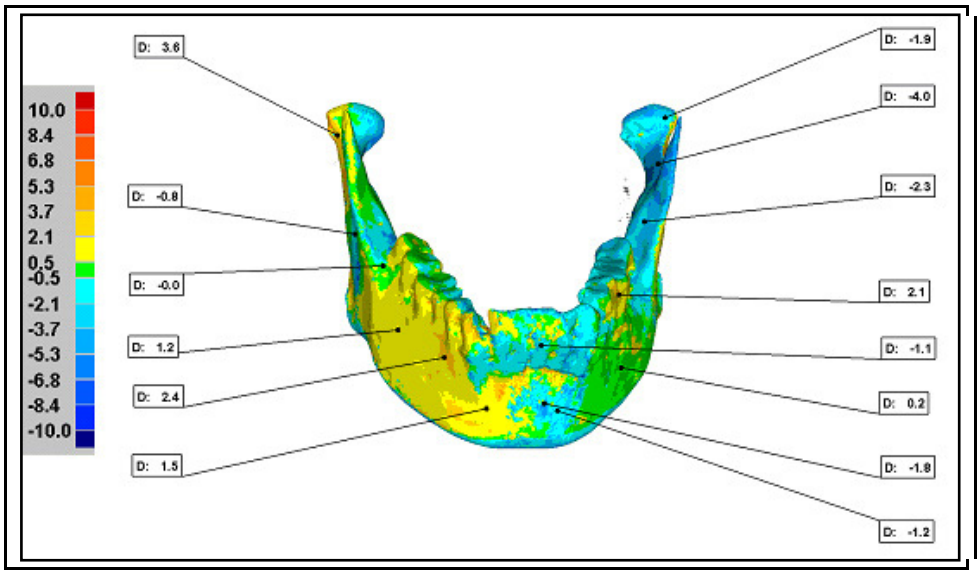

Name	Dev	Ref X	Ref Y	Ref Z	Dev Radius	Dev X	Dev Y	Dev Z	Test X	Test Y	Test Z
A001	1.240	-34.741	-72.284	-27.048	1.000	-0.852	0.269	0.859	-35.593	-72.015	-26.189
A002	-0.018	-40.041	-54.562	-39.009	1.000	-0.000	-0.009	-0.016	-40.042	-54.571	-39.025
A003	3.572	-56.965	-14.051	-65.544	1.000	-2.807	-0.876	2.028	-59.771	-14.927	-63.516
A004	-0.822	-49.096	-45.219	-46.926	1.000	0.751	0.136	-0.304	-48.345	-45.083	-47.230
A005	2.439	-21.232	-78.893	-14.687	1.000	-1.446	-1.116	1.615	-22.679	-80.009	-13.071
A006	-1.878	45.777	-7.566	-73.596	1.000	0.023	-0.175	-1.870	45.800	-7.741	-75.466
A007	-3.956	42.410	-23.064	-64.758	1.000	3.120	-1.987	-1.401	45.531	-25.051	-66.159
A008	-2.266	36.800	-41.308	-53.702	1.000	1.533	-0.604	-1.556	38.333	-41.913	-55.258
A009	2.128	25.910	-62.338	-20.915	1.000	1.783	-0.531	1.033	27.693	-62.870	-19.881
A010	0.240	27.301	-82.937	-28.846	1.000	0.191	-0.081	0.121	27.492	-83.018	-28.725
A011	1.507	-10.004	-92.540	-14.784	1.000	-0.445	-0.548	1.331	-10.450	-93.088	-13.452
A012	-1.106	4.106	-74.700	-1.011	1.000	0.107	0.779	-0.778	4.214	-73.920	-1.789
A013	-1.156	8.953	-93.239	-15.756	1.000	-0.593	0.106	-0.987	8.359	-93.133	-16.743
A014	-1.767	5.304	-90.988	-13.337	1.000	-0.821	0.138	-1.558	4.483	-90.850	-14.895

Units: mm.

Mandible D standard deviations

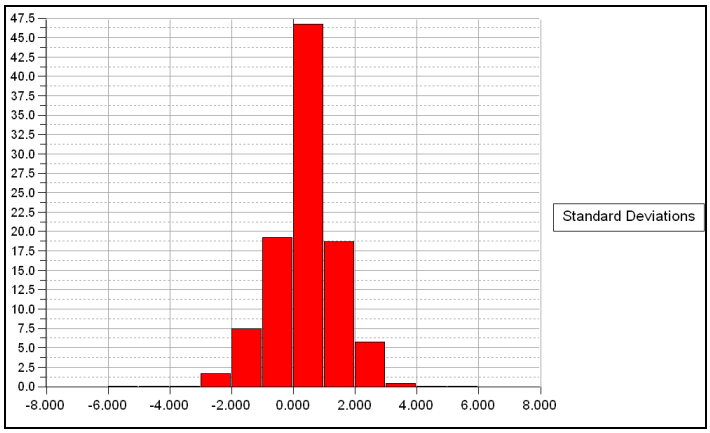

Mandible D deviation distribution.

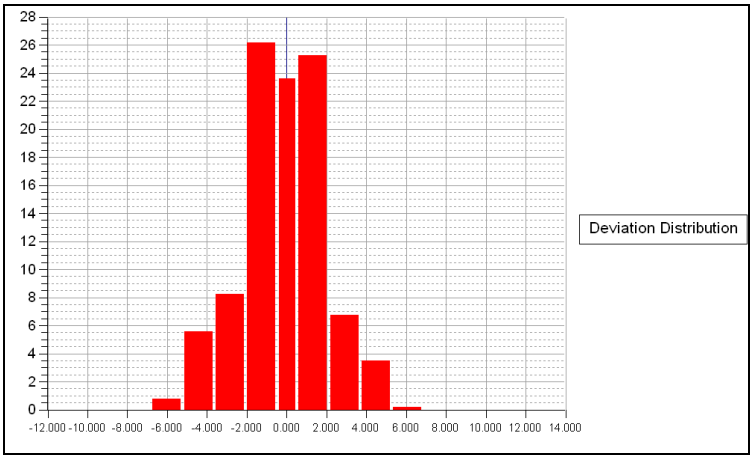

Vertical axis = percentage;
horizontal axis = millimetres

Skull D comparison and superimposition

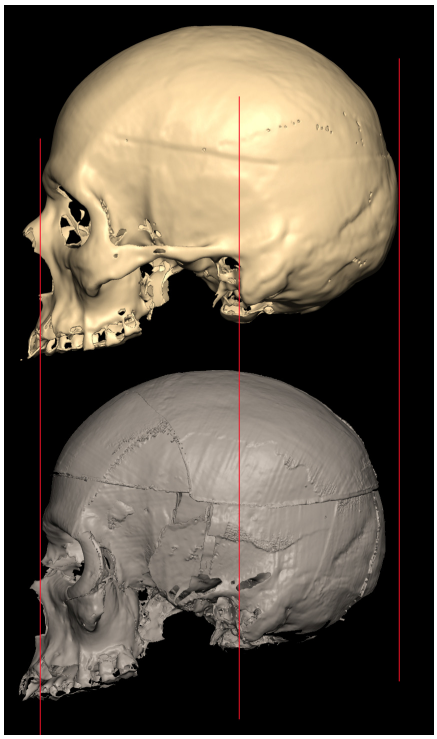

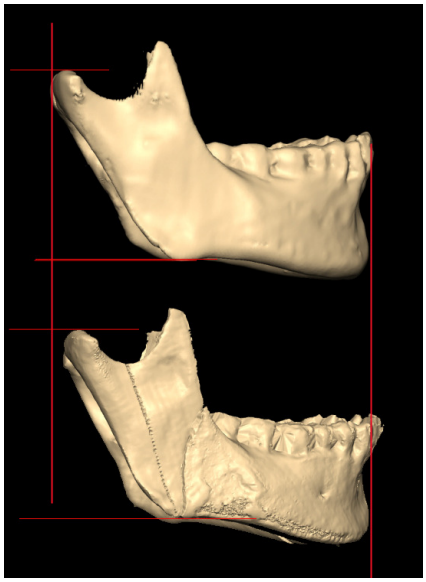

Lower image = after restoration

Cream = before restoration; grey = after restoration.

Appendix 7

Cranium E shell deviation tables

Reference Model	skull E cranium
Test Model	# cranium
# Data Points	459073

Tolerances	mm
Max Tol +	10.000
Min Tol +	0.500
Min Tol -	-0.500
Max Tol -	-10.000

Deviation	mm
Max Dev +	9.200
Max Dev -	-9.200
Average +/-	2.931 / -2.287
Std Dev	3.482

Percentage Deviations

>=Min	<Max	# Points	%
-10.000	-8.417	3365	0.733
-8.417	-6.833	8757	1.908
-6.833	-5.250	12525	2.728
-5.250	-3.667	21574	4.699
-3.667	-2.083	38363	8.357
-2.083	-0.500	84225	18.347
-0.500	0.500	78581	17.117
0.500	2.083	81991	17.860
2.083	3.667	47577	10.364
3.667	5.250	33725	7.346
5.250	6.833	23703	5.163
6.833	8.417	17399	3.790
8.417	10.000	7288	1.588

Out of Max Tol +	0	0.000
Out of Max Tol -	0	0.000

Standard Deviations

Distribution ()	# Points	%
-6 * Std Dev	0	0.000
-5 * Std Dev	0	0.000
-4 * Std Dev	0	0.000
-3 * Std Dev	2097	0.457
-2 * Std Dev	22843	4.976
-1 * Std Dev	72436	15.779
1 * Std Dev	218431	47.581
2 * Std Dev	94375	20.558
3 * Std Dev	44439	9.680
4 * Std Dev	4452	0.970
5 * Std Dev	0	0.000
6 * Std Dev	0	0.000

Cranium E shell deviation maps.

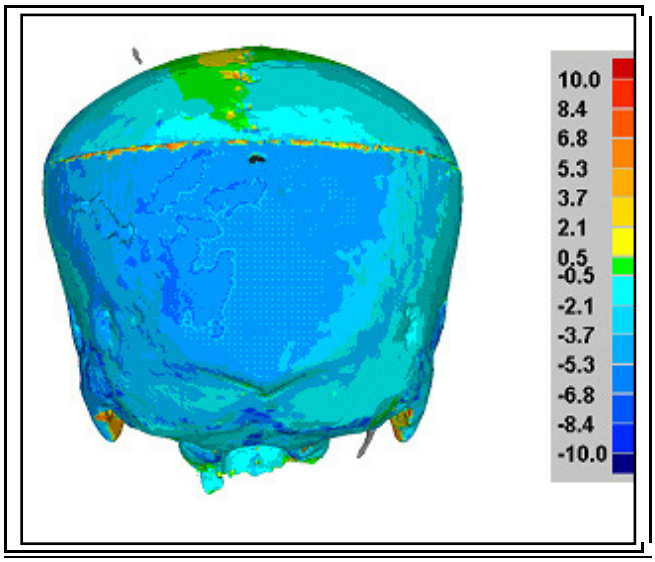

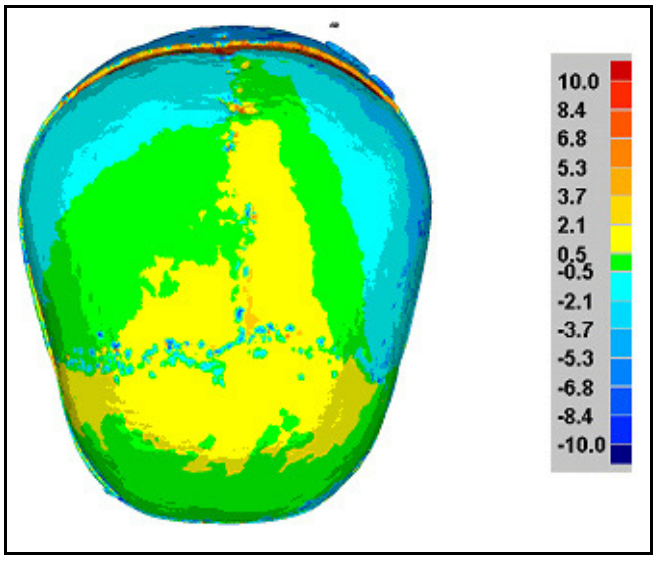

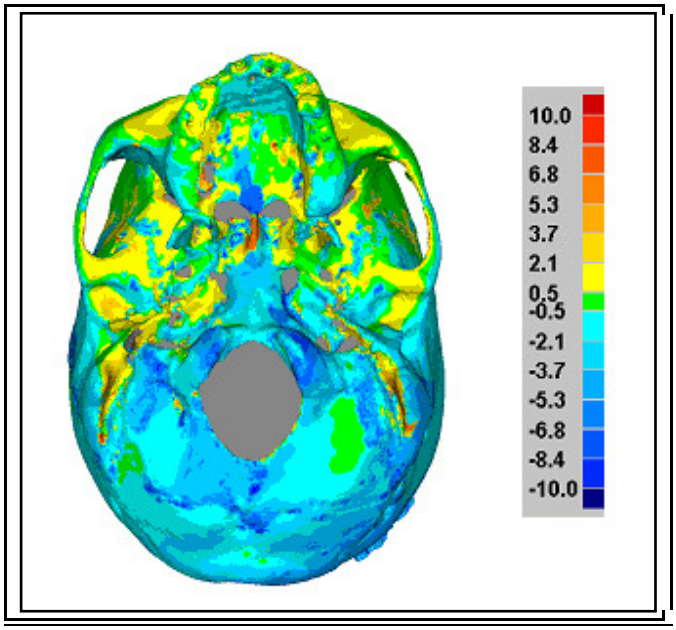
10.0
8.4
6.8
5.3
3.7
2.1
0.5
-0.5
-2.1
-3.7
-5.3
-6.8
-8.4
-10.0

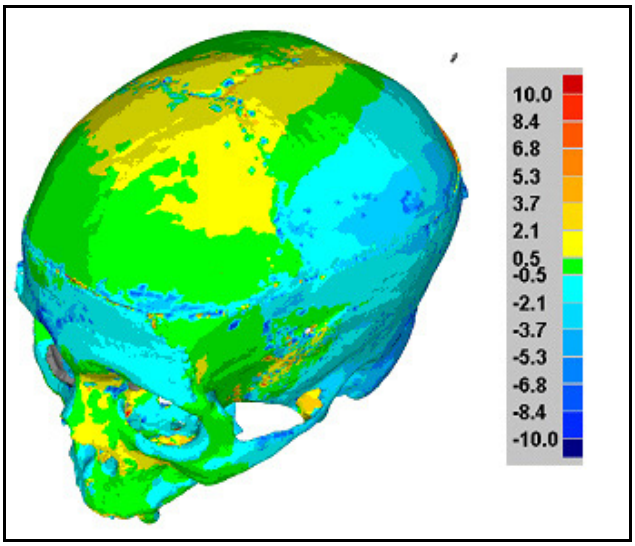
10.0
8.4
6.8
5.3
3.7
2.1
0.5
-0.5
-2.1
-3.7
-5.3
-6.8
-8.4
-10.0

Cranium E annotated map and deviation table.

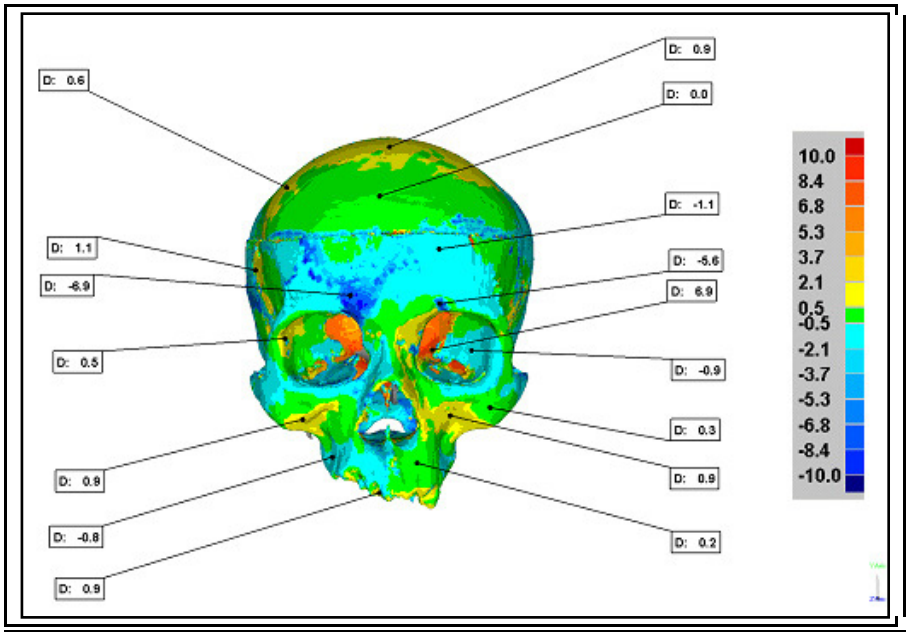

Name	Dev	Ref X	Ref Y	Ref Z	Dev Radius	Dev X	Dev Y	Dev Z	Test X	Test Y	Test Z
A001	0.036	-5.389	80.494	0.089	1.000	-0.002	-440.021	0.029	-5.391	80.515	0.118
A002	0.868	-1.350	105.040	-28.853	1.000	0.047	0.767	0.404	-1.303	105.807	-28.449
A003	-1.058	19.044	58.031	8.780	1.000	-0.203	-0.036	-1.038	18.841	57.996	7.742
A004	-5.649	19.214	35.747	8.824	1.000	-1.110	3.449	-4.335	18.104	39.196	4.489
A005	-0.907	34.499	15.720	-21.280	1.000	0.610	-0.086	-0.666	35.108	15.634	-21.946
A006	6.857	22.335	11.446	-153.287	1.000	-3.452	3.634	4.679	18.883	15.079	-148.608
A007	0.261	41.348	-7.914	-7.183	1.000	0.108	-0.093	0.219	41.456	-8.007	-6.965
A008	0.890	24.381	-11.312	-7.232	1.000	0.370	-0.515	0.624	24.751	-11.827	-6.608
A009	0.158	10.147	-29.675	5.215	1.000	0.054	0.016	0.147	10.201	-29.658	5.363
A010	-0.763	-25.795	-29.209	-10.294	1.000	0.672	-0.087	-0.350	-25.123	-29.297	-10.645
A011	0.895	-37.974	-12.708	-4.978	1.000	-0.076	-0.607	0.654	-38.050	-13.315	-4.324
A012	0.493	-45.705	21.187	-7.839	1.000	0.436	0.004	0.230	-45.269	21.191	-7.609
A013	1.135	-63.002	51.431	-48.468	1.000	-1.055	-0.048	0.416	-64.057	51.383	-48.053
A014	-6.905	-17.303	39.162	11.721	1.000	2.071	1.341	-6.450	-15.233	40.503	5.271
A015	0.575	-47.029	87.295	-30.437	1.000	-0.374	0.389	0.200	-47.403	87.684	-30.237
A016	0.936	-5.511	-41.734	6.006	1.000	-0.626	-0.405	0.566	-6.137	-42.139	6.572

Units: mm.

Cranium E standard deviations.

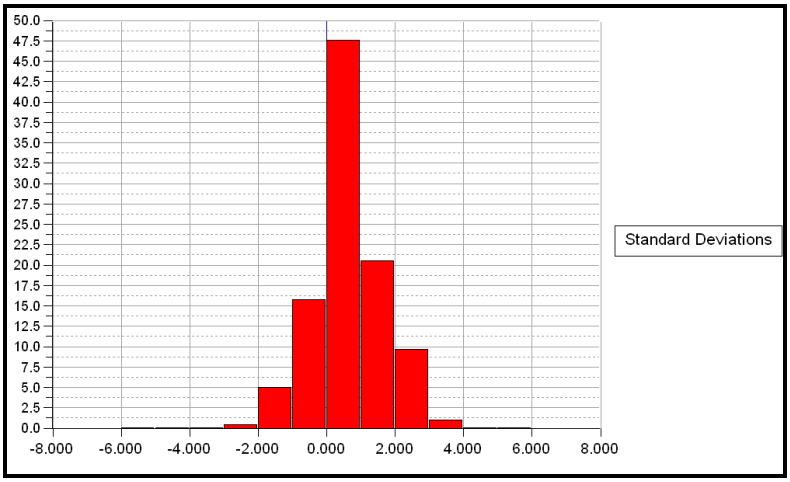

Cranium E deviation distribution.

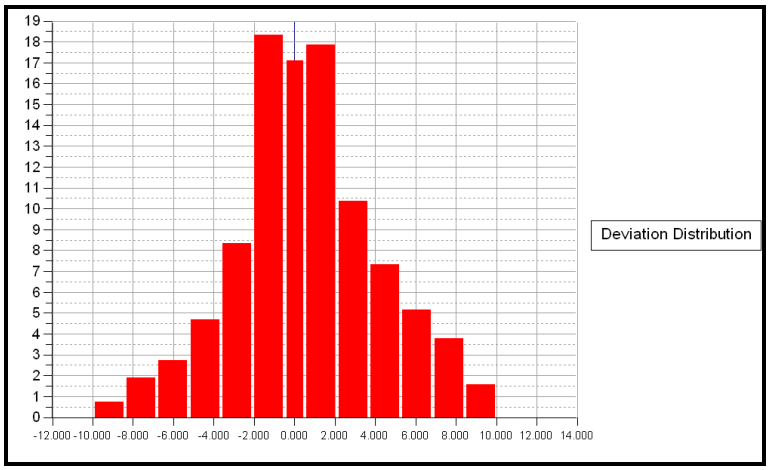

Vertical axis = percentage;
horizontal axis = millimetres.

Mandible E shell deviation tables.

Reference Model	skull E mand
Test Model	# skull e
# Data Points	248310

Tolerances	mm
Max Tol +	10.000
Min Tol +	0.500
Min Tol -	-0.500
Max Tol -	-10.000

Deviation	mm
Max Dev +	5.400
Max Dev -	-5.400
Average +/-	0.875 / -1.822
Std Dev	1.940

Percentage Deviations

>=Min	<Max	# Points	%
-10.000	-8.417	0	0.000
-8.417	-6.833	0	0.000
-6.833	-5.250	1549	0.624
-5.250	-3.667	21164	8.523
-3.667	-2.083	26053	10.492
-2.083	-0.500	45457	18.307
-0.500	0.500	102538	41.294
0.500	2.083	36884	14.854
2.083	3.667	7201	2.900
3.667	5.250	7004	2.821
5.250	6.833	460	0.185
6.833	8.417	0	0.000
8.417	10.000	0	0.000

Out of Max Tol +	0	0.000
Out of Max Tol -	0	0.000

Standard Deviations

Distribution ()	# Points	%
-6 * Std Dev	0	0.000
-5 * Std Dev	0	0.000
-4 * Std Dev	0	0.000
-3 * Std Dev	6659	2.682
-2 * Std Dev	27919	11.244
-1 * Std Dev	39348	15.846
1 * Std Dev	149266	60.113
2 * Std Dev	14157	5.701
3 * Std Dev	9280	3.737
4 * Std Dev	1681	0.677
5 * Std Dev	0	0.000
6 * Std Dev	0	0.000

Mandible E shell deviation maps.

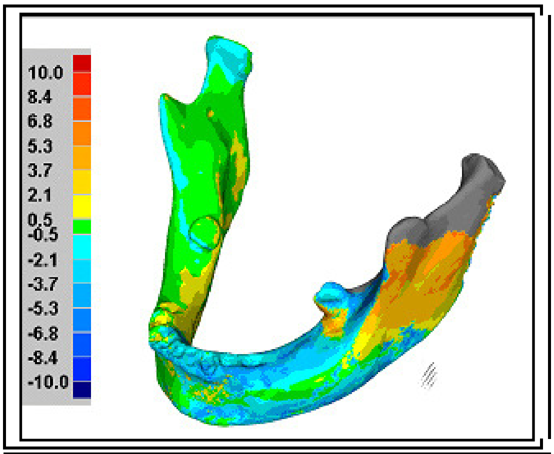

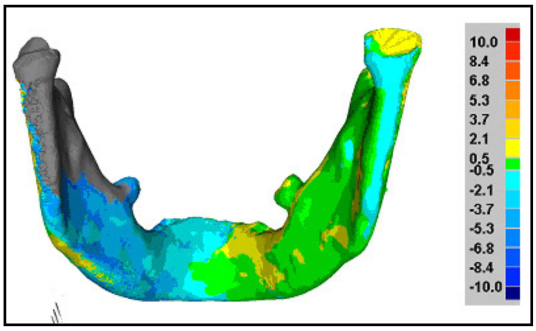

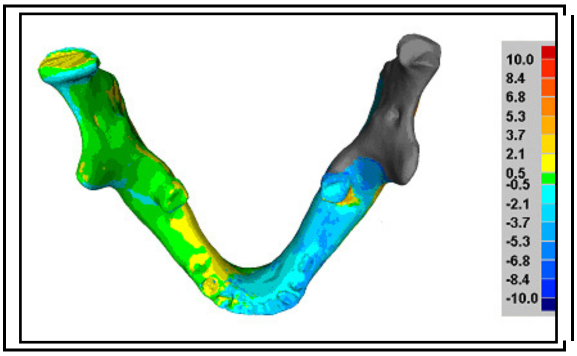

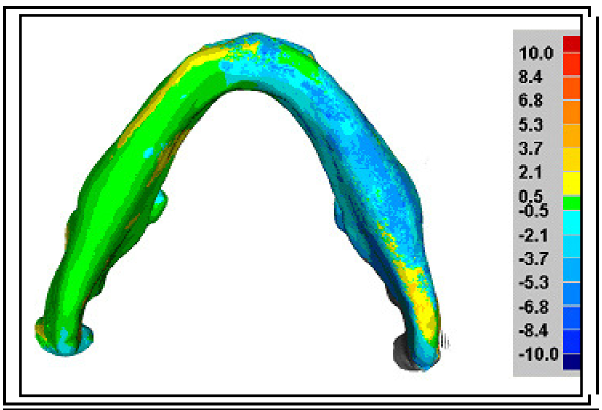

Mandible E annotated map and deviation

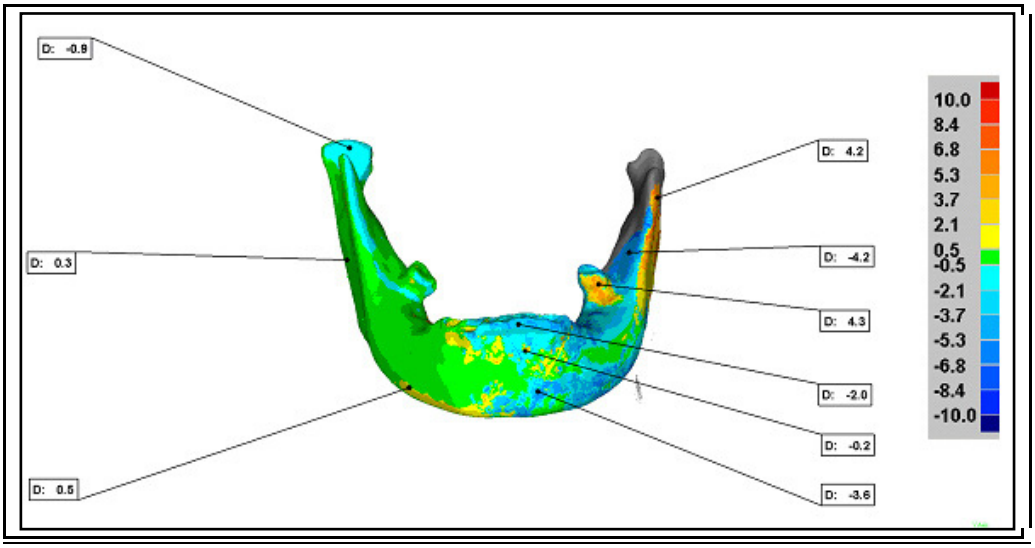

Name	Dev	Ref X	Ref Y	Ref Z	Dev Radius	Dev X	Dev Y	Dev Z	Test X	Test Y	Test Z
A001	-0.882	-48.885	-9.917	-61.266	1.000	-0.208	-0.097	-0.852	-49.094	-10.014	-62.118
A002	0.270	-47.954	-44.738	-48.436	1.000	-0.253	-0.053	0.077	-48.207	-44.791	-48.359
A003	0.517	-26.989	-79.347	-14.441	1.000	-0.393	-0.207	0.265	-27.381	-79.554	-14.177
A004	-1.995	1.798	-61.390	6.689	1.000	0.059	0.093	-1.992	1.857	-61.297	4.697
A005	-0.169	3.570	-68.264	3.441	1.000	-0.019	0.023	-0.166	3.551	-68.241	3.274
A006	-3.568	6.840	-78.577	2.555	1.000	-2.007	-0.431	-2.919	4.834	-79.008	-0.364
A007	4.275	25.018	-51.795	-28.971	1.000	1.004	-2.052	3.613	26.021	-53.847	-25.358
A008	-4.224	34.568	-42.724	-37.569	1.000	3.445	-1.667	-1.788	38.013	-44.391	-39.357
A009	4.164	42.461	-27.083	-35.573	1.000	3.731	-0.212	1.836	46.192	-27.295	-33.737

Units: mm.

Mandible E standard deviations.

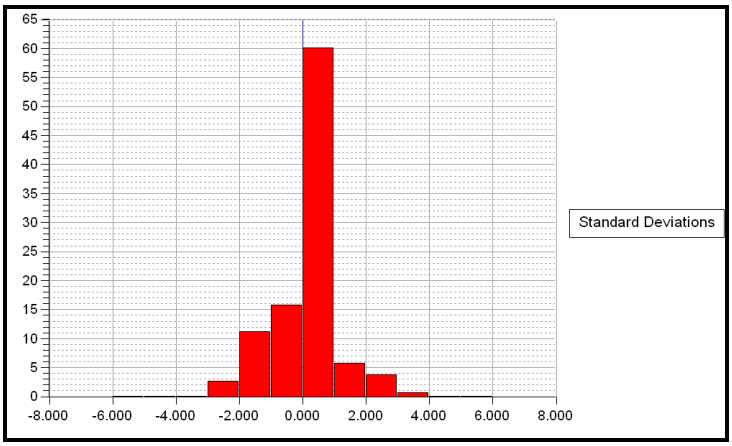

Mandible E deviation distribution

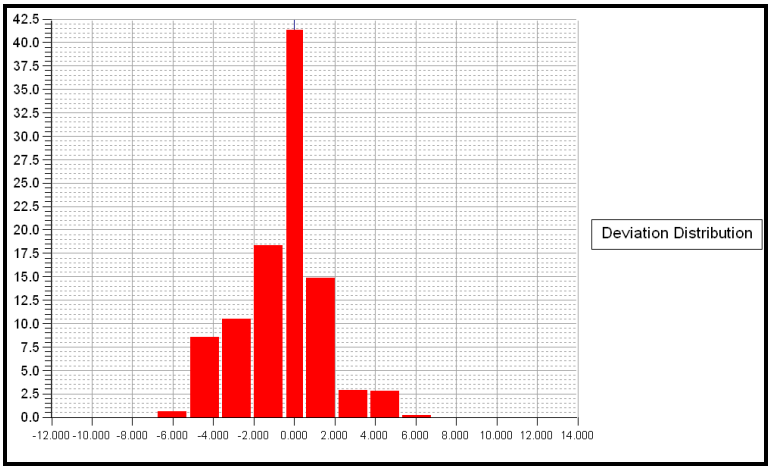

.

Vertical axis = percentage;
horizontal axis = millimetres

Skull E comparison and superimposition

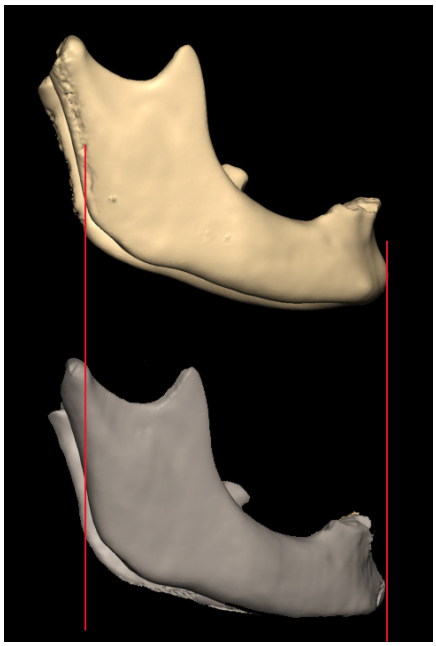

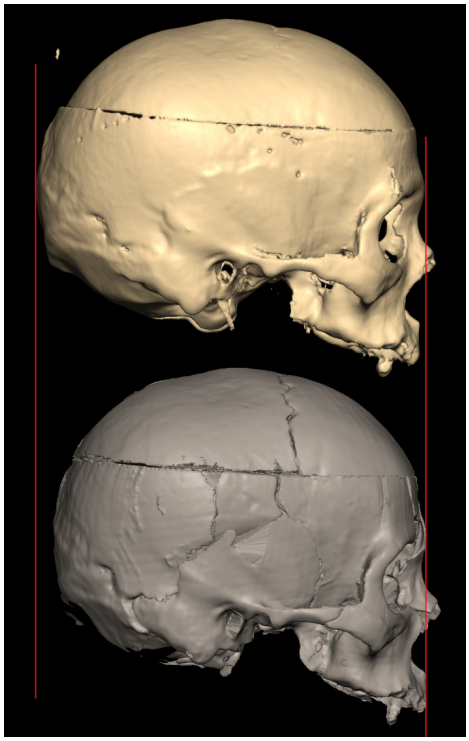

Lower image = after restoration

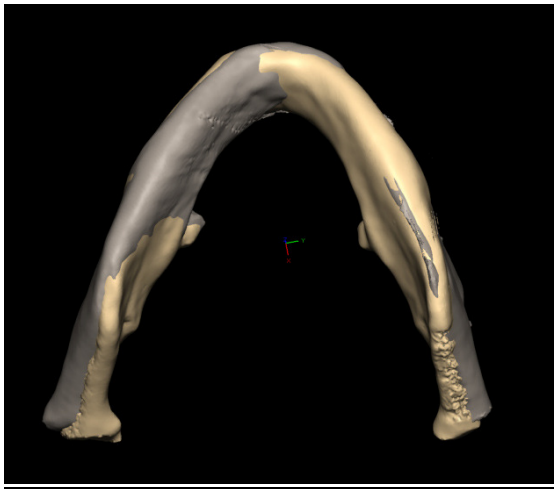

Cream = before restoration; grey = after restoration